CHAPTER 1

MECHANICS OF PNEUMATIC TIRES

Aside from aerodynamic and gravitational forces, all other major forces and moments affecting the motion of a ground vehicle are applied through the running gear–ground contact. An understanding of the basic characteristics of the interaction between the running gear and the ground is, therefore, essential to the study of performance characteristics, ride quality, and handling behavior of ground vehicles. The running gear of a ground vehicle is generally required to fulfill the following functions:

- To support the weight of the vehicle
- To cushion the vehicle over surface irregularities
- To provide sufficient traction for driving and braking
- To provide adequate steering control and direction stability

Pneumatic tires can perform these functions effectively and efficiently; thus, they are universally used in road vehicles, and are also widely used in off-road vehicles. The study of the mechanics of pneumatic tires is of fundamental importance to the understanding of the performance and characteristics of ground vehicles. Two basic types of problem in the mechanics of tires are of special interest to vehicle engineers. One is the mechanics of tires on hard surfaces, which is essential to the study of the characteristics of road vehicles. The other is the mechanics of tires on deformable surfaces (unprepared terrain), which is of prime importance to the study of off-road vehicle performance.

The mechanics of tires on hard surfaces is discussed in this chapter, whereas the behavior of tires over unprepared terrain is discussed in Chapter 2.

A pneumatic tire is a flexible structure of the shape of a toroid filled with compressed air. The most important structural element of the tire is the

carcass. It is made up of a number of layers of flexible cords of high modulus of elasticity encased in a matrix of low modulus rubber compounds, as shown in Fig. 1.1. The cords are made of fabrics of natural, synthetic, or metallic composition, and are anchored around the beads made of high tensile strength steel wires. The beads serve as the "foundations" for the carcass and provide adequate seating of the tire on the rim. The ingredients of the rubber compounds are selected to provide the tire with specific properties. The rubber compounds for the sidewall are generally required to be highly resistant to fatigue and scuffing, and styrene—butadiene compounds are widely used [1.1].[1] The rubber compounds for the tread vary with the type of tire. For instance, for heavy truck tires, the high load intensities necessitate the use of tread compounds with high resistance to abrasion, tearing, and crack growth, and with low hysteresis to reduce internal heat generation and rolling resistance. Consequently, natural rubber compounds are widely used for truck tires, although they intrinsically provide lower values of the coefficient of road adhesion, particularly on wet surfaces, than various synthetic rubber compounds universally used for passenger car and racing car tires [1.1]. For tubeless tires, which have become dominant, a thin layer of rubber with high impermeability to air (such as butyl rubber compounds) is attached to the inner surface of the carcass.

The load transmission of a pneumatic tire is analogous to that of a bicycle wheel, where the hub hangs on the spokes from the upper part of the rim, which in turn is supported at its lower part by the ground. For an inflated pneumatic tire, the inflation pressure causes tension to be developed in the cords comprising the carcass. The load applied through the rim of the wheel hangs primarily on the cords in the sidewalls through the beads.

The design and construction of the carcass determine, to a great extent, the characteristics of the tire. Among the various design parameters, the geometric dispositions of layers of rubber-coated cords (plies), particularly their directions, play a significant role in the behavior of the tire. The direction of the cords is usually defined by the crown angle, which is the angle between the cord and the circumferential center line of the tire, as shown in Fig. 1.1. When the cords have a low crown angle, the tire will have good cornering characteristics, but a harsh ride. On the other hand, if the cords are at right angle to the centerline of the tread, the tire will be capable of providing a comfortable ride, but poor handling performance.

A compromise is adopted in a bias-ply tire, in which the cords extend diagonally across the carcass from bead to bead with a crown angle of approximately 40°, as shown in Fig. 1.1(a). A bias-ply tire has two plies (for light-load tires) or more (up to 20 plies for heavy-load tires). The cords in adjacent plies run in opposite directions. Thus, the cords overlap in a diamond-shaped (criss-cross) pattern. In operation, the diagonal plies flex and rub, thus elongating the diamond-shaped elements and the rubber-filler. This flexing action produces

[1]Numbers in brackets designate references at the end of the chapter.

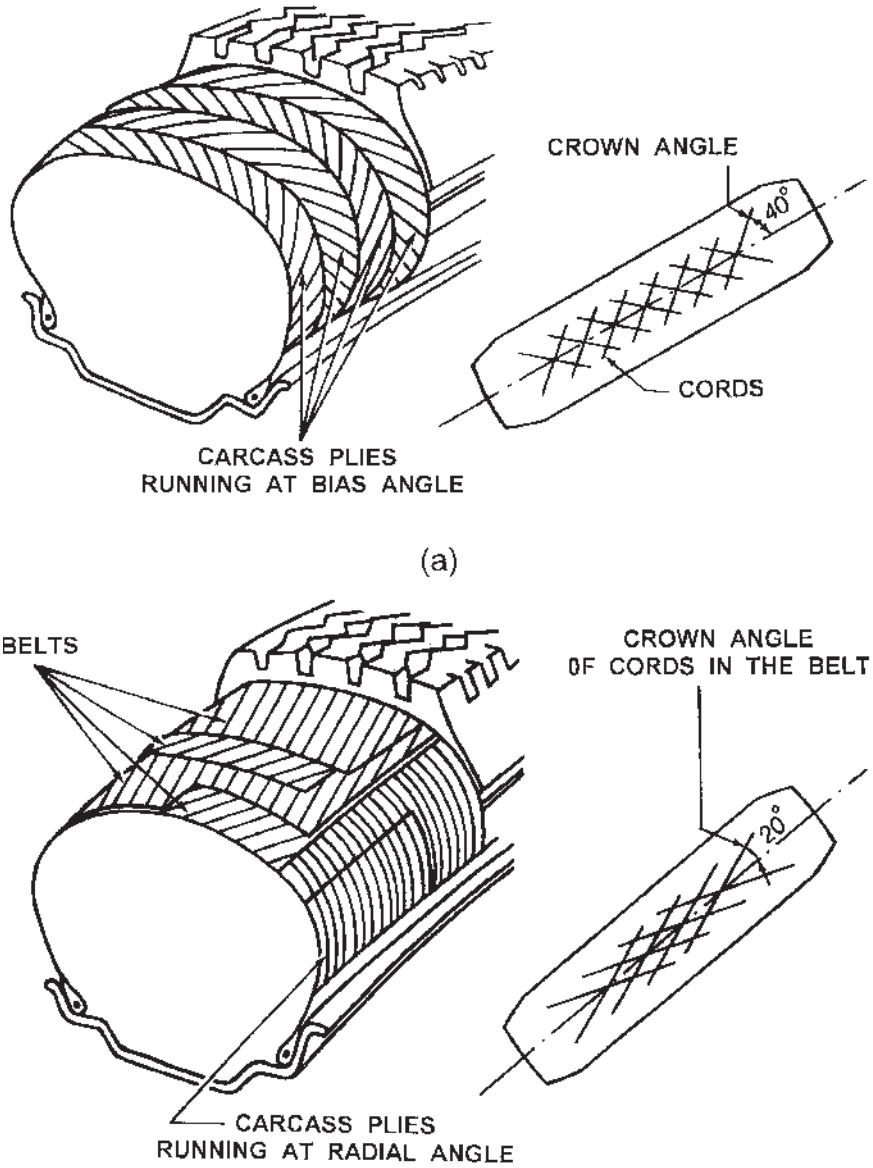

Fig. 1.1 Tire construction. (a) Bias-ply tire. (b) Radial-ply tire.

a wiping motion between the tread and the road, which is one of the main causes of tire wear and high rolling resistance [1.2, 1.3].

The radial-ply tire, on the other hand, is constructed very differently from the bias-ply tire. It was first introduced by Michelin in 1948 and has now become dominant for passenger cars and trucks and increasingly for heavy-duty earth-moving machinery. However, the bias-ply tire is still in use for motorcycles, certain agricultural machinery, and some military equipment. The radial-ply tire has one or more layers of cords in the carcass extending radially from bead to bead, resulting in a crown angle of 90°, as shown in Fig. 1.1(b). A belt of several layers of cords of high modulus of elasticity (usually steel or other high-strength materials) is fitted under the tread, as shown in Fig. 1.1(b). The cords in the belt are laid at a low crown angle of approximately 20°. The belt is essential to the proper functioning of the radial-ply tire. Without it, a radial-ply carcass can become unstable since the tire periphery may develop into a series of buckles due to the irregularities in cord spacing when inflated. For passenger car tires, usually there are two radial plies in the carcass made of synthetic material, such as rayon or polyester, and two plies of steel cords and two plies of cords made of synthetic material, such as nylon, in the belt. For truck tires, usually there is one radial steel ply in the carcass and four steel plies in the belt. For the radial-ply tire, flexing of the carcass involves very little relative movement of the cords forming the belt. In the absence of a wiping motion between the tire and the road, the power dissipation of the radial-ply tire could be as low as 60% of that of the bias-ply tire under similar conditions, and the life of the radial-ply tire could be as long as twice that of the equivalent bias-ply tire [1.3]. For a radial-ply tire, there is a relatively uniform ground pressure over the entire contact area. In contrast, the ground pressure for a bias-ply tire varies greatly from point to point as tread elements passing through the contact area undergo complex localized wiping motion.

There are also tires built with belts in the tread on bias-ply construction. This type of tire is usually called the bias-belted tire. The cords in the belt are of materials with a higher modulus of elasticity than those in the bias plies. The belt provides high rigidity to the tread against distortion, and reduces tread wear and rolling resistance in comparison with the conventional bias-ply tire. Generally, the bias-belted tire has characteristics midway between those of the bias-ply and the radial-ply tire.

In the United States, the Department of Transportation requires tire manufacturers to provide information on tire dimensions and ratings on the sidewall of every tire. For instance, for a tire P185/70 R14 87S, "P" indicates a passenger car tire; "185" is the nominal width of the cross section in millimeters; "70" is the aspect ratio, which is the ratio of the height of the sidewall to the cross-sectional width; "R" stands for radial-ply tire; "14" is the rim diameter in inches; "87" is a code indicating the maximum load the tire can carry at its maximum rated speed; "S" is a speed rating which indicates the maximum speed that the tire can sustain without failure: S, 112 mph (180 km/h); T, 118 mph (190 km/h); H, 130 mph (210 km/h); V,

149 mph (240 km/h); Z, 149 mph (240 km/h) or more. Traction and temperature capabilities are indicated on a scale from A to C, A being the best and C the worst. The traction rating is based on straight-line stopping ability on a wet surface. The temperature rating is an index of the tire's ability to withstand the heat that high speeds, heavy loads, and hard driving generate. Tread-wear index is an indication of expected tire life. It is rated against a reference tire with an index of 100. For instance, a tread-wear rating of 420 means that the tire should last 4.2 times as long as the reference tire. A tread-wear index of 180 is considered to be quite low and an index of 500, quite high.

Although the construction of pneumatic tires differs from one type to another, the basic issues involved are not dissimilar. In the following sections, the mechanics fundamental to all types of tire are discussed. The characteristics peculiar to a particular kind of tire are also described.

1.1 TIRE FORCES AND MOMENTS

To describe the characteristics of a tire and the forces and moments acting on it, it is necessary to define an axis system that serves as a reference for the definition of various parameters. One of the commonly used axis systems recommended by the Society of Automotive Engineers is shown in Fig. 1.2 [1.4].

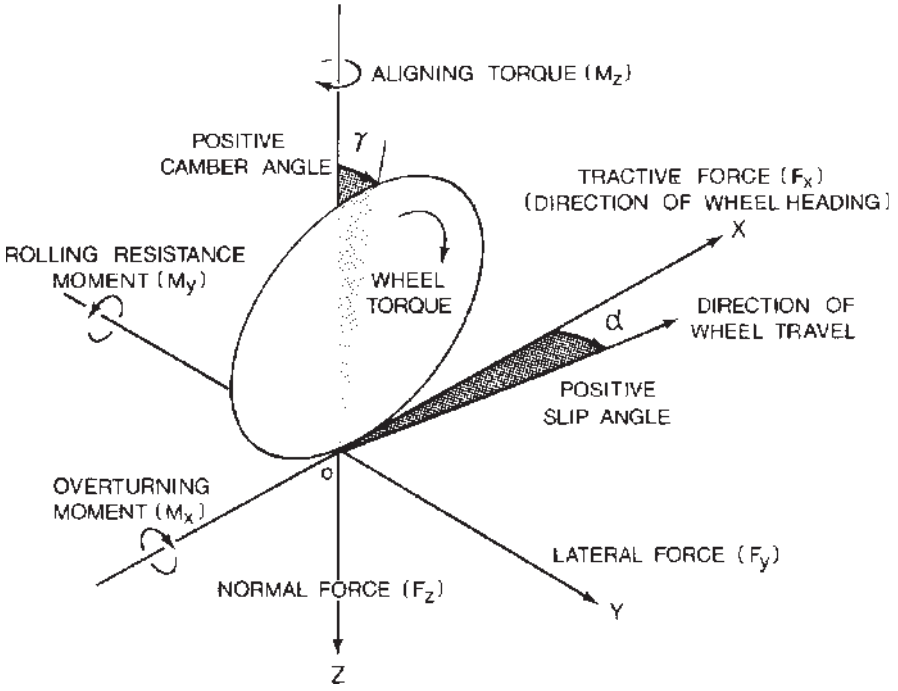

Fig. 1.2 Tire axis system.

The origin of the axis system is the center of tire contact. The X axis is the intersection of the wheel plane and the ground plane with a positive direction forward. The Z axis is perpendicular to the ground plane with a positive direction downward. The Y axis is in the ground plane, and its direction is chosen to make the axis system orthogonal and right hand.

Three forces and three moments act on the tire from the ground. Tractive force (or longitudinal force) F_x is the component in the X direction of the resultant force exerted on the tire by the road. Lateral force F_y is the component in the Y direction, and normal force F_z is the component in the Z direction. Overturning moment M_x is the moment about the X axis exerted on the tire by the road. Rolling resistance moment M_y is the moment about the Y axis, and aligning torque M_z is the moment about the Z axis.

With this axis system, many performance parameters of the tire can be conveniently defined. For instance, the longitudinal shift of the center of normal pressure is determined by the ratio of the rolling resistance moment to the normal load. The lateral shift of the center of normal pressure is defined by the ratio of the overturning moment to the normal load. The integration of longitudinal shear stresses over the entire contact patch represents the tractive or braking force. A driving torque about the axis of rotation of the tire produces a force for accelerating the vehicle, and a braking torque produces a force for decelerating the vehicle.

There are two important angles associated with a rolling tire: the slip angle and the camber angle. Slip angle α is the angle formed between the direction of wheel travel and the line of intersection of the wheel plane with the road surface. Camber angle γ is the angle formed between the XZ plane and the wheel plane. The lateral force at the tire–ground contact patch is a function of both the slip angle and the camber angle.

1.2 ROLLING RESISTANCE OF TIRES

The rolling resistance of tires on hard surfaces is primarily caused by the hysteresis in tire materials due to the deflection of the carcass while rolling. Friction between the tire and the road caused by sliding, the resistance due to air circulating inside the tire, and the fan effect of the rotating tire on the surrounding air also contribute to the rolling resistance of the tire, but they are of secondary importance. Available experimental results give a breakdown of tire losses in the speed range 128–152 km/h (80–95 mph) as 90–95% due to internal hysteresis losses in the tire, 2–10% due to friction between the tire and the ground, and 1.5–3.5% due to air resistance [1.5, 1.6]. Of the total energy losses within the tire structure, it is found that for a radial truck tire, hysteresis in the tread region, including the belt, contributes 73%, the sidewall 13%, the region between the tread and the sidewall, commonly known as the shoulder region, 12%, and the beads 2%.

When a tire is rolling, the carcass is deflected in the area of ground contact. As a result of tire distortion, the normal pressure in the leading half of the

contact patch is higher than that in the trailing half. The center of normal pressure is shifted in the direction of rolling. This shift produces a moment about the axis of rotation of the tire, which is the rolling resistance moment. In a free-rolling tire, the applied wheel torque is zero; therefore, a horizontal force at the tire–ground contact patch must exist to maintain equilibrium. This resultant horizontal force is generally known as the rolling resistance. The ratio of the rolling resistance to the normal load on the tire is defined as the coefficient of rolling resistance.

A number of factors affect the rolling resistance of a pneumatic tire. They include the structure of the tire (construction and materials) and its operating conditions (surface conditions, inflation pressure, speed, temperature, etc.). Tire construction has a significant influence on its rolling resistance. Figure 1.3 shows the rolling resistance coefficient at various speeds of a range of bias-ply and radial-ply passenger car tires at rated loads and inflation pressures on a smooth road [1.7]. The difference in rolling resistance coefficient between a bias-ply and a radial-ply truck tire of the same size under rated conditions is shown in Fig. 1.4 [1.8]. Thicker treads and sidewalls and an increased number of carcass plies tend to increase the rolling resistance because of greater hysteresis losses. Tires made of synthetic rubber compounds generally have higher rolling resistance than those made of natural rubber. Tires made of butyl rubber compounds, which are shown to have better traction and roadholding properties, have an even higher rolling resistance than those made of conventional synthetic rubber. It is found that the rolling resistance of tires

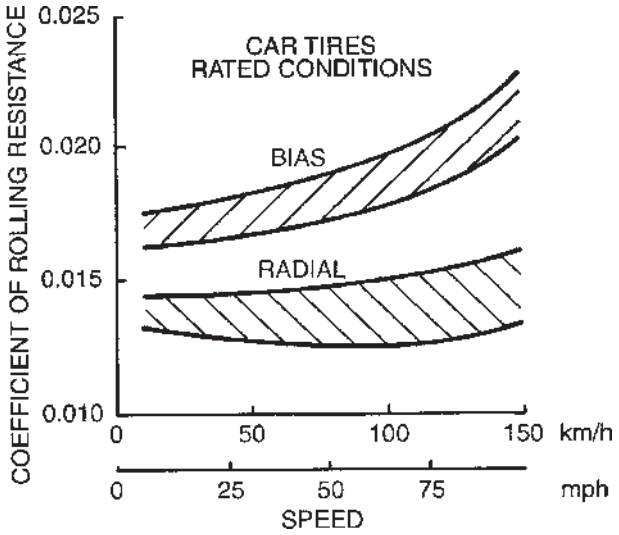

Fig. 1.3 Variation of rolling resistance coefficient of radial-ply and bias-ply car tires with speed on a smooth, flat road surface under rated load and inflation pressure. (Reproduced with permission from *Automotive Handbook,* 2nd ed., Robert Bosch, Germany.)

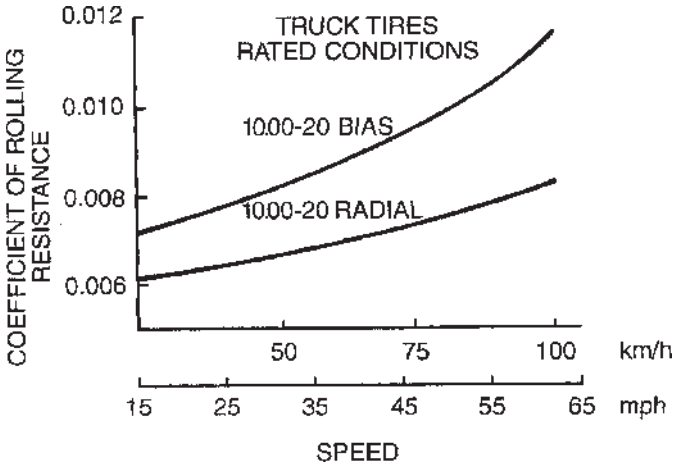

Fig. 1.4 Variation of rolling resistance coefficient of radial-ply and bias-ply truck tires with speed under rated load and inflation pressure. (Reproduced with permission from reference 1.8.)

with tread made of synthetic rubber compounds and that made of butyl rubber compounds are approximately 1.06 and 1.35 times that made of natural rubber compounds, respectively [1.9].

Surface conditions also affect the rolling resistance. On hard, smooth surfaces, the rolling resistance is considerably lower than that on a rough road. On wet surfaces, a higher rolling resistance than on dry surfaces is usually observed. Figure 1.5 shows a comparison of the rolling resistance of passenger

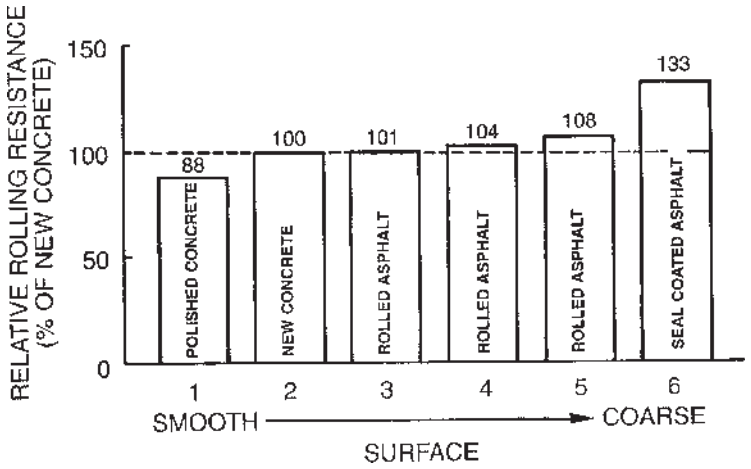

Fig. 1.5 Variation of tire rolling resistance with pavement surface texture. (Reproduced with permission of the Society of Automotive Engineers from reference 1.10.)

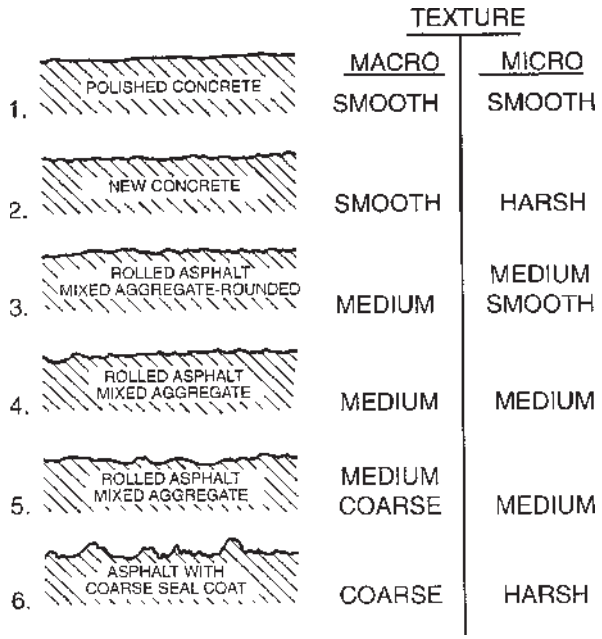

Fig. 1.6 Texture of various types of pavement surface. (Reproduced with permission of the Society of Automotive Engineers from reference 1.10.)

car tires over six road surfaces with different textures, ranging from polished concrete to coarse asphalt [1.10]. The profiles of these six surfaces are shown in Fig. 1.6. It can be seen that on the asphalt surface with coarse sealcoat (surface no. 6) the rolling resistance is 33% higher than that on a new concrete surface (surface no. 2), while on the polished concrete (surface no. 1), it shows a 12% reduction in comparison with that on the new concrete surface.

Inflation pressure affects the flexibility of the tire. Depending on the deformability of the ground, the inflation pressure affects the rolling resistance of the tire in different manners. On hard surfaces, the rolling resistance generally decreases with the increase in inflation pressure. This is because, with higher inflation pressure, the deflection of the tire decreases, with consequently lower hysteresis losses. Figure 1.7 shows the effects of inflation pressure on the rolling resistance of a radial-ply tire (GR78-15), a bias-ply tire, and a bias-belted tire (both G78-15) under various normal loads, expressed in terms of the percentage of the rated load at an inflation pressure of 165 kPa (24 psi) [1.11]. The results were obtained with the inflation pressure being regulated, that is, the pressure was maintained at a specific level throughout the tests. It can be seen that inflation pressure has a much more significant effect on the rolling resistance of the bias and bias-belted tires than the radial-ply tire. On deformable surfaces, such as sand, high inflation pressure results in increased ground penetration work, and therefore higher rolling resistance, as shown in Fig. 1.8 [1.12]. Conversely, lower inflation pressure, while decreasing ground

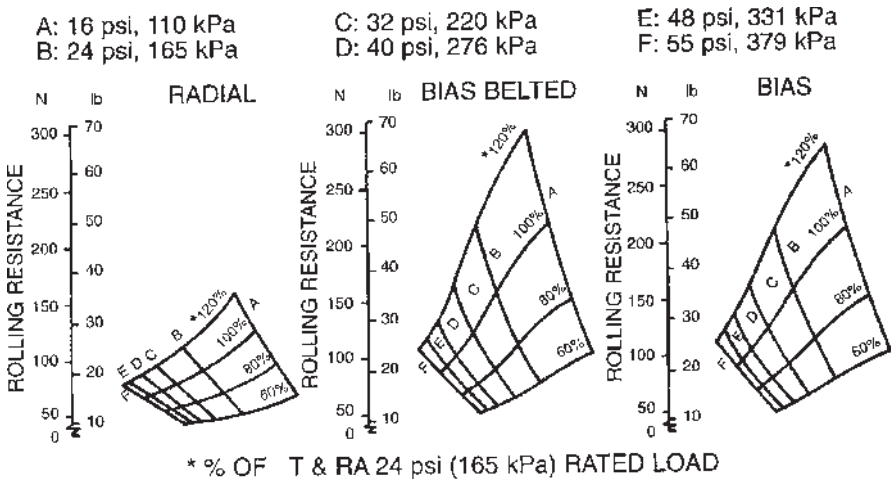

Fig. 1.7 Variation of rolling resistance of radial-ply, bias-belted, and bias-ply car tires with load and inflation pressure. (Reproduced with permission of the Society of Automotive Engineers from reference 1.11.)

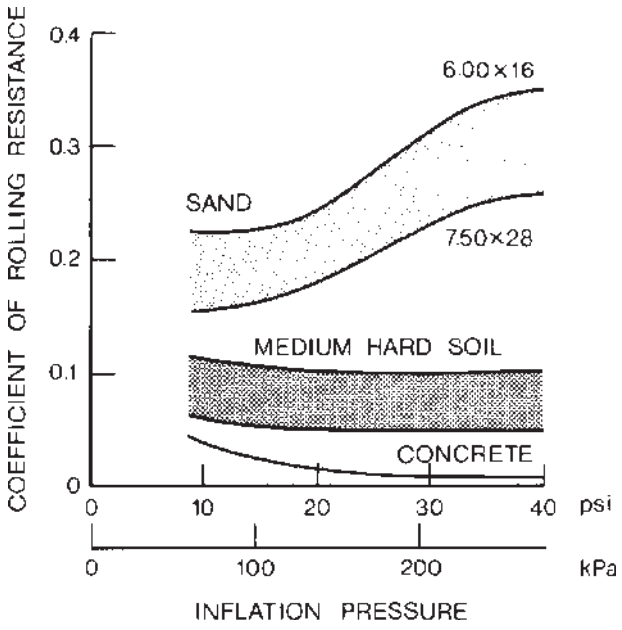

Fig. 1.8 Variation of rolling resistance coefficient with inflation pressure of tires on various surfaces. (Reproduced with permission from reference 1.12.)

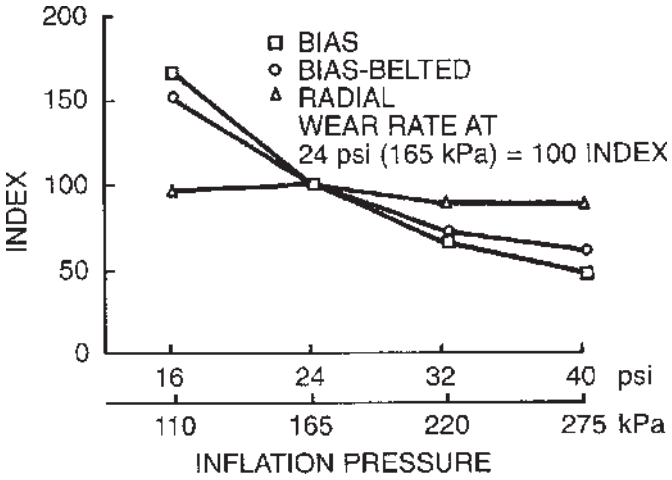

Fig. 1.9 Variation of shoulder-crown wear with inflation pressure for radial-ply, bias-ply, and bias-belted car tires. (Reproduced with permission of the Society of Automotive Engineers from reference 1.11.)

penetration, increases the deflection of the tire and hence internal hysteresis losses. Therefore, an optimum inflation pressure exists for a particular tire on a given deformable surface, which minimizes the sum of ground penetration work and internal losses of the tire.

Inflation pressure affects not only the rolling resistance, but also the tread wear of a tire. Figure 1.9 shows the effects of inflation pressure on tread wear of a radial-ply, a bias-ply, and a bias-belted tire [1.11]. The wear rate at 165 kPa (24 psi) is used as a reference for comparison. It can be seen that the effects of inflation pressure on tread wear are more significant for the bias-ply and bias-belted tire than the radial-ply tire.

Rolling resistance is also affected by driving speed because of the increase of work in deforming the tire and of vibrations in the tire structure with the increase in speed. The effects of speed on the rolling resistance of bias-ply and radial-ply passenger car and truck tires are illustrated in Figs. 1.3 and 1.4, respectively. For a given tire under a particular operating condition, there exists a threshold speed above which the phenomenon popularly known as standing waves will be observed, as shown in Fig. 1.10. The approximate value of the threshold speed V_{th} may be determined by the expression $V_{th} = \sqrt{F_t/\rho_t}$, where F_t is the circumferential tension in the tire and ρ_t is the density of tread material per unit area [1.13]. Standing waves are formed because, owing to high speed, the tire tread does not recover immediately from distortion originating from tire deflection after it leaves the contact surface, and the residual deformation initiates a wave. The amplitude of the wave is greatest immediately on leaving the ground, and is damped out in an exponential manner around the circumference of the tire. The formation of the standing wave greatly increases energy losses, which in turn cause considerable heat

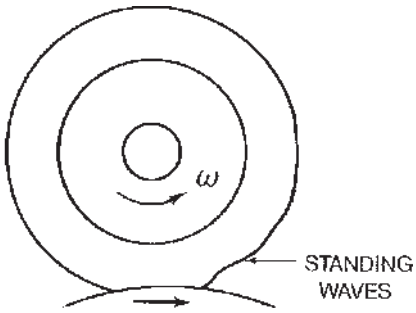

Fig. 1.10 Formation of standing waves of a tire at high speeds.

generation that could lead to tire failure. This places an upper limit on the safe operating speed of tires.

Operating temperature, tire diameter, and tractive force also have effects on the rolling resistance of a tire. Tire temperature affects the rolling resistance in two ways: one is by changing the temperature of the air in the tire cavity, and thereby changing the operating inflation pressure; and the other is by changing the stiffness and hysteresis of the rubber compounds. Figure 1.11 shows the dependence of the rolling resistance on the internal tire temperature for an automobile tire [1.5]. The variation of rolling resistance coefficient with shoulder temperature of a radial-ply passenger car tire is shown in Fig. 1.12 [1.14]. It can be seen that the rolling resistance at a shoulder temperature of -10°C is approximately 2.3 times that at 60°C for the tire examined. It is also found that the shoulder temperature of the tire, and not the ambient temperature, is a basic determining factor of the tire rolling resistance coefficient. The effect of tire diameter on the coefficient of rolling resistance is shown in Fig. 1.13 [1.12]. It can be seen that the effect of tire diameter is negligible on

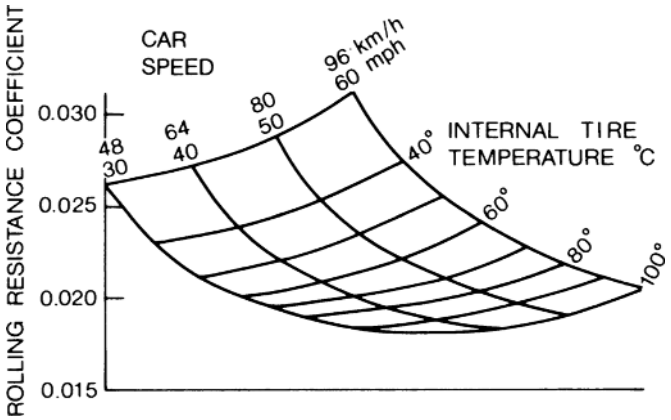

Fig. 1.11 Effect of internal temperature on rolling resistance coefficient of a car tire. (Reproduced with permission of the Council of the Institution of Mechanical Engineers from reference 1.5.)

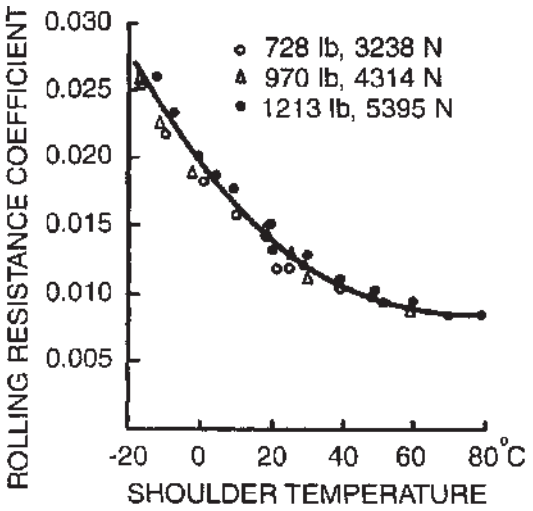

Fig. 1.12 Variation of rolling resistance coefficient with shoulder temperature for a car tire P195/75R14. (Reproduced with permission of the Society of Automotive Engineers from reference 1.14.)

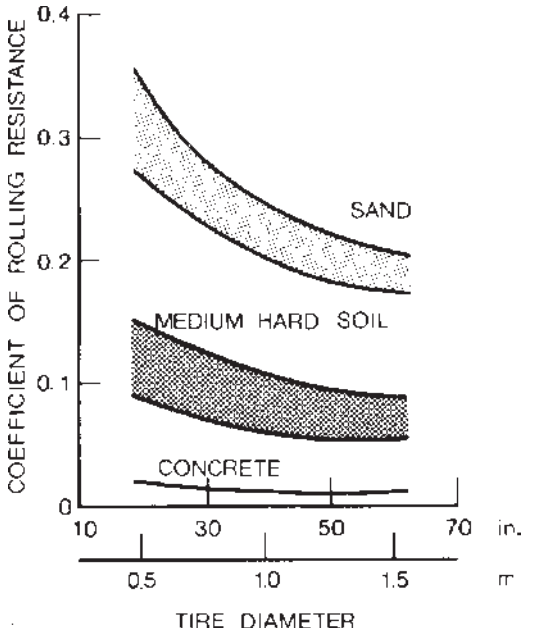

Fig. 1.13 Effect of tire diameter on rolling resistance coefficient on various surfaces. (Reproduced with permission from reference 1.12.)

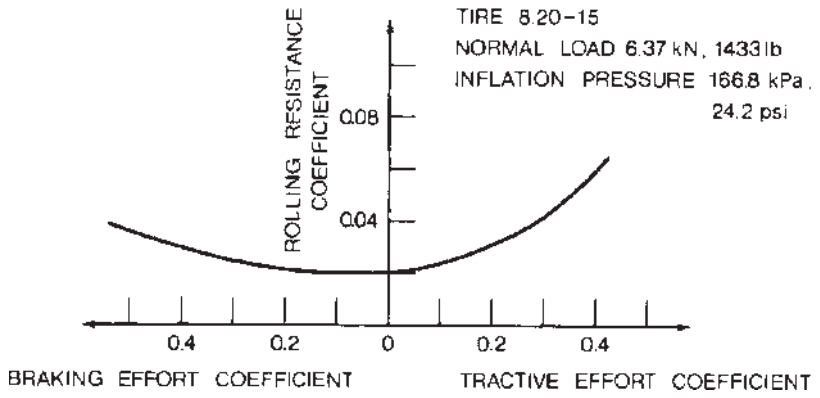

Fig. 1.14 Effect of tractive and braking effort on rolling resistance coefficient of a car tire. (Reproduced with permission from *Mechanics of Pneumatic Tires,* edited by S.K. Clark, Monograph 122, National Bureau of Standards, 1971.)

hard surfaces (concrete), but is considerable on deformable or soft ground. Figure 1.14 shows the effect of the braking and tractive effort coefficient on the rolling resistance coefficient [1.6].

When considering the effects of material, construction, and design parameters of tires on rolling resistance, it is necessary to have a proper perspective of the energy losses in the tire and the characteristics of the tire–vehicle system as a whole. Although it is desirable to keep the rolling resistance as low as possible, it should be judged against other performance parameters, such as tire endurance and life, traction, cornering properties, cushioning effect, and cost. For instance, from the standpoint of rolling resistance, synthetic rubber compounds are less favorable than natural rubber compounds, yet because of significant advantages in cost, tread life, wet-road grip, and tire squeal, they have virtually displaced natural rubber compounds from passenger car tires, particularly for treads. For high-performance vehicles, there may be some advantage for using butyl rubber tires because of the marked gains in traction, roadholding, silence, and comfort, in spite of their poor hysteresis characteristics [1.5].

The complex relationships between the design and operational parameters of the tire and its rolling resistance make it extremely difficult, if not impossible, to develop an analytic method for predicting the rolling resistance. The determination of the rolling resistance, therefore, relies almost entirely on experiments. To provide a uniform basis for collecting experimental data, the Society of Automotive Engineers recommends rolling resistance measurement procedures for various types of tire on different surfaces, which may be found in the *SAE Handbook*.

Based on experimental results, many empirical formulas have been proposed for calculating the rolling resistance of tires on hard surfaces. For instance, based on the experimental data shown in Fig. 1.3, for radial-ply

passenger car tires under rated loads and inflation pressures on a smooth road, the relationship between rolling resistance coefficient f_r and speed V (up to 150 km/h or 93 mph) may be expressed by

$$f_r = 0.0136 + 0.40 \times 10^{-7} V^2 \tag{1.1}$$

and for bias-ply passenger car tires,

$$f_r = 0.0169 + 0.19 \times 10^{-6} V^2 \tag{1.2}$$

where V is in km/h.

Based on the experimental data shown in Fig. 1.4, for the radial-ply truck tire under rated load and inflation pressure, the relationship between the rolling resistance coefficient f_r and speed V (up to 100 km/h or 62 mph) may be described by

$$f_r = 0.006 + 0.23 \times 10^{-6} V^2 \tag{1.3}$$

and for the bias-ply truck tire,

$$f_r = 0.007 + 0.45 \times 10^{-6} V^2 \tag{1.4}$$

where V is in km/h.

The rolling resistance coefficient of truck tires is usually lower than that of passenger car tires on road surfaces. This is primarily due to the higher inflation pressure used in truck tires (typically 620–827 kPa or 90–120 psi as opposed to 193–248 kPa or 28–36 psi for passenger car tires).

In preliminary performance calculations, the effect of speed may be ignored, and the average value of f_r for a particular operating condition may be used. The average values of f_r for various types of tire over different surfaces are summarized in Table 1.1.

TABLE 1.1 Coefficient of Rolling Resistance

Road surface	Coefficient of rolling resistance
Car tires	
Concrete, asphalt	0.013
Rolled gravel	0.02
Tarmacadam	0.025
Unpaved road	0.05
Field	0.1–0.35
Truck tires	
Concrete, asphalt	0.006–0.01

Source: Automotive Handbook, 4th edition, Bosch, 1996. (Reproduced with permission of Robert Bosch, Germany.)

1.3 TRACTIVE (BRAKING) EFFORT AND LONGITUDINAL SLIP (SKID)

When a driving torque is applied to a pneumatic tire, a tractive force is developed at the tire–ground contact patch, as shown in Fig. 1.15 [1.6]. At the same time, the tire tread in front of and within the contact patch is subjected to compression. A corresponding shear deformation of the sidewall of the tire is also developed.

As tread elements are compressed before entering the contact region, the distance that the tire travels when subject to a driving torque will be less than that in free rolling. This phenomenon is usually referred to as longitudinal slip. The longitudinal slip of the vehicle running gear, when a driving torque is applied, is usually defined by

$$i = \left(1 - \frac{V}{r\omega}\right) \times 100\% = \left(1 - \frac{r_e}{r}\right) \times 100\% \tag{1.5}$$

where V is the linear speed of the tire center, ω is the angular speed of the tire, r is the rolling radius of the free-rolling tire, and r_e is the effective rolling

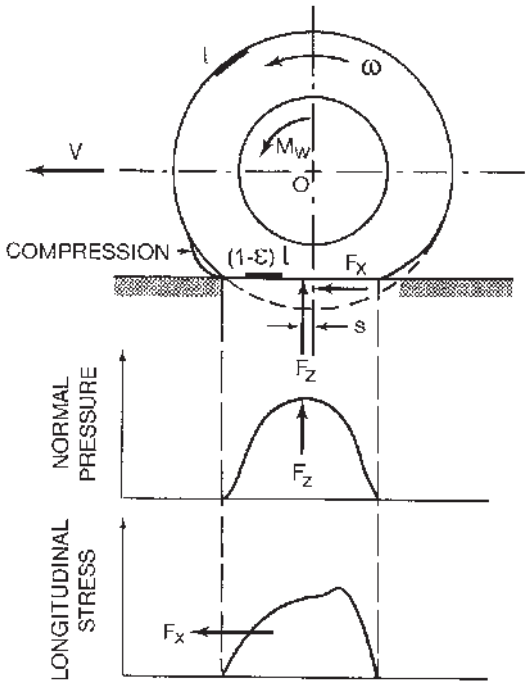

Fig. 1.15 Behavior of a tire under the action of a driving torque. (Reproduced with permission from *Mechanics of Pneumatic Tires,* edited by S.K. Clark, Monograph 122, National Bureau of Standards, 1971.)

radius of the tire, which is the ratio of the linear speed of the tire center to the angular speed of the tire.

When a driving torque is applied, the tire rotates without the equivalent translatory progression; therefore, $r\omega > V$ and a positive value for slip results. If a tire is rotating at a certain angular speed but the linear speed of the tire center is zero, then, in accordance with Eq. 1.5, the longitudinal slip of the tire will be 100%. This is often observed on an icy surface, where the driven tires are spinning at high angular speeds, while the vehicle does not move forward. The definition of longitudinal slip given by Eq. 1.5 is adopted in the analysis of the mechanics of tires in this book.

A definition of longitudinal slip different from that given by Eq. 1.5 appears in some publications. For instance, in the *SAE Handbook Supplement, Vehicle Dynamics Terminology J670e* [1.4], longitudinal slip is defined as "the ratio of the longitudinal slip velocity to the spin velocity of the straight free-rolling tire expressed as a percentage." The longitudinal slip velocity is taken as "the difference between the spin velocity of the driven or braked tire and the spin velocity of the straight free-rolling tire." Both spin velocities are measured at the same linear velocity at the wheel center in the X direction (Fig. 1.2). A positive value of slip results from a driving torque. In essence, the definition of longitudinal slip i' suggested by the SAE can be expressed by

$$i' = \left(\frac{r\omega}{V} - 1\right) \times 100\% = \left(\frac{r}{r_e} - 1\right) \times 100\% \tag{1.6}$$

where V, ω, r, and r_e are defined in the same way as that for Eq. 1.5. It should be noted that in accordance with the definition suggested by the SAE, when a tire is rotating at a certain angular speed but the linear speed of the tire center is zero, the longitudinal slip i' of the tire will be denoted as infinite.

As the tractive force developed by a tire is proportional to the applied wheel torque under steady-state conditions, slip is a function of tractive effort. Generally speaking, at first the wheel torque and tractive force increase linearly with slip because, initially, slip is mainly due to elastic deformation of the tire tread. This corresponds to section OA of the curve shown in Fig. 1.16. A further increase of wheel torque and tractive force results in part of the tire tread sliding on the ground. Under these circumstances, the relationship between the tractive force and the slip is nonlinear. This corresponds to section AB of the curve shown in Fig. 1.16. Based on available experimental data, the maximum tractive force of a pneumatic tire on hard surfaces is usually reached somewhere between 15 and 20% slip. Any further increase of slip beyond that results in an unstable condition, with the tractive effort falling rapidly from the peak value $\mu_p W$ to the pure sliding value $\mu_s W$, as shown in Fig. 1.16, where W is the normal load on the tire and μ_p and μ_s are the peak and sliding values of the coefficient of road adhesion, respectively.

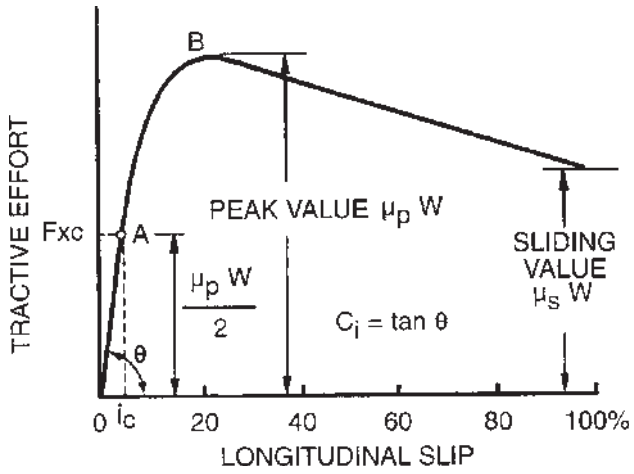

Fig. 1.16 Variation of tractive effort with longitudinal slip of a tire.

A general theory that can accurately predict the relationship between the tractive effort and the longitudinal slip of pneumatic tires on hard surfaces has yet to be evolved. However, several theories have been proposed that could provide a basic understanding of the physical nature of the processes involved. One of the earliest theoretical treatises on the relationship between the tractive effort and the longitudinal slip of pneumatic tires was presented by Julien [1.15].

In Julien's theory, it is assumed that the tire tread can be regarded as an elastic band, and that the contact patch is rectangular and the normal pressure is uniformly distributed [1.15]. It is further assumed that the contact patch can be divided into an adhesion region and a sliding region. In the adhesion region, the interacting forces depend on the elastic properties of the tire, whereas in the sliding region, the interacting forces depend upon the adhesive properties of the tire–ground interface. When a driving torque is applied to a tire, in the region in front of the contact patch, the driving torque produces a longitudinal strain ϵ (in compression) in the tread. It remains constant in the adhesion region of the contact patch, where no sliding between the tire tread and the ground takes place. Let e_0 be the longitudinal deformation of the tire tread in front of the contact patch, and let e be the longitudinal deformation of the tread at a point at a distance x behind the front contact point

$$e = e_0 + x\epsilon \tag{1.7}$$

Assume that e_0 is proportional to ϵ, and $e_0 = \lambda\epsilon$. Then

$$e = (\lambda + x)\epsilon \tag{1.8}$$

It is further assumed that, within the adhesion region, where no sliding between the tire tread and the ground takes place, the tractive force per unit contact length is proportional to the deformation of the tread. Thus,

$$\frac{dF_x}{dx} = k_t e = k_t(\lambda + x)\epsilon \tag{1.9}$$

where k_t is the tangential stiffness of the tire tread and F_x is the tractive force. Based on experimental data of a sample of heavy truck tires under rated loads and inflation pressures, it is found that the value of k_t varies in a narrow range from approximately 3930 kN/m^2 (570 lb/in.^{2}) for a radial-ply tire to 4206 kN/m^2 (610 lb/in.^{2}) for a bias-ply tire.

$$F_x = \int_0^x k_t(\lambda + x)\epsilon \, dx = k_t \lambda x \epsilon \left(1 + \frac{x}{2\lambda}\right) \tag{1.10}$$

Let p be the normal pressure, b the width of the contact patch, and μ_p the peak value of the coefficient of road adhesion. Then no sliding will take place between the tread and the ground if the following condition is satisfied:

$$\frac{dF_x}{dx} = k_t(\lambda + x)\epsilon \leq \mu_p p b \tag{1.11}$$

This implies that if a point at a distance of x behind the front contact point is in the adhesion region, then x must be less than a characteristic length l_c, which defines the length of the region where no sliding between the tire tread and the ground takes place; that is,

$$x \leq l_c = \frac{\mu_p p b}{k_t \epsilon} - \lambda = \frac{\mu_p W}{l_t k_t \epsilon} - \lambda \tag{1.12}$$

where W is the normal load on the tire and l_t is the contact length of the tire.

If $l_t \leq l_c$, then the entire contact area is an adhesion region. Letting $x = l_t$ in Eq. 1.10, the tractive force becomes

$$F_x = k_t \lambda l_t \epsilon \left(1 + \frac{l_t}{2\lambda}\right) = K_t \epsilon \tag{1.13}$$

where $K_t = k_t \lambda \, l_t[1 + l_t/2\lambda]$.

Since the longitudinal strain ϵ is a measure of the longitudinal slip i of the tire, it is concluded that if the entire contact patch is an adhesion region, the relationship between the tractive force F_x and the slip i is linear. This corresponds to the region between points O and A on the tractive effort–slip curve shown in Fig. 1.16.

The condition for sliding at the rear edge of the contact area is given by

$$l_t = l_c = \frac{\mu_p W}{l_t k_t i} - \lambda \tag{1.14}$$

This means that, if the slip or tractive force reaches the respective critical value i_c or F_{xc} given below, sliding in the trailing part of the contact patch begins:

$$i_c = \frac{\mu_p W}{l_t k_t (l_t + \lambda)} \tag{1.15}$$

$$F_{xc} = \frac{\mu_p W[1 + (l_t/2\lambda)]}{1 + (l_t/\lambda)} \tag{1.16}$$

A further increase of slip or tractive force beyond the respective critical value results in the spread of the sliding region from the trailing edge toward the leading part of the contact patch. The tractive force F_{xs} developed in the sliding region is given by

$$F_{xs} = \mu_p W(1 - l_c/l_t) \tag{1.17}$$

and the tractive force F_{xa} developed in the adhesion region is given by

$$F_{xa} = k_t \lambda i l_c \left(1 + \frac{l_c}{2\lambda}\right) \tag{1.18}$$

where l_c is determined by Eq. 1.12.

Hence, the relationship between the total tractive force and the slip when part of the tire tread sliding on the ground is expressed by

$$F_x = F_{xs} + F_{xa} = \mu_p W - \frac{\lambda(\mu_p W - K' i)^2}{2 l_t K' i} \tag{1.19}$$

where $K' = l_t k_t \lambda$.

This equation clearly indicates the nonlinear behavior of the tractive effort–longitudinal slip relationship when sliding occurs in part of the contact area. This corresponds to the region beyond point A of the curve shown in Fig. 1.16.

When sliding extends over the entire contact patch, the tractive force F_x is equal to $\mu_p W$. Under this condition, the slip i is obtained by setting l_c to zero in Eq. 1.14. The value of the slip i_m where the maximum tractive effort occurs is equal to $\mu_p W/l_t k_t \lambda$ and corresponds to point B shown in Fig. 1.16. A further increase of tire slip results in an unstable situation, with the coefficient of road adhesion falling rapidly from the peak value μ_p to the pure sliding value μ_s.

In practice, the normal pressure distribution over the tire–ground contact patch is not uniform. There is a gradual drop of pressure near the edges. It is expected, therefore, that a small sliding region will be developed in the trailing part of the contact area, even at low slips.

Using Julien's theory to define the relationship between tractive effort and longitudinal slip, in addition to the parameters μ_p, W, and l_t, the value of λ, which determines the longitudinal deformation of the tire tread prior to entering the contact patch, must be known. To determine the value of λ for a given tire would require considerable effort and elaborate experiments. In view of this, a simplified theory has been developed in which the effect of λ is neglected. From Eq. 1.9, by neglecting the term λ, the tractive force per unit contact length in the adhesion region at a distance of x from the front contact point is given by

$$\frac{dF_x}{dx} = k_t x\epsilon = k_t x i \tag{1.20}$$

If there is no sliding between the tire tread and the ground for the entire contact patch, the relationship between the tractive force and slip can be expressed by

$$F_x = \int_0^{l_t} k_t i x \, dx = (k_t l_t^2/2) i \tag{1.21}$$

The term $k_t l_t^2/2$ may be taken as the slope C_i of the tractive effort–slip curve at the origin as shown in Fig. 1.16; that is,

$$\frac{k_t l_t^2}{2} = C_i = \tan\,\theta = \left.\frac{\partial F_x}{\partial i}\right|_{i=0} \tag{1.22}$$

where C_i is usually referred to as the longitudinal stiffness of the tire.

If no sliding takes place on the contact patch, the relationship between the tractive force and the slip will, therefore, be linear:

$$F_x = C_i i \tag{1.23}$$

Equation 1.23 applies to section OA of the curve shown in Fig. 1.16.

With the increase of slip beyond point A shown in Fig. 1.16, the tractive force per unit contact length at the trailing edge of the contact patch reaches the adhesion limit, and sliding between the tread and the ground takes place.

$$\frac{dF_x}{dx} = k_t l_t i = \mu_p p b = \frac{\mu_p W}{l_t} \tag{1.24}$$

This indicates that when the slip or tractive force reaches the respective critical value i_c or F_{xc} given below, sliding in the trailing part of the contact patch begins:

$$i_c = \frac{\mu_p W}{k_t l_t^2} = \frac{\mu_p W}{2C_i} \tag{1.25}$$

$$F_{xc} = C_i i_c = \frac{\mu_p W}{2} \tag{1.26}$$

In other words, if slip $i \leq i_c$ or the tractive force $F_x \leq F_{xc}$, the relationship between the tractive force and slip is linear, as shown in Fig. 1.16. Equation 1.26 indicates that the upper limit for the linear range of the tractive force–slip relationship is identified by the tractive force being equal to one-half of its maximum value ($\mu_p W/2$).

A further increase of slip or tractive force beyond the respective critical value (i.e., $i > i_c$ or $F_x > F_{xc}$) results in the spread of the sliding region from the trailing edge towards the leading part of the contact patch. The tractive force F_{xs} developed in the sliding region is given by

$$F_{xs} = \mu_p W \left(1 - \frac{l_c}{l_t}\right) = \mu_p W \left(1 - \frac{\mu_p W}{2C_i i}\right) \tag{1.27}$$

and the tractive force F_{xa} developed in the adhesion region is expressed by

$$F_{xa} = \frac{1}{2}\frac{\mu_p W l_c}{l_t} = \frac{\mu_p^2 W^2}{4C_i i} \tag{1.28}$$

Hence, the relationship between the total tractive force and the slip when part of the tread is sliding on the ground (i.e., $i > i_c$ or $F_x > F_{xc}$) is given by

$$F_x = F_{xs} + F_{xa} = \mu_p W \left(1 - \frac{\mu_p W}{4C_i i}\right) \tag{1.29}$$

The equation above indicates the nonlinear nature of the tractive effort–longitudinal slip relationship when sliding occurs in part of the contact patch. It is applicable to predicting the tractive effort–slip relation when the tractive effort is lower than its maximum value $\mu_p W$.

In comparison with Julien's theory, the simplified theory described above requires only three parameters, μ_p, W, and C_i, to define the tractive effort–longitudinal slip relationship. As pointed out previously, the value of C_i can easily be identified from the initial slope of the measured tractive effort–slip curve.

When a braking torque is applied to the tire, a stretching of the tread elements occurs prior to entering the contact area, as shown in Fig. 1.17, in contrast with the compression effect for a driven tire. The distance that the

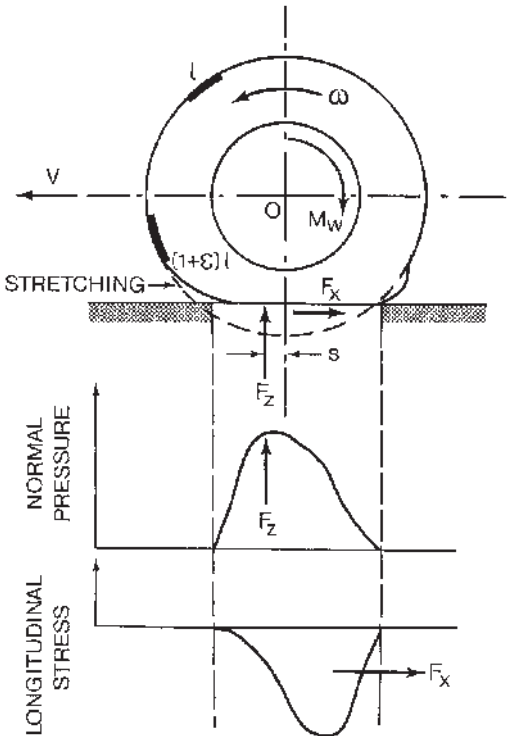

Fig. 1.17 Behavior of a tire under the action of a braking torque. (Reproduced with permission from *Mechanics of Pneumatic Tires,* edited by S.K. Clark, Monograph 122, National Bureau of Standards, 1971.)

tire travels when a braking torque is applied, therefore, will be greater than that in free rolling. The severity of braking is often measured by the skid of the tire i_s, which is defined as

$$\begin{aligned} i_s &= \left(1 - \frac{r\omega}{V}\right) \times 100\% \\ &= \left(1 - \frac{r}{r_e}\right) \times 100\% \end{aligned} \tag{1.30}$$

For a locked wheel, the angular speed ω of the tire is zero, whereas the linear speed of the tire center is not zero. Under this condition, the skid is denoted 100%. It should be noted that using the definition of slip suggested by the SAE and given by Eq. 1.6, for a locked tire, the slip will be -100%.

A simplified theory for the relationship between the braking effort and the skid can also be developed, following an approach similar to that for the relationship between the tractive force and the slip described previously.

According to the definitions of slip i and skid i_s given by Eqs. 1.5 and 1.30, respectively, the expressions for slip i and skid i_s are related by

$$|i| = |i_s/(1 - i_s)| \tag{1.31}$$

If no sliding takes place on the contact patch, the relationship between the braking effort and the skid can be established by replacing C_i and i in Eq. 1.23 with C_s and $i_s/(1 - i_s)$, respectively.

$$F_x = C_s i_s/(1 - i_s) \tag{1.32}$$

where F_x is the braking effort acting in the opposite direction of motion of the tire center, and C_s is the slope of the braking effort–skid curve at the origin, and is given by [1.8]

$$C_s = \left.\frac{\partial F_x}{\partial i_s}\right|_{i_s=0} \tag{1.33}$$

C_s is referred to as the longitudinal stiffness of the tire during braking. Similar to the parameter C_i, the value of C_s can easily be identified from the initial slope of the measured braking effort–skid curve.

It is interesting to note from Eq. 1.32 that, using the definition of skid given by Eq. 1.30, the relationship between braking effort and skid is nonlinear, even at low skids, where no sliding takes place between the tread and the ground.

The critical value of skid i_{sc}, at which sliding between the tread and the ground begins, can be established by replacing C_i and i in Eq. 1.25 with C_s and $i_s/(1 - i_s)$, respectively:

$$i_{sc} = \frac{\mu_p W}{2C_s + \mu_p W} \tag{1.34}$$

The corresponding critical value of braking effort F_{xc}, above which sliding between the tread and the ground begins, is given by

$$F_{xc} = \frac{C_s i_{sc}}{1 - i_{sc}} = \frac{\mu_p W}{2} \tag{1.35}$$

When sliding takes place in part of the contact patch (i.e., $i_s > i_{sc}$), the relationship between the braking effort and the skid can be established by replacing C_i and i in Eq. 1.29 with C_s and $i_s/(1 - i_s)$, respectively.

$$F_x = \mu_p W \left[1 - \frac{\mu_p W(1 - i_s)}{4C_s i_s}\right] \tag{1.36}$$

While the theory described above represents a simplified model for the highly complex phenomenon of tire–ground interaction, it has been proven to be

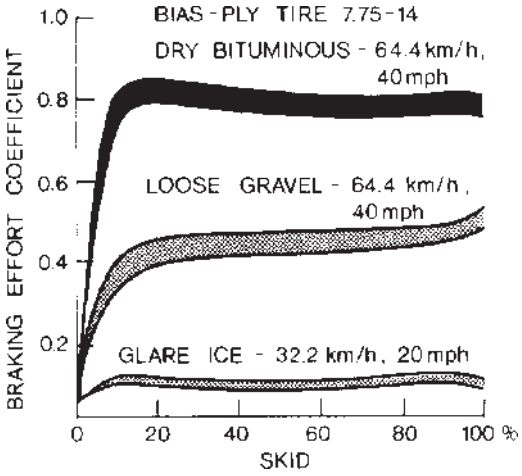

Fig. 1.18 Variation of braking effort coefficient with skid of a car tire on various surfaces. (Reproduced with permission of the Society of Automotive Engineers from reference 1.17.)

useful in representing tire behavior in the simulations of the dynamics of passenger cars [1.8, 1.16].

Figure 1.18 shows the variation of the braking effort coefficient, which is the ratio of the braking effort to the normal load, with skid for a bias-ply passenger car tire over various surfaces [1.17]. The peak and sliding values of the coefficient of road adhesion of a bias-ply, a bias-belted, and a radial-ply passenger car tire of the same size with various inflation pressures at a speed of 64 km/h (40 mph) on a dry, aggregate asphalt surface are shown in Fig. 1.19 [1.11]. It appears that on a dry surface, the coefficient of road adhesion does not vary significantly with tire construction and inflation pressure. Average peak and sliding values of the coefficient of road adhesion μ_p and μ_s on various surfaces are given in Table 1.2 [1.12].

TABLE 1.2 Average Values of Coefficient of Road Adhesion

Surface	Peak value μ_p	Sliding value μ_s
Asphalt and concrete (dry)	0.8–0.9	0.75
Asphalt (wet)	0.5–0.7	0.45–0.6
Concrete (wet)	0.8	0.7
Gravel	0.6	0.55
Earth road (dry)	0.68	0.65
Earth road (wet)	0.55	0.4–0.5
Snow (hard-packed)	0.2	0.15
Ice	0.1	0.07

Source: Reference 1.12.

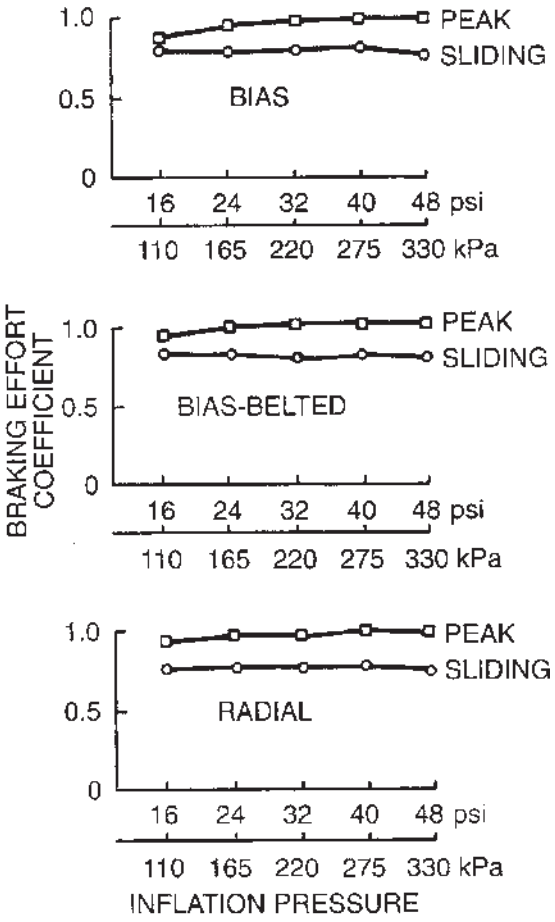

Fig. 1.19 Variation of peak and sliding values of braking effort coefficient with inflation pressure for bias-ply, bias-belted, and radial-ply car tires on dry pavement. (Reproduced with permission of the Society of Automotive Engineers from reference 1.11.)

Among the operational parameters, speed and normal load have noticeable effects on the tractive (braking) effort–slip (skid) characteristics. Figure 1.20 shows the influence of speed on the braking effort coefficient–skid characteristics of a bias-ply truck tire on a dry asphalt surface [1.18]. As shown in Fig. 1.20, speed appears to have a significant effect on the tractive (braking) performance of a tire. Therefore, it has been suggested that to improve the prediction of the relationship between the tractive (braking) effort and the slip (skid), the effect of the sliding speed between the tire tread and the ground should be incorporated into the theories described previously [1.8]. Figure 1.21 shows the effect of normal load on the braking performance of a

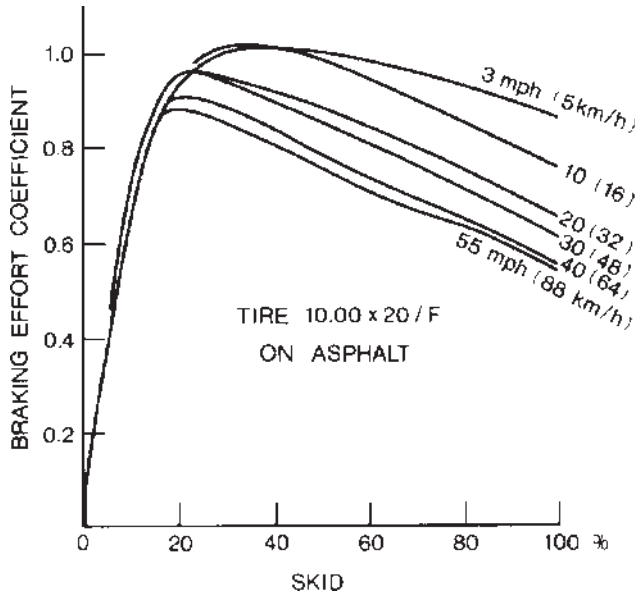

Fig. 1.20 Effect of speed on braking performance of a truck tire on asphalt. (Reproduced with permission from reference 1.18.)

bias-ply truck tire on a dry asphalt surface [1.18]. The value of the longitudinal stiffness C_s increases noticeably with an increase of the normal load. This is because the tire contact length increases with the normal load for a given inflation pressure. According to Eq. 1.21, to develop a given longitudinal force, the longer tire contact length results in lower longitudinal slip (or skid).

A sample of the peak and sliding values of the coefficient of road adhesion μ_p and μ_s for truck tires at 64 km/h (40 mph) on dry and wet concrete pavements is shown in Table 1.3 [1.19]. The pavements were aggressively textured, like those of relatively new roads meeting the requirements of the U.S. Federal Interstate Highway System.

It can be seen from Table 1.3 that the ratio of the peak value μ_p to the sliding value μ_s for truck tires on dry concrete pavement is around 1.4, whereas on wet concrete pavement, it ranges from approximately 1.3 to 1.6. It is also noted that there appear to be no clear distinctions between the tractive (braking) performance of bias-ply and radial-ply truck tires.

The significant difference between the peak values μ_p and the sliding value μ_s of the coefficient of road adhesion indicates the importance of avoiding wheel lockup during braking (skid $i_s = 100\%$) or wheel spinning during acceleration (slip $i = 100\%$). This is one of the impetuses to the development of antilock brake systems and traction control systems for road vehicles, which is discussed in Chapter 3.

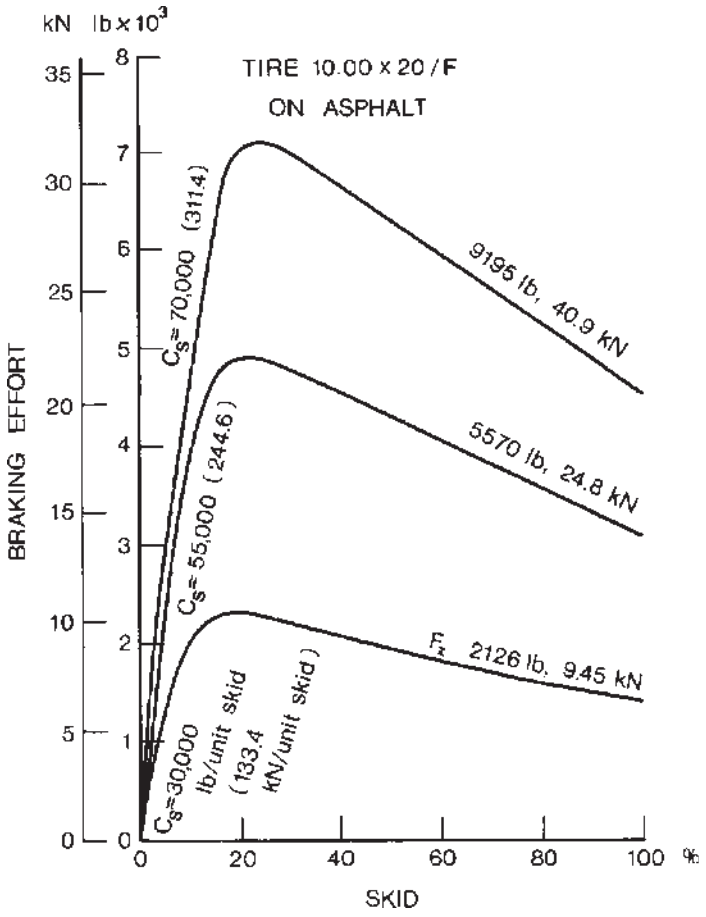

Fig. 1.21 Effect of normal load on braking performance of a truck tire on asphalt. (Reproduced with permission from reference 1.18.)

1.4 CORNERING PROPERTIES OF TIRES

1.4.1 Slip Angle and Cornering Force

When a pneumatic tire is not subject to any force perpendicular to the wheel plane (i.e., side force), it will move along the wheel plane. If, however, a side force F_s is applied to a tire, a lateral force will be developed on the contact patch, and the tire will move along a path at an angle α with the wheel plane, as OA shown in Fig. 1.22. The angle α is usually referred to as the slip angle, and the phenomenon of side slip is mainly due to the lateral elasticity of the tire.

The lateral force developed on the tire–ground contact patch is usually called the cornering force $F_{y\alpha}$ when the camber angle of the wheel is zero. The relationship between the cornering force and the slip angle is of fundamental importance to the directional control and stability of road vehicles.

TABLE 1.3 Values of Coefficient of Road Adhesion for Truck Tires on Dry and Wet Concrete Pavement at 64 km/h (40 mph)

Tire type	Tire construction	Dry		Wet	
		μ_p	μ_s	μ_p	μ_s
Goodyear Super Hi Miler (rib)	Bias-ply	0.850	0.596	0.673	0.458
General GTX (rib)	Bias-ply	0.826	0.517	0.745	0.530
Firestone Transteel (rib)	Radial-ply	0.809	0.536	0.655	0.477
Firestone Transport 1 (rib)	Bias-ply	0.804	0.557	0.825	0.579
Goodyear Unisteel R-1 (rib)	Radial-ply	0.802	0.506	0.700	0.445
Firestone Transteel Traction (lug)	Radial-ply	0.800	0.545	0.600	0.476
Goodyear Unisteel L-1 (lug)	Radial-ply	0.768	0.555	0.566	0.427
Michelin XZA (rib)	Radial-ply	0.768	0.524	0.573	0.443
Firestone Transport 200 (lug)	Bias-ply	0.748	0.538	0.625	0.476
Uniroyal Fleet Master Super Lug	Bias-ply	0.739	0.553	0.513	0.376
Goodyear Custom Cross Rib	Bias-ply	0.716	0.546	0.600	0.455
Michelin XZZ (rib)	Radial-ply	0.715	0.508	0.614	0.459
Average		0.756	0.540	0.641	0.467

Source: UMTRI, reference 1.19.

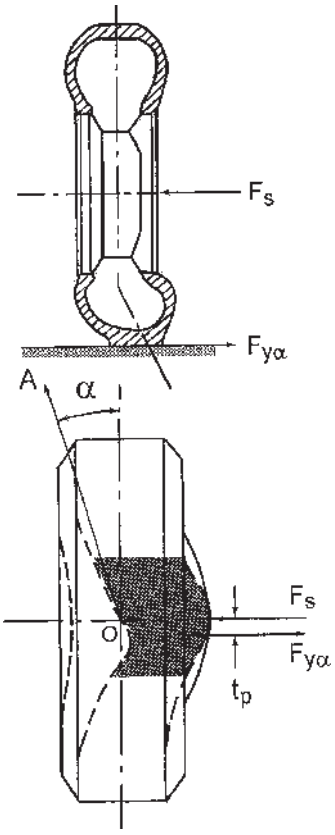

Fig. 1.22 Behavior of a tire subject to a side force. (Reproduced with permission from *Mechanics of Pneumatic Tires,* edited by S.K. Clark, Monograph 122, National Bureau of Standards, 1971.)

When the tire is moving at a uniform speed in the direction of OA, the side force F_s applied at the wheel center and the cornering force $F_{y\alpha}$ developed in the ground plane are usually not collinear, as shown in Fig. 1.22. At small slip angles, the cornering force in the ground plane is normally behind the applied side force, giving rise to a torque (or couple), which tends to align the wheel plane with the direction of motion. This torque is called the aligning or self-aligning torque, and is one of the primary restoring moments that help the steered tire return to the original position after negotiating a turn. The distance t_p between the side force and the cornering force is called the pneumatic trail, and the product of the cornering force and the pneumatic trail determines the self-aligning torque.

The relationships between the slip angle and the cornering force of various types of tire under a variety of operating conditions have been investigated extensively. Typical plots of the cornering force as a function of the slip angle for a bias-ply and a radial-ply passenger car tire are shown in Fig. 1.23 [1.6]. It can be seen that for slip angles below a certain value, such as 4° shown in Fig. 1.23, the cornering force is approximately proportional to the slip angle. Beyond that, the cornering force increases at a lower rate with an increase of the slip angle, and it reaches a maximum value where the tire begins sliding laterally. For passenger car tires, the maximum cornering force may occur at a slip angle of about 18°, while for racing car tires, the cornering force may peak at approximately 6°. Figure 1.23 shows that the cornering force of a bias-ply tire increases more slowly with an increase of the slip angle than that of a radial-ply tire. These characteristics are considered to be more

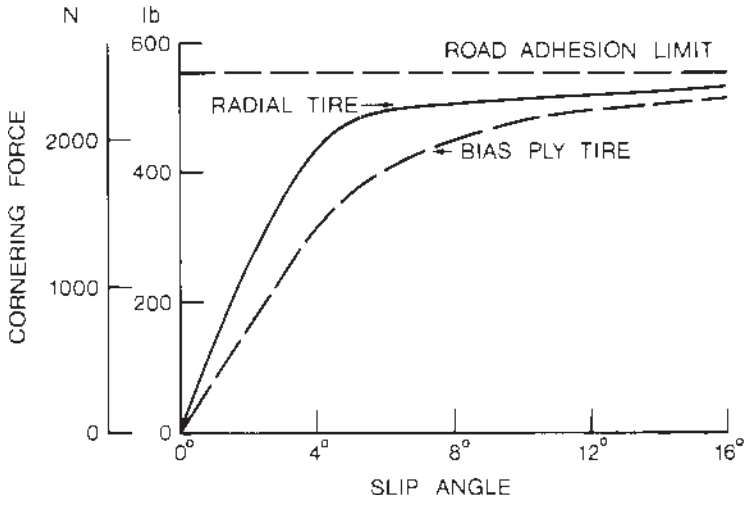

Fig. 1.23 Cornering characteristics of a bias-ply and a radial-ply car tire. (Reproduced with permission from *Mechanics of Pneumatic Tires,* edited by S.K. Clark, Monograph 122, National Bureau of Standards, 1971.)

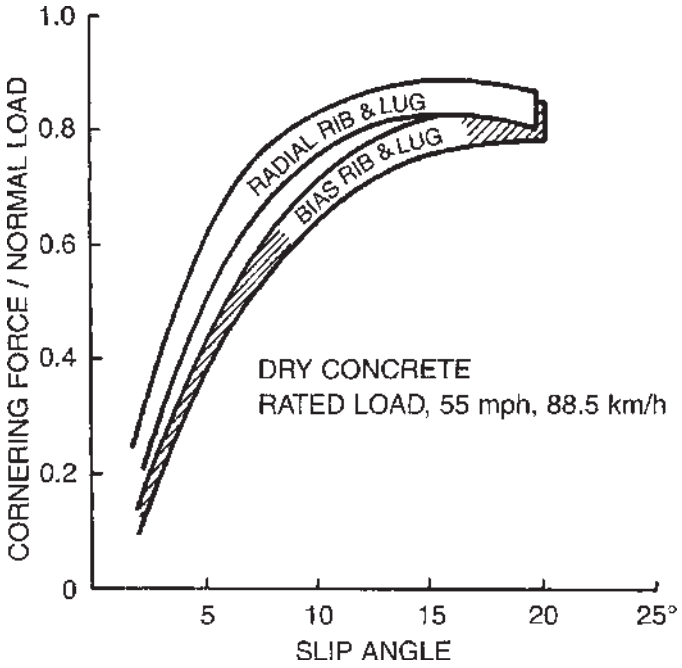

Fig. 1.24 Cornering characteristics of bias-ply and radial-ply truck tires on dry concrete. (Reproduced with permission from reference 1.8.)

suited to two-wheeled vehicles, such as motorcycles. A more gradual increase of the cornering force with the slip angle enables the driver to exercise better control over a two-wheeled vehicle. This is one of the reasons why bias-ply tires are used for motorcycles [1.1]. Figure 1.24 shows the variations of the ratio of the cornering force to the normal load with the slip angle for radial-ply and bias-ply truck tires of size 10.00–20 with different tread designs (ribbed or lugged) [1.8]. Similar to that shown in Fig. 1.23 for passenger car tires, the cornering force of radial-ply truck tires increases more rapidly with an increase of the slip angle than that of bias-ply truck tires.

A number of factors affect the cornering behavior of pneumatic tires. The normal load on the tire strongly influences the cornering characteristics. Some typical results are shown in Fig. 1.25 [1.6]. It can be seen that for a given slip angle, the cornering force generally increases with an increase of the normal load. However, the relationship between the cornering force and the normal load is nonlinear. Thus, the transfer of load from the inside to the outside tire during a turning maneuver will reduce the total cornering force that a pair of tires can develop. Consider a pair of tires on a beam axle, each with normal load F_z, as shown in Fig. 1.26. The cornering force per tire with normal load F_z is F_y for a given slip angle. If the vehicle undergoes a steady-state turn, owing to lateral load transfer, the normal load on the inside tire will

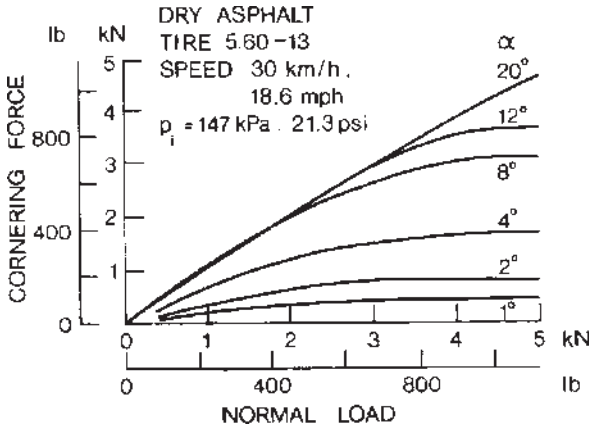

Fig. 1.25 Effect of normal load on the cornering characteristics of a car tire. (Reproduced with permission from *Mechanics of Pneumatic Tires,* edited by S.K. Clark, Monograph 122, National Bureau of Standards, 1971.)

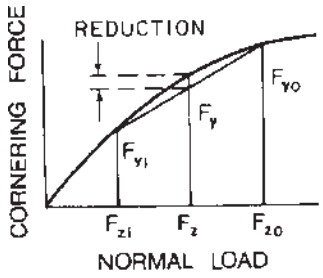

Fig. 1.26 Effect of lateral load transfer on the cornering capability of a pair of tires on an axle.

be reduced to F_{zi} and that on the outside tire will be increased to F_{zo}. As a result, the total cornering force of the two tires will be the sum of F_{yi} and F_{yo}, which is less than $2F_y$, as shown in Fig. 1.26. This implies that for a pair of tires on a beam axle to develop the required amount of cornering force to balance a given centrifugal force during a turn, the lateral load transfer results in an increase in the slip angle of the tires.

To provide a measure for comparing the cornering behavior of different tires, a parameter called cornering stiffness C_α is used. It is defined as the derivative of the cornering force $F_{y\alpha}$ with respect to slip angle α evaluated at zero slip angle:

$$C_\alpha = \left.\frac{\partial F_{y\alpha}}{\partial \alpha}\right|_{\alpha=0} \tag{1.37}$$

Figure 1.27 shows a comparison of the relationships between the cornering stiffness and the normal load for a sample of passenger car, light truck, and

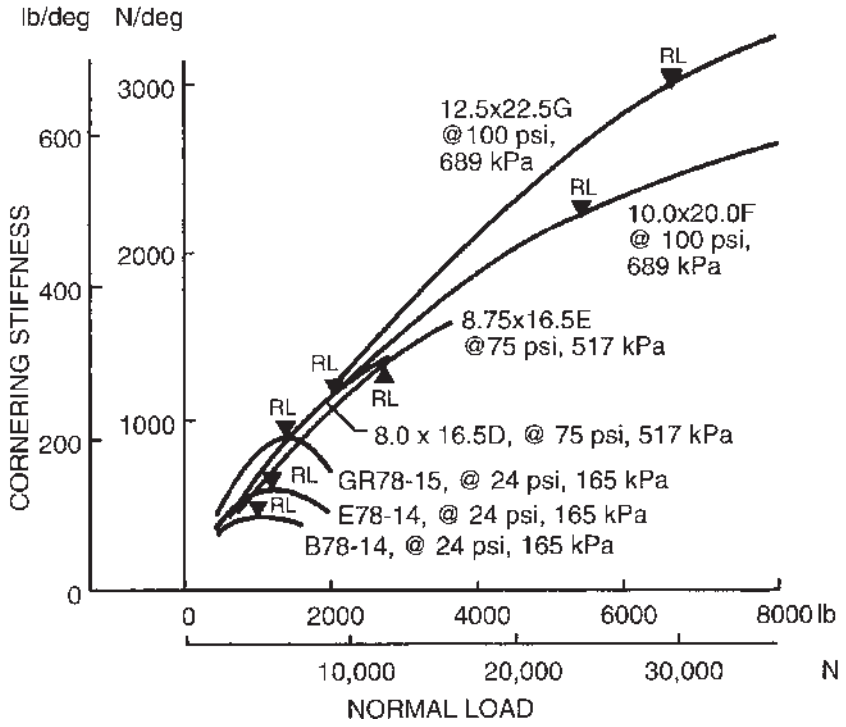

Fig. 1.27 Comparison of cornering stiffness of car, light truck, and heavy truck tires. (Reproduced with permission from reference 1.8.)

heavy truck tires [1.8]. In the figure, RL indicates the rated load for a specific tire. For the three passenger car tires tested, the cornering stiffness reaches a maximum at the rated load, and decreases with a further increase in the normal load. However, for the light truck and heavy truck tires shown, the cornering stiffness keeps increasing beyond the rated load, although at a lower rate.

To evaluate the effect of the normal load on the cornering ability of tires, a parameter called the cornering coefficient, which is defined as the cornering stiffness per unit normal load, is often used. Figure 1.28 shows a typical relationship between the cornering coefficient and the normal load of a tire [1.12]. It shows that the cornering coefficient decreases with an increase in the normal load.

Inflation pressure usually has a moderate effect on the cornering properties of a tire. In general, the cornering stiffness of tires increases with an increase of the inflation pressure. Figure 1.29 shows a comparison of the cornering coefficients at different inflation pressures of a radial-ply, a bias-belted, and a bias-ply passenger car tire [1.11]. Table 1.4 shows a sample of the values of the cornering coefficient for truck tires at rated loads and inflation pressures (unless specified) [1.19].

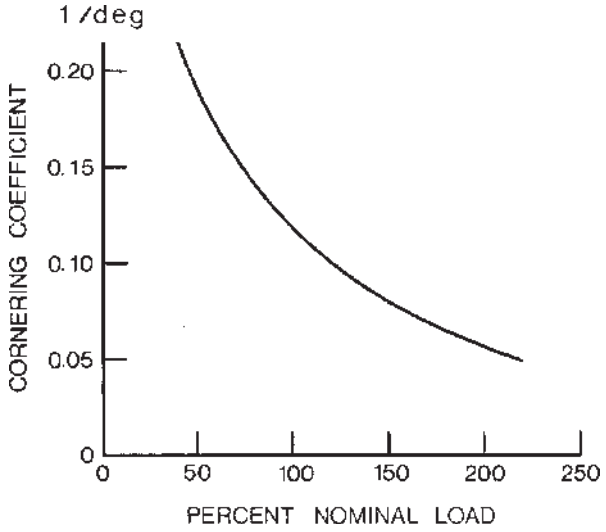

Fig. 1.28 Effect of normal load on the cornering coefficient of a tire. (Reproduced with permission from reference 1.12.)

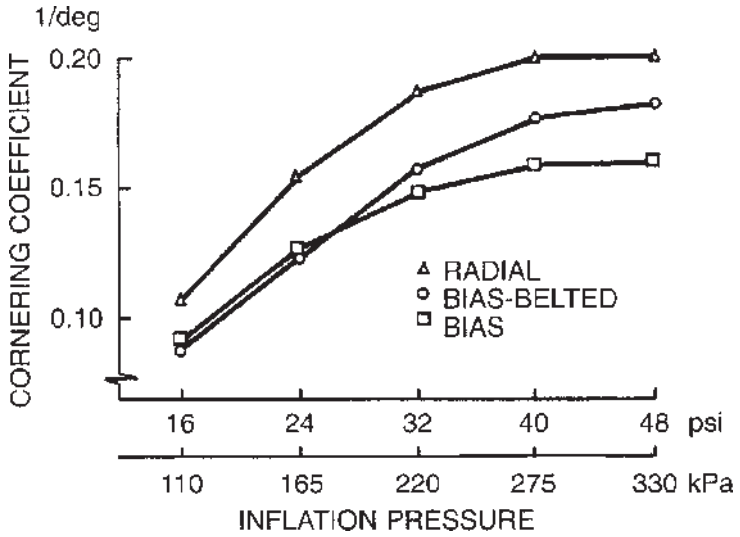

Fig. 1.29 Variation of cornering coefficient with inflation pressure for radial-ply, bias-ply, and bias-belted car tires. (Reproduced with permission of the Society of Automotive Engineers from reference 1.11.)

TABLE 1.4 Cornering Coefficients for Truck Tires at Rated Loads and Inflation Pressures (Unless Specified)

Tire type	Tire construction	Cornering coefficient (deg^{-1})
Michelin Radial XZA (1/3 tread)	Radial-ply	0.1861
Michelin Radial XZA (1/2 tread)	Radial-ply	0.1749
Michelin Pilote XZA	Radial-ply	0.1648
Michelin Radial XZA	Radial-ply	0.1472
Goodyear Unisteel G159, 11R22.5 LRF at 655 kPa (95 psi)	Radial-ply	0.1413
Michelin XZZ	Radial-ply	0.1370
Goodyear Unisteel 11, 10R22.5 LRF at 620 kPa (90 psi)	Radial-ply	0.1350
Goodyear Unisteel G159, 11R22.5 LRG at 792 kPa (115 psi)	Radial-ply	0.1348
Goodyear Unisteel 11, 10R22.5 LRF at 758 kPa (110 psi)	Radial-ply	0.1311
Firestone Transteel	Radial-ply	0.1171
Firestone Transteel Traction	Radial-ply	0.1159
Goodyear Unisteel R-1	Radial-ply	0.1159
Goodyear Unisteel L-1	Radial-ply	0.1121
Firestone Transport 1	Bias-ply	0.1039
General GTX	Bias-ply	0.1017
Goodyear Super Hi Miler	Bias-ply	0.0956
Goodyear Custom Cross Rib	Bias-ply	0.0912
Uniroyal Fleet Master Super Lub	Bias-ply	0.0886
Firestone Transport 200	Bias-ply	0.0789

Source: UMTRI and TRIF, reference 1.19.

1.4.2 Slip Angle and Aligning Torque

As mentioned in Section 1.4.1, the side force F_s applied at the wheel center and the cornering force $F_{y\alpha}$ developed in the ground plane are usually not collinear, as shown in Fig. 1.22. This gives rise to a torque commonly known as the aligning or self-aligning torque. Figure 1.30 shows a plot of the cornering force versus the aligning torque for a passenger car tire at various slip angles and under different normal loads [1.20]. Figures 1.31 and 1.32 show the variations of the aligning torque with the slip angle and the normal load for a bias-ply truck tire (10.00-20/*F*) and for a radial-ply truck tire (10.00-20/*G*), respectively [1.8]. It is interesting to note that with a given normal load, the aligning torque first increases with an increase of the slip angle. It reaches a maximum at a particular slip angle, and then decreases with a further increase of the slip angle. This is mainly caused by the sliding of the tread in the trailing part of the contact patch at high slip angles, which results in shifting the point of application of the cornering force forward. Table 1.5 shows a sample of measured values of pneumatic trail for truck tires at a slip angle of 1° and

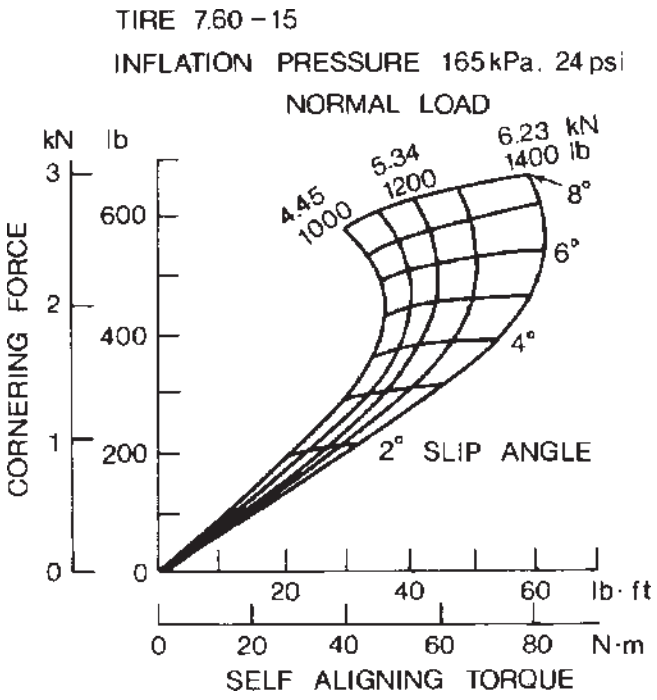

Fig. 1.30 Variation of self-aligning torque with cornering force of a car tire under various normal loads. (Reproduced with permission of the Society of Automotive Engineers from reference 1.20.)

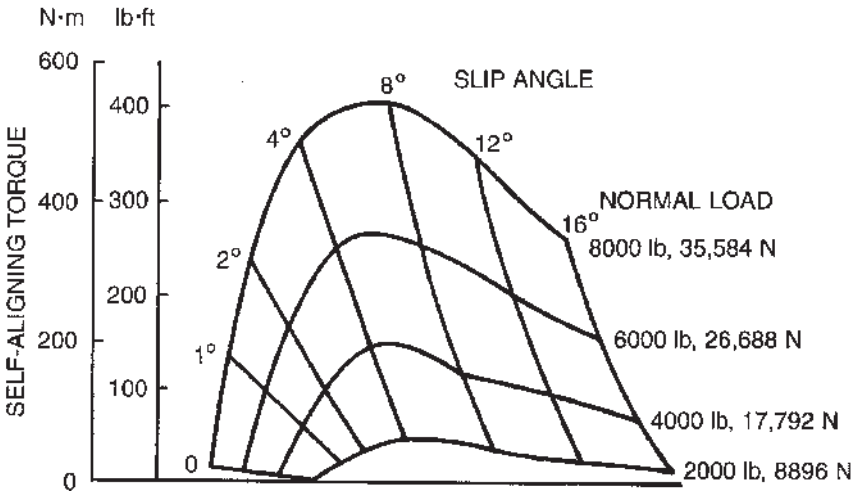

Fig. 1.31 Variation of self-aligning torque with normal load and slip angle for a bias-ply truck tire, 10.00–20/*F*. (Reproduced with permission from reference 1.8.)

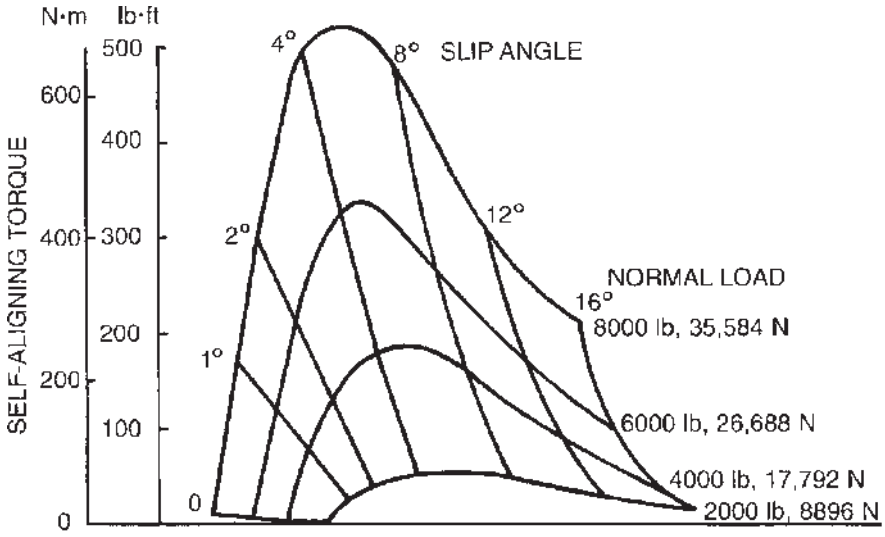

Fig. 1.32 Variation of self-aligning torque with normal load and slip angle for a radial-ply truck tire, 10.00–20/*G*. (Reproduced with permission from reference 1.8.)

TABLE 1.5 Pneumatic Trails for Truck Tires at a Slip Angle of 1° Under Rated Loads and Inflation Pressures (Unless Specified)

		Pneumatic trails	
Tire type	Tire construction	cm	in.
Michelin Radial 11R22.5 XZA (1/3 Tread)	Radial-ply	6.17	2.43
Goodyear Unisteel II, 10R22.5 LRF at 620 kPa (90 psi)	Radial-ply	6.15	2.42
Michelin Radial 11R22.5 XZA (1/2 Tread)	Radial-ply	5.89	2.32
Goodyear Unisteel G159, 11R22.5 LRG at 655 kPa (95 psi)	Radial-ply	5.87	2.31
Michelin Radial 11R22.5 XZA	Radial-ply	5.51	2.17
Goodyear Unisteel G159, 11R22.5 LRG at 792 kPa (115 psi)	Radial-ply	5.46	2.15
Goodyear Unisteel II, 10 R22.5 LRF at 758 kPa (110 psi)	Radial-ply	5.41	2.13
Michelin Radial 11R22.5 XZA	Radial-ply	5.38	2.12
Michelin Pilote 11/80R22.5 XZA	Radial-ply	4.62	1.82
New Unspecified Model 10.00-20/F	Bias-ply	5.89	2.32
Half-Worn Unspecified Model 10.00-20/F	Bias-ply	7.14	2.81
Fully-Worn Unspecified Model 10.00-20/F	Bias-ply	6.55	2.58

Source: UMTRI, reference 1.19.

under rated loads and inflation pressures (unless specified) [1.19]. It is shown that the pneumatic trail for truck tires varies in the range from 4.6 cm (1.8 in.) to 7.1 cm (2.8 in.). A typical value for a new bias-ply truck tire is 5.8 cm (2.3 in.), while that for a new radial-ply tire is 5.3 cm (2.1 in.).

Longitudinal force affects the aligning torque significantly. Generally speaking, the effect of a driving torque is to increase the aligning torque for a given slip angle, while a braking torque has the opposite effect. Inflation pressure and normal load also have noticeable effects on the aligning torque because they affect the size of the tire contact patch. Higher normal load and lower inflation pressure result in longer tire contact length, and hence pneumatic trail. This causes an increase in the aligning torque.

1.4.3 Camber and Camber Thrust

Camber is the inclination of the wheel plane from a plane perpendicular to the road surface when viewed from the fore and aft directions of the vehicle, as shown in Fig. 1.33. Its main purpose is to achieve axial bearing pressure and to decrease the kingpin offset. Camber on passenger cars is between 1/2 and 1°. High camber angles promote excessive tire wear [1.12].

Camber causes a lateral force developed on the contact patch. This lateral force is usually referred to as camber thrust $F_{y\gamma}$, and the development of this thrust may be explained in the following way. A free-rolling tire with a camber angle would revolve about point O, as shown in Fig. 1.33. However, the cambered tire in a vehicle is constrained to move in a straight line. A lateral force in the direction of the camber is, therefore, developed in the ground plane. It is interesting to note that the camber thrust acts ahead of the wheel center, and therefore forms a small camber torque. The relationship between the camber thrust and the camber angle (at zero slip angle) for a bias-ply passenger car tire is illustrated in Fig. 1.34 [1.21]. It has been shown

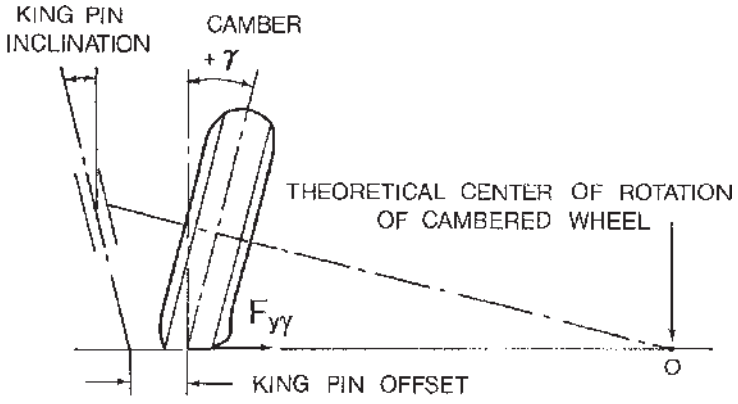

Fig. 1.33 Behavior of a cambered tire.

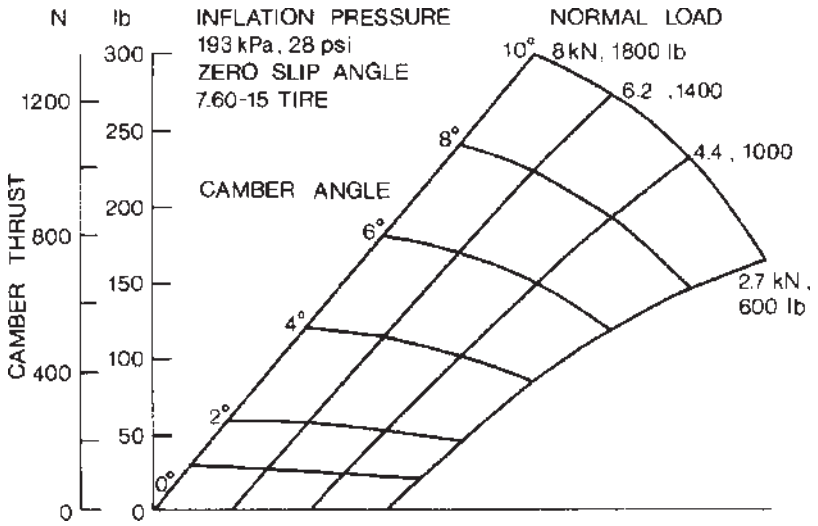

Fig. 1.34 Variation of camber thrust with camber angle and normal load for a car tire. (Reproduced with permission of the Society of Automotive Engineers from reference 1.21.)

that the camber thrust is approximately one-fifth the value of the cornering force obtained from an equivalent slip angle for a bias-ply tire and somewhat less for a radial-ply tire. To provide a measure for comparing the camber characteristics of different tires, a parameter called "camber stiffness" is often used. It is defined as the derivative of the camber thrust with respect to the camber angle evaluated at zero camber angle.

$$C_\gamma = \left.\frac{\partial F_{y\gamma}}{\partial \gamma}\right|_{\gamma=0} \tag{1.38}$$

Similar to the cornering stiffness, the normal load and inflation pressure have an influence on the camber stiffness. Figure 1.35 shows the variations of the camber stiffness with normal load for three truck tires at an inflation pressure of 620 kPa (90 psi) [1.8]. It is found that for truck tires, the value of the camber stiffness is approximately one-tenth to one-fifth of that of the cornering stiffness under similar operating conditions.

The total lateral force of a cambered tire operating at a slip angle is the sum of the cornering force $F_{y\alpha}$ and the camber thrust $F_{y\gamma}$:

$$F_y = F_{y\alpha} \pm F_{y\gamma} \tag{1.39}$$

If the cornering force and the camber thrust are in the same direction, the positive sign should be used in the above equation. For small slip and camber

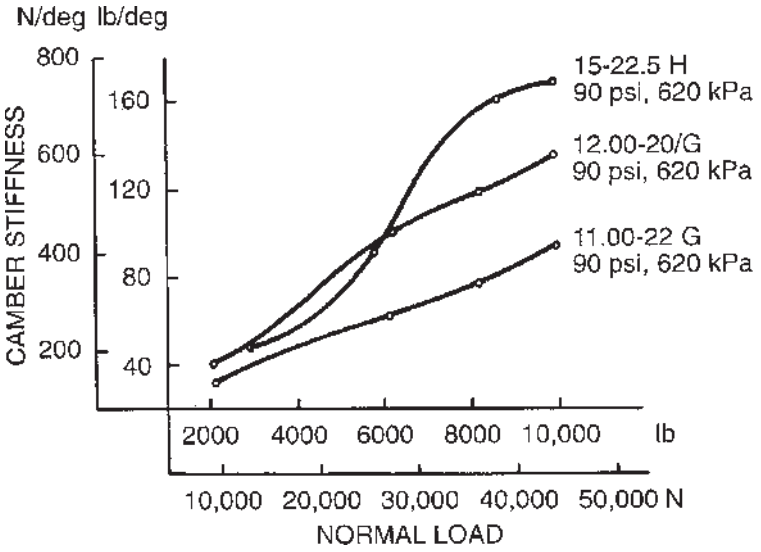

Fig. 1.35 Variation of camber stiffness with normal load for heavy truck tires. (Reproduced with permission from reference 1.8.)

angles, the relationship between the cornering force and the slip angle and that between the camber thrust and the camber angle are essentially linear; the total lateral force of a cambered tire at a slip angle can, therefore, be determined by

$$F_y = C_\alpha \alpha \pm C_\gamma \gamma \tag{1.40}$$

As discussed previously, the lateral forces due to slip angle and camber angle produce an aligning torque. The aligning torque due to slip angle, however, is usually much greater.

1.4.4 Characterization of Cornering Behavior of Tires

A number of attempts have been made to develop mathematical models for the cornering behavior of pneumatic tires. There are two basic types of model. One is based on the assumption that the tread of the tire is equivalent to a stretched string restrained by lateral springs, representative of the sidewall with the wheel rim acting as the base of the springs, as shown in Fig. 1.36(a). In the other model, the tread is considered equivalent to an elastic beam with continuous lateral elastic support, as shown in Fig. 1.36(b) [1.15, 1.22].

In both models, it is assumed that the cornering behavior of a tire can be deduced from the characteristics of the equatorial line of the tire, which is the intersection of the undeformed tire tread with the wheel plane. The portion of the equatorial line in the contact area is called the contact line. One of the

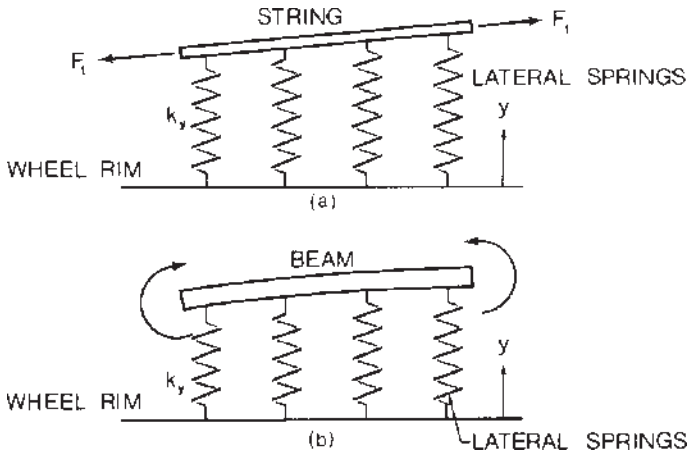

Fig. 1.36 Models for cornering behavior of tires. (a) Stretched string model. (b) Beam on elastic foundation model. (Reproduced with permission from *Vehicle Dynamics* by J.R. Ellis, Business Books, 1969.)

major differences in these two basic models is that in the stretched-string model, discontinuities of the slope of the equatorial line are permissible, whereas for the beam model, that is not the case. It has been shown that for small slip angles, the stretched-string model can provide a basic understanding of the lateral behavior of a pneumatic tire. In the following, the stretched-string model as proposed by Temple and von Schlippe is discussed [1.15].

Consider a tire in a steady-state motion with a fixed slip angle. The shape of the equatorial line BC in the contact area shown in Fig. 1.37 is the path of the tire, and it is immobile relative to the ground when no sliding takes place. Let the chained line AB in the figure represent the projection of the portion of the equatorial line outside and in front of the contact patch. As the tire rolls forward, points of AB becomes points of BC. This indicates that AB and BC must have a common tangent at point B. At the rear of the contact patch, such conditions do not hold, and a kink may be present at point C. Thus, it can be stated that for a rolling tire, the slope of the equatorial line is continuous at the front edge of the contact area, but not necessarily at the rear.

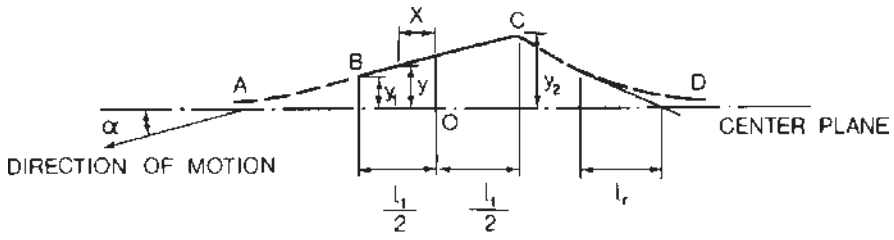

Fig. 1.37 Behavior of the equatorial line of a rolling tire subject to a side force.

Consider an element of the distorted equatorial line shown in Fig. 1.37. Let the lateral deflection from the wheel center plane be y, and the distance measured along the undistorted equatorial line be x, with the origin at the center of the contact patch. It is assumed that the lateral force applied to the rim by the element due to lateral deflection y is given, in differential form, by

$$dF_{y1} = k_y y\, dx \tag{1.41}$$

where k_y is the lateral stiffness of the tire. This equation applies at all points of the periphery. Based on experimental data of a sample of bias-ply and radial-ply heavy truck tires under rated loads and inflation pressures, it is found that the value of k_y varies in a narrow range. The average value is approximately 2275 kN/m^2 (330 lb/in.^{2})

In an element of the equatorial line, there is another force component acting in the lateral direction, which is due to the tension in the string. This component is proportional to the curvature of the equatorial line, and for small deflection is given, in differential form, by

$$dF_{y2} = -F_t \frac{d^2y}{dx^2} dx \tag{1.42}$$

where F_t represents the tension in the string. It is usually convenient to write $F_t = k_y l_r^2$,where l_r is termed the "relaxation length," in which the lateral deflection, described by an exponential function, decreases to 1/2.718 of its prior value, as shown in Fig. 1.37.

Let l_t be the contact length with the origin for x at the center, and let y_1 and y_2 be the deflections of the equatorial line at the front and rear ends of the contact patch, as shown in Fig. 1.37. Over the part of the tire not in contact with the ground (i.e., free region) having total length l_h, the tire is not loaded by external means, and therefore from Eqs. 1.41 and 1.42,

$$k_y \left(y - l_r^2 \frac{d^2y}{dx^2} \right) = 0 \tag{1.43}$$

The solution of this differential equation will yield the deflected shape of the equatorial line in the free region, which is given by

$$y = \frac{y_2 \sinh\, [(x - l_t/2)/l_r] + y_1 \sinh\, [(l_t/2 + l_h - x)/l_r]}{\sinh\, (l_h/l_r)} \tag{1.44}$$

If r is the tire radius, under normal conditions l_h lies between $4.5r$ and $6r$, whereas l_r is approximately equal to r [1.15]. Hence, Eq. 1.44 may be approximated by an exponential function. For the free region near the front of the contact area (i.e., $x > l_t/2$),

$$y = y_1 \exp \left[\frac{-(x - l_t/2)}{l_r} \right] \tag{1.45}$$

For the free region near the rear of the contact area (i.e., $x < l_t/2 + l_h$),

$$y = y_2 \exp\left[\frac{-(l_t/2 + l_h - x)}{l_r}\right] \tag{1.46}$$

Thus, in the free region not in contact with the ground but near either end of the contact patch, the shape of the equatorial line is an exponential curve.

The expressions for the lateral deflection and the lateral forces acting on an element of the tread described above permit the determination of the cornering force and the aligning torque in terms of constants k_y and l_r and contact length l_t. This can be achieved in two ways:

1. Integrating the lateral force exerted on the tire over the contact length, but including an infinitesimal length of the equatorial line in the free region at either end, as proposed by Temple.
2. Integrating the lateral force exerted on the rim by the tire over the entire circumference, including the contact length, as proposed by von Schlippe. The essence of these two methods is illustrated in Fig. 1.38.

Following Temple's method, and assuming that the equatorial line in the contact region is a straight line, one can obtain the total lateral force F_y by integration:

$$\begin{aligned} F_y &= k_y \int_{-l_t/2}^{l_t/2} \left(y - l_r^2 \frac{d^2y}{dx^2}\right) dx \\ &= k_y \int_{-l_t/2}^{l_t/2} y \, dx - k_y l_r^2 \left(\frac{dy}{dx}\right)\Bigg]_{-l_t/2}^{l_t/2} \end{aligned}$$

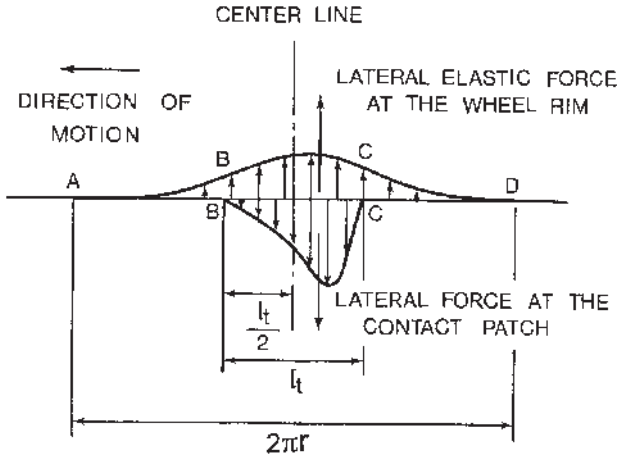

Fig. 1.38 Lateral force acting on the wheel rim and on the tire–road contact patch.

$$= k_y(y_1 + y_2)l_t/2 + k_y l_r(y_1 + y_2)$$
$$= k_y(y_1 + y_2)(l_r + l_t/2) \tag{1.47}$$

For a nonrolling tire subject to a pure side force,

$$y_1 = y_2 = y_0 \text{ and } F_y = 2k_y y_0(l_r + l_t/2) \tag{1.48}$$

The moment of lateral force about a vertical axis through the center of contact (i.e., the aligning torque) is given by

$$M_z = k_y \int_{-l_t/2}^{l_t/2} x\left(y - l_r^2 \frac{d^2y}{dx^2}\right) dx$$
$$= k_y \int_{-l_t/2}^{l_t/2} xy\ dx - k_y l_r^2 \left(x\frac{dy}{dx} - y\right)\Bigg]_{-l_t/2}^{l_t/2}$$
$$= k_y \frac{(l_t/2)^2}{3}(y_1 - y_2) + k_y l_r \left(l_r + \frac{l_t}{2}\right)(y_1 - y_2)$$
$$= k_y(y_1 - y_2)\left[\frac{(l_r/2)^2}{3} + l_r\left(l_r + \frac{l_t}{2}\right)\right] \tag{1.49}$$

Following von Schlippe's approach, one can obtain the same expressions.

For a tire rolling at a slip angle α, the slope of the equatorial line in the contact area is equal to tan α if the tread in the contact patch is not sliding. Thus,

$$\alpha \simeq \tan\alpha = \frac{y_1 - y_2}{l_t} = -\frac{y_1}{l_r} \tag{1.50}$$

Substituting the above expression into Eqs. 1.47 and 1.49, the relationships between the magnitudes of the lateral force and the self-aligning torque and the slip angle become

$$\frac{F_y}{\alpha} = 2k_y\left(l_r + \frac{l_t}{2}\right)^2 \tag{1.51}$$

$$\frac{M_z}{\alpha} = k_y l_t\left[\frac{(l_t/2)^2}{3} + l_r\left(l_r + \frac{l_t}{2}\right)\right] \tag{1.52}$$

The pneumatic trail t_p is given by

$$t_p = \frac{M_z}{F_y} = \frac{(l_t/2)[(l_t/2)^2/3 + l_r(l_r + l_t/2)]}{(l_r + l_t/2)^2} \tag{1.53}$$

The two basic parameters k_y and l_r, which specify the characteristics of the lateral elasticity of the pneumatic tire, can be measured by suitable tests. It is noted that the ratio of F_y/α to M_z/α is independent of k_y, and therefore l_r can be determined from the measured values of F_y/α and M_z/α (contact length of the tire l_t being known). On the other hand, the ratio of $(F_y/y_0)^2$ of a nonrolling tire to F_y/α is independent of l_r, and therefore k_y can be determined from the measured values of $(F_y/y_0)^2$ and F_y/α. Measurements of k_y and l_r have been carried out by several investigators. For instance, values of l_r for a family of aircraft tires of different sizes but with similar proportion were found by von Schlippe to vary from $0.6r$ to $0.9r$ approximately. Values of k_y measured by von Schlippe were about 90% of the inflation pressure [1.15].

Equations 1.51 and 1.52 indicate that, if no sliding between the tread and the ground occurs, the lateral force and the aligning torque increase linearly with the slip angle. This is the case for small slip angles, as shown in Fig. 1.23. As the slip angle increases, sliding between the tread and the ground occurs. The assumption that the equatorial line in the contact patch is a straight line is no longer valid. Thus, the theory proposed by Temple and von Schlippe is restricted to small slip angles.

As noted above, using Temple's or von Schlippe's theory to define the relationship between the cornering force and the slip angle, the values of k_y and l_r must be known. Their determination is usually quite an involved process. In view of this, a simplified theory has been proposed [1.8]. In the simplified model, it is assumed that if no sliding takes place, the lateral deflection of y' of a tread element on the ground at a longitudinal distance of x from the front of the contact patch (along the wheel plane) is proportional to $\tan\alpha$ and is given by

$$y' = x\tan\alpha \tag{1.54}$$

where the lateral deflection y' is measured with respect to the front contact point and perpendicular to the wheel plane, and α is the slip angle.

If k'_y is the equivalent lateral stiffness of the tire, then when no lateral sliding between the tire tread and the ground takes place, the lateral force per unit contact length is given by

$$\frac{dF_{y\alpha}}{dx} = k'_y x\tan\alpha \tag{1.55}$$

and the cornering force developed on the entire contact patch is expressed by

$$\begin{aligned} F_{y\alpha} &= \int_0^{l_t} k'_y x\tan\alpha\ dx \\ &= (k'_y l_t^2/2)\tan\alpha \end{aligned} \tag{1.56}$$

where l_t is the contact length of the tire.

The term $(k'_y l_t^2/2)$ may be taken as the cornering stiffness C_α defined by Eq. 1.37, that is, the slope of the cornering force–slip angle curve at the origin, which can easily be identified:

$$\frac{k'_y l_t^2}{2} = C_\alpha = \left.\frac{\partial F_{y\alpha}}{\partial \alpha}\right|_{\alpha=0} \tag{1.57}$$

Therefore, when no lateral sliding takes place on the contact patch, the relationship between the cornering force and the slip angle is expressed by

$$F_{y\alpha} = C_\alpha \tan\alpha \tag{1.58}$$

If the slip angle α is small, $\tan\alpha \approx \alpha$, and Eq. 1.58 may be rewritten as

$$F_{y\alpha} = C_\alpha \alpha \tag{1.59}$$

Following an approach similar to that for analyzing the relationship between the tractive effort and the longitudinal slip described in Section 1.3, the critical values of the slip angle α_c and the cornering force $F_{y\alpha c}$, at which lateral sliding in the trailing part of the contact patch begins, can be determined. The critical value of α_c is given by

$$\alpha_c = \frac{\mu_p W}{2C_\alpha} \tag{1.60}$$

and the critical value of $F_{y\alpha c}$ is given by

$$F_{y\alpha c} = \frac{\mu_p W}{2} \tag{1.61}$$

Similar to the relationship between the tractive effort–longitudinal slip described in Section 1.3, Eq. 1.61 indicates that the relationship between the cornering force and the slip angle will be linear and no lateral sliding will take place, if the cornering force is less than one-half of its peak value $(\mu_p W/2)$.

When lateral sliding between the tire tread and the ground takes place (i.e., $\alpha > \alpha_c$ or $F_{y\alpha} > F_{y\alpha c}$), the relationship between the cornering force and the slip angle, analogous to Eq. 1.29, is expressed by

$$F_{y\alpha} = \mu_p W\left(1 - \frac{\mu_p W}{4C_\alpha \tan\alpha}\right) = \mu_p W\left(1 - \frac{\mu_p W}{4C_\alpha \alpha}\right) \tag{1.62}$$

The above equation indicates the nonlinear nature of the cornering force–slip angle relationship when lateral sliding takes place in part of the contact patch.

While the theories described above provide physical insight into certain aspects of the cornering behavior of the pneumatic tire, they are simplified

representations of a highly complex process. In the simulations of the lateral dynamic behavior of road vehicles, to more accurately represent tire characteristics, measured tire data, rather than theoretical relationships, are often used. Measured tire data in tabular form or represented by empirical equations may be entered as input to the simulation models. For instance, the following empirical equation has been proposed to represent the relationship between the cornering force $F_{y\alpha}$ and the slip angle α [1.22]:

$$F_{y\alpha} = c_1\alpha + c_2\alpha^2 + c_3\alpha^3 \tag{1.63}$$

where c_1, c_2, and c_3 are empirical constants derived from fitting Eq. 1.63 to the measured data of a given tire.

As mentioned previously, normal load has a significant influence on the development of cornering force. To take the effects of normal load into account, the coefficients c_1, c_2, and c_3 may be expressed as a quadratic function of normal load [1.22]. This would require an additional curve-fitting exercise.

In the discussion of the cornering behavior of pneumatic tires described above, the effect of the longitudinal force has not been considered. However, quite often both the side force and the longitudinal force are present, such as braking in a turn. In general, tractive (or braking) effort will reduce the cornering force that can be generated for a given slip angle; the cornering force decreases gradually with an increase of the tractive or braking effort. At low values of tractive (or braking) effort, the decrease in the cornering force is mainly caused by the reduction of the cornering stiffness of the tire. A further increase of the tractive (or braking) force results in a pronounced decrease of the cornering force for a given slip angle. This is due to the mobilization of the available local adhesion by the tractive (or braking) effort, which reduces the amount of adhesion available in the lateral direction.

The difference in behavior between a bias-ply and a radial-ply passenger car tire is shown in Fig. 1.39 [1.6]. It is interesting to note that for a radial-ply tire, the cornering force available at a given slip angle is more or less the same for both braking and driving conditions. For a bias-ply tire, however, at a given slip angle, a higher cornering force is obtained during braking than when the tire is driven. The fact that the presence of the tractive (or braking) effort requires a higher slip angle to generate the same cornering force is also illustrated in Fig. 1.39. Figure 1.40 shows the effects of longitudinal force on the development of cornering force for a truck tire at different slip angles [1.23]. Similar to that shown in Fig. 1.39, for a truck tire, the cornering force available at a given slip angle also decreases with an increase of the longitudinal force. Note that if an envelope around each family of curves of Fig. 1.39 is drawn, a curve approximately semielliptical in shape may be obtained. This enveloping curve is often referred to as the friction ellipse.

The friction ellipse concept is based on the assumption that the tire may slide on the ground in any direction if the resultant of the longitudinal force

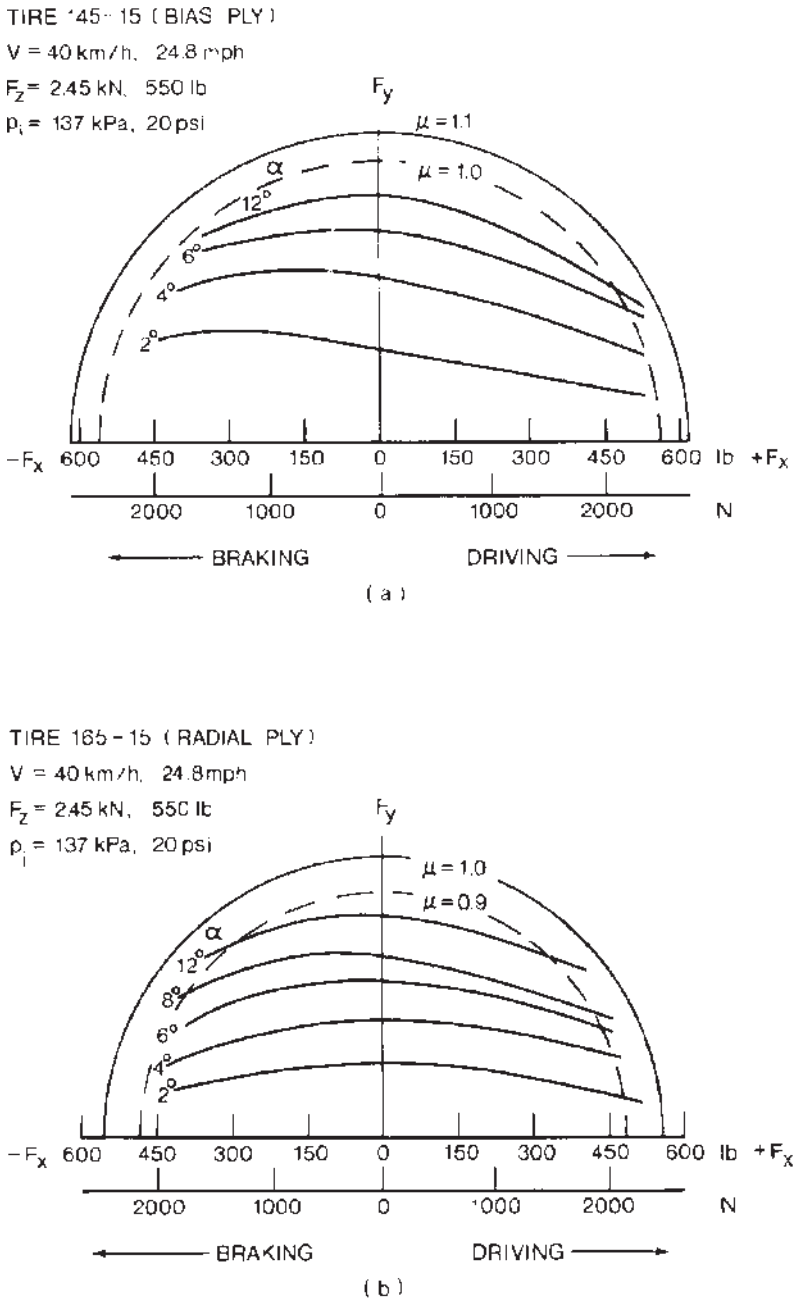

Fig. 1.39 Effect of tractive and braking effort on the cornering characteristics of (a) a bias-ply and (b) a radial-ply car tire. (Reproduced with permission from *Mechanics of Pneumatic Tires,* edited by S.K. Clark, Monograph 122, National Bureau of Standards, 1971.)

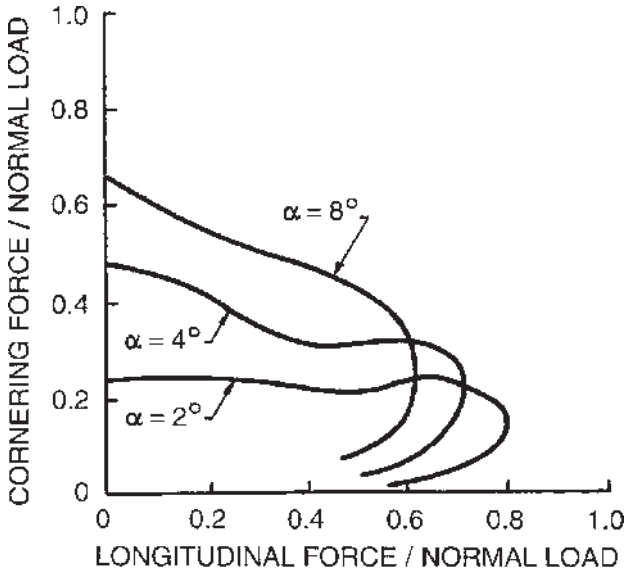

Fig. 1.40 Effect of longitudinal force on the cornering characteristics of a truck tire. (Reproduced with permission of the Society of Automotive Engineers from reference 1.23.)

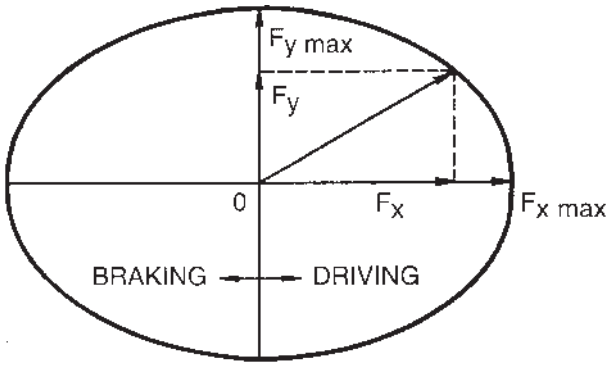

Fig. 1.41 The friction ellipse concept relating the maximum cornering force to a given longitudinal force.

(either tractive or braking) and lateral (cornering) force reaches the maximum value defined by the coefficient of road adhesion and the normal load on the tire. However, the longitudinal and lateral force components may not exceed their respective maximum values F_{xmax} and F_{ymax}, as shown in Fig. 1.41. F_{xmax} and F_{ymax} can be identified from measured tire data, and constitute the major and minor axes of the friction ellipse, respectively, as shown in Fig. 1.41.

Based on the experimental observations described above, attempts have been made to formulate an analytical framework for predicting the longitudinal force and cornering force as functions of combined longitudinal slip (or skid) and slip angle.

One of the simplest theories for predicting the cornering force available at a specific slip angle in the presence of a tractive or braking force is based on the friction ellipse concept described above. The procedure for determining the available cornering force based on this simple theory is outlined below.

1. From measured tire data, the relationship between the cornering force and the slip angle under free rolling conditions (i.e., in the absence of tractive or braking effort) is first plotted, as shown in Fig. 1.42(a).
2. The cornering forces at various slip angles under free rolling conditions are then marked on the vertical axis of Fig. 1.42(b), as shown. For instance, the cornering force developed at a slip angle of 4° is identified as F_{y4} on the vertical axis, which constitutes the minor axis of an ellipse to be established.
3. From measured tire data, the maximum tractive or braking force, $F_{x\,\max}$, in the absence of lateral force, is marked on the horizontal axis in Fig. 1.42(b) as shown, which constitutes the major axis of the ellipse.
4. The available cornering force F_y at a given slip angle, such as the 4° angle shown in Fig. 1.42(b), for any given tractive or braking force F_x is then determined from the following equation:

$$(F_y/F_{y4})^2 + (F_x/F_{x\,\max})^2 = 1 \tag{1.64}$$

The above equation describes an ellipse with the measured values of $F_{x\,\max}$ and F_{y4} as the major and minor axes, respectively.

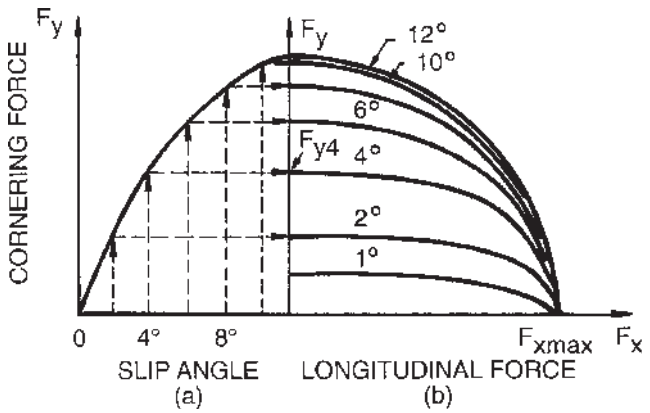

Fig. 1.42 Construction of a friction ellipse relating cornering force to longitudinal force for a given slip angle.

Following the procedure outlined above, the available cornering force at any slip angle in the presence of any given tractive or braking force can be determined, and a set of curves illustrating the relationships between he cornering force and the tractive (or braking) force at various slip angles can be plotted, as shown in Fig. 1.42(b). It is noted that for a given slip angle, the cornering force is reduced as a tractive (or braking) force is applied to the tire. This is consistent with the trends of the measured data shown in Figs. 1.39 and 1.40.

Based on the simplified theory for the relationship between the braking force and the longitudinal skid described in Section 1.3 and that between the cornering force and the slip angle described earlier in this section, another semiempirical method for predicting the braking force and cornering force in the presence of both the longitudinal skid and slip angle has been proposed [1.8]. In this method, it is assumed that when no sliding takes place, the braking force per unit contact length at a distance of x from the front contact point is given by (see Eqs. 1.20 and 1.31)

$$\frac{dF_x}{dx} = k_t x i_s/(1 - i_s) \tag{1.65}$$

where i_s is the longitudinal skid, as defined by Eq. 1.30.

If, at the same time, the tire develops a slip angle α, then due to the longitudinal skid, the tread in contact with the ground will be elongated at a rate equal to $1/(1 - i_s)$. As a result, the lateral deflection y' of a point on the tread in contact with the ground is given by (see Eq. 1.54)

$$y' = x \tan\alpha/(1 - i_s) \tag{1.66}$$

The corresponding lateral force per unit contact length is, therefore, expressed by (see Eq. 1.55)

$$\frac{dF_{y\alpha}}{dx} = k'_y x \tan\alpha/(1 - i_s) \tag{1.67}$$

Let p be the uniform normal pressure on the contact patch, b the contact width, and μ the coefficient of road adhesion. Then, based on the concept of friction ellipse described above, no sliding will take place at a point located at a distance of x from the front contact point if the resultant of the braking force and lateral force per unit contact length is less than a minimum value defined by the coefficient of road adhesion μ and the normal pressure p, that is,

$$\sqrt{[k_t x i_s/(1 - i_s)]^2 + [k'_y x \tan\alpha/(1 - i_s)]^2} = \mu p b = \frac{\mu W}{l_t} \tag{1.68}$$

where W is the normal load and l_t is the contact length of the tire.

This implies that if a point at a distance x from the front contact point is in the adhesion region, then x must be less than a characteristic length l_c, which defines the length of the adhesion region where no sliding between the tire tread and the ground takes place. The value of l_c in relation to the contact length l_t can be derived from Eq. 1.68, and is given by

$$\frac{l_c}{l_t} = \frac{\mu W(1-i_s)}{2\sqrt{(k_t l_t^2 i_s/2)^2 + (k_y' l_t^2 \tan\alpha/2)^2}}$$
$$= \frac{\mu W(1-i_s)}{2\sqrt{(C_s i_s)^2 + (C_\alpha \tan\alpha)^2}} \tag{1.69}$$

where $k_t l_t^2/2 = C_s$ and $k_y' l_t^2/2 = C_\alpha$, as described by Eqs. 1.33 and 1.57, respectively.

If $l_c/l_t \geq 1$, the entire contact patch is an adhesion region. The braking force is given by

$$F_x = \int_0^{l_t} [k_t x i_s/(1-i_s)]\, dx = k_t l_t^2 i_s/2(1-i_s)$$
$$= C_s i_s/(1-i_s) \tag{1.70}$$

and the cornering force $F_{y\alpha}$ as a function of slip angle α and skid i_s is expressed by

$$F_{y\alpha} = \int_0^{l_t} [k_y' x \tan\alpha/(1-i_s)]\ dx$$
$$= k_y' l_t^2 \tan\alpha/2(1-i_s)$$
$$= C_\alpha \tan\alpha/(1-i_s) \tag{1.71}$$

If $l_c/l_t < 1$, then sliding between the tread and the ground will take place. The braking force developed on the adhesion region F_{xa} is given by

$$F_{xa} = \int_0^{l_c} [k_t x i_s/(1-i_s)]\, dx$$
$$= \frac{\mu^2 W^2 C_s i_s(1-i_s)}{4[(C_s i_s)^2 + (C_\alpha \tan\alpha)^2]} \tag{1.72}$$

and the braking force developed on the sliding region F_{xs} is expressed by

$$F_{xs} = \frac{\mu W C_s i_s}{\sqrt{(C_s i_s)^2 + (C_\alpha \tan\alpha)^2}} \left[1 - \frac{\mu W(1-i_s)}{2\sqrt{(C_s i_s)^2 + (C_\alpha \tan\alpha)^2}}\right] \tag{1.73}$$

The total braking force F_x is given by

$$\begin{aligned} F_x &= F_{xa} + F_{xs} \\ &= \frac{\mu W C_s i_s}{\sqrt{(C_s i_s)^2 + (C_\alpha \tan\alpha)^2}} \left[1 - \frac{\mu W (1 - i_s)}{4\sqrt{(C_s i_s)^2 + (C_\alpha \tan\alpha)^2}} \right] \end{aligned} \tag{1.74}$$

Similarly, if sliding between the tread and the ground takes place, then the cornering force developed on the adhesion region is given by

$$\begin{aligned} F_{y\alpha a} &= \int_0^{l_c} [k_y' x \tan\alpha/(1 - i_s)] dx \\ &= \frac{\mu^2 W^2 C_\alpha \tan\alpha (1 - i_s)}{4[(C_s i_s)^2 + (C_\alpha \tan\alpha)^2]} \end{aligned} \tag{1.75}$$

and the cornering force developed on the sliding region is expressed by

$$F_{y\alpha s} = \frac{\mu W C_\alpha \tan\alpha}{\sqrt{(C_s i_s)^2 + (C_\alpha \tan\alpha)^2}} \left[1 - \frac{\mu W (1 - i_s)}{2\sqrt{(C_s i_s)^2 + (C_\alpha \tan\alpha)^2}} \right] \tag{1.76}$$

The total cornering force $F_{y\alpha}$ is given by

$$\begin{aligned} F_{y\alpha} &= F_{y\alpha a} + F_{y\alpha s} \\ &= \frac{\mu W C_\alpha \tan\alpha}{\sqrt{(C_s i_s)^2 + (C_\alpha \tan\alpha)^2}} \left[1 - \frac{\mu W (1 - i_s)}{4\sqrt{(C_s i_s)^2 + (C_\alpha \tan\alpha)^2}} \right] \end{aligned} \tag{1.77}$$

The parameters, μ, W, C_s, and C_α may change with operating conditions. For instance, it has been found that on a given surface, the values of μ, C_s, and C_α are functions of the normal load and operating speed of the tire. In a dynamic maneuver involving both braking and steering, the normal load and speed of the tires on a vehicle change as the maneuver proceeds. To achieve more accurate predictions, the effects of normal load and speed on the values of μ, C_s, C_α, and other tire parameters should be properly taken into account [1.8].

The semiempirical method for modeling tire behavior described above has been incorporated into a computer model for simulating the directional response and braking performance of commercial vehicles [1.8]. The method presented above is for predicting the braking force and cornering force of a tire during combined braking and cornering. Following the same approach, however, a method for predicting the tractive force and cornering force as functions of combined longitudinal slip and slip angle can be formulated.

Example 1.1. A truck tire $10 \times 20/F$ with a normal load of 24.15 kN (5430 lb) is traveling on a dry asphalt pavement with a coefficient of road adhesion $\mu = 0.85$. The cornering stiffness of the tire C_α is 133.30 kN/rad (523 lb/deg) and the longitudinal stiffness C_s is 186.82 kN/unit skid (42,000 lb/unit skid).

Estimate the braking force and the cornering force that the tire can develop at a slip angle $\alpha = 4^\circ$ and a longitudinal skid of 10%.

Solution. To determine whether sliding takes place on the tire contact patch under the given operating conditions, the ratio l_c/l_t is calculated using Eq. 1.69:

$$\frac{l_c}{l_t} = \frac{\mu W(1 - i_s)}{2\sqrt{(C_s i_s)^2 + (C_\alpha \tan\alpha)^2}}$$

$$= \frac{0.85 \times 24.15 \times (1 - 0.1)}{2\sqrt{186.82 \times 0.1)^2 + (133.30 \times 0.0699)^2}} = 0.442$$

Since $l_c/l_t < 1$, sliding takes place in part of the contact patch.

The braking force can be predicted using Eq. 1.74:

$$F_x = F_{xa} + F_{xs}$$

$$= \frac{\mu W C_s i_s}{\sqrt{(C_s i_s)^2 + (C_\alpha \tan\alpha)^2}} \left[1 - \frac{\mu W(1 - i_s)}{4\sqrt{(C_s i_s)^2 + (C_\alpha \tan\alpha)^2}}\right]$$

$$= \frac{0.85 \times 24.15 \times 186.82 \times 0.1}{\sqrt{(186.82 \times 0.1)^2 + (133.30 \times 0.0699)^2}}$$

$$\cdot \left[1 - \frac{0.85 \times 24.15 \times (1 - 0.1)}{4\sqrt{(186.82 \times 0.1)^2 + (133.30 \times 0.0699)^2}}\right.$$

$$= 14.30 \text{ kN } (3215 \text{ lb})$$

The cornering force can be predicted using Eq. 1.77:

$$F_{y\alpha} = F_{y\alpha a} + F_{y\alpha s}$$

$$= \frac{\mu W C_\alpha \tan\alpha}{\sqrt{(C_s i_s)^2 + (C_\alpha \tan\alpha)^2}} \left[1 - \frac{\mu W(1 - i_s)}{4\sqrt{(C_s i_s)^2 + (C_\alpha \tan\alpha)^2}}\right]$$

$$= \frac{0.85 \times 24.15 \times 133.30 \times 0.0699}{\sqrt{(186.82 \times 0.1)^2 + (133.30 \times 0.0699)^2}}$$

$$\cdot \left[1 - \frac{0.85 \times 24.15 \times (1 - 0.1)}{4\sqrt{(186.82 \times 0.1)^2 + (133.30 \times 0.0699)^2}}\right]$$

$$= 7.14 \text{ kN } (1605 \text{ lb})$$

In recent years, an empirical method for characterizing tire behavior known as the Magic Formula has been developed and used in vehicle handling simulations [1.24–1.27]. The Magic Formula, in its basic form, can be used to fit experimental tire data for characterizing the relationships between the cornering force and slip angle, self-aligning torque and slip angle, or braking effort and skid. It is expressed by [1.24–1.27]

$$y(x) = D \sin \{C \arctan [Bx - E(Bx - \arctan Bx)]\} \tag{1.78}$$

$$Y(X) = y(x) + S_v$$

$$x = X + S_h \tag{1.79}$$

where $Y(X)$ represents cornering force, self-aligning torque, or braking effort, and X denotes slip angle or skid. Coefficient B is called the stiffness factor, C the shape factor, D the peak factor, and E the curvature factor. S_h and S_v are the horizontal shift and vertical shift, respectively.

Equation 1.78 produces a curve that passes through the origin, $x = y = 0$, and reaches a maximum at $x = x_m$, as shown in Fig. 1.43. Beyond that it decreases and finally approaches an asymptote y_a. For given values of the coefficients, the curve shows an antisymmetric shape with respect to the origin, $x = y = 0$. To allow the curve to have an offset with respect to the origin, two shifts S_h and S_v are introduced, as shown in Fig. 1.43. Consequently, a new set of coordinates X and Y, representing cornering force, self-aligning torque, or braking effort and slip angle or skid, respectively, is established. This enables the effects of ply-steer, conicity, or rolling resistance

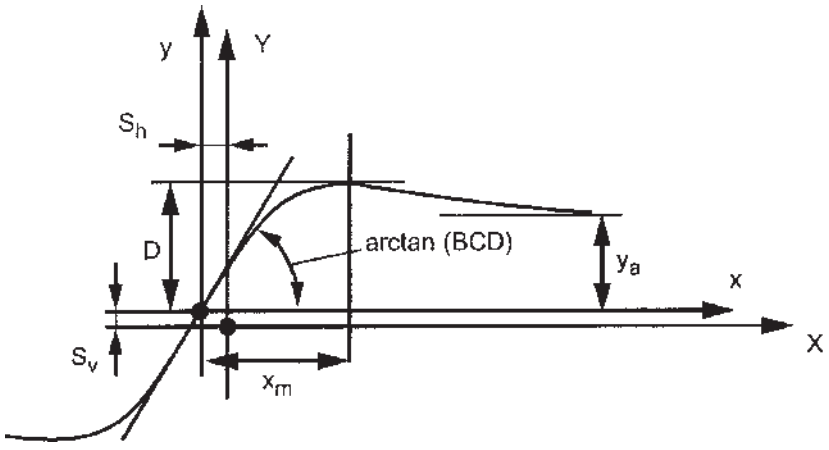

Fig. 1.43 Characteristics of the Magic Formula for fitting tire test data. (From Pacejka, H.B. and Besselink, I.J.M. (1997), *Proceedings of the 2nd International Colloquium on Tyre Models for Vehicle Dynamic Analysis,* pp. 234–249, © Swets & Zeitlinger. Used with permission.)

on cornering force, self-aligning torque, or braking effort to be taken into account.

Figure 1.43 illustrates the meaning of some of the coefficients in Eq. 1.78. For instance, if Fig. 1.43 represents the cornering force and slip angle relationship of a tire, then coefficient D represents the peak value with respect to x, y coordinates and the product BCD corresponds to the slope of the curve at the origin, representing the cornering stiffness of the tire, as defined by Eq. 1.37.

The Magic Formula is capable of producing characteristics that closely match measured data. Figures 1.44, 1.45, and 1.46 show a comparison of the experimental data and fitted curves using Eqs. 1.78 and 1.79 for the relationships of cornering force and slip angle, self-aligning torque and slip angle, and braking effort and skid of a passenger car tire, respectively [1.25].

As an example, the values of the coefficients in Eqs. 1.78 and 1.79 for predicting cornering force F_y, self-aligning torque, M_z, and braking effort F_x of a car tire are given in Table 1.6. In using the values of the coefficients in the table to predict the cornering force, self-aligning torque, and braking effort, the resulting values are in N, N·m, and N, respectively, and that the slip angle is in degrees and skid is defined by Eq. 1.30 and considered to be a negative value.

It is found that some of the coefficients in Eqs. 1.78 and 1.79 are functions of the normal load and/or camber angle of the tire [1.24]. For instance, peak factor D may be expressed as a function of normal load F_z as follows:

$$D = a_1 F_z^2 + a_2 F_z \tag{1.80}$$

where F_z is in kN, and a_1 and a_2 are empirical coefficients.

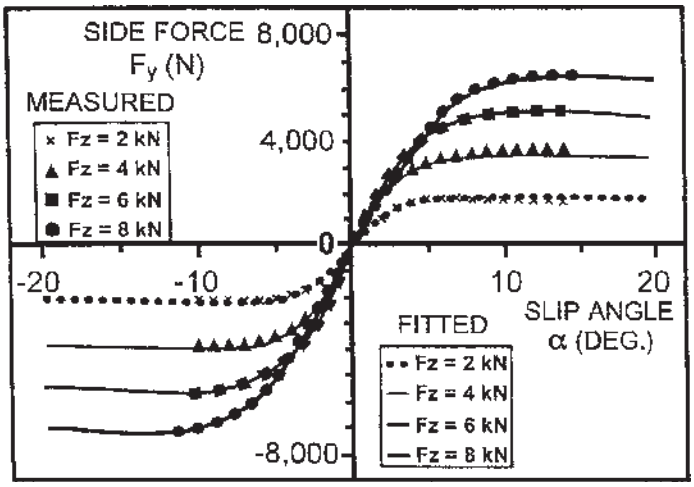

Fig. 1.44 Comparison of the measured and fitted relationships between side force and slip angle using the Magic Formula. (Reprinted with permission from SAE paper No. 890087 © 1989 Society of Automotive Engineers, Inc.)

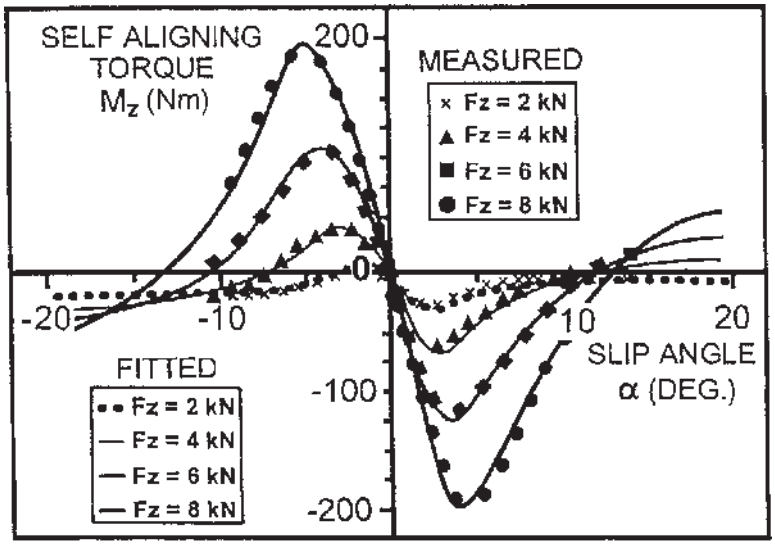

Fig. 1.45 Comparison of the measured and fitted relationships between self-aligning torque and slip angle using the Magic Formula. (Reprinted with permission from SAE paper No. 890087 © 1989 Society of Automotive Engineers, Inc.)

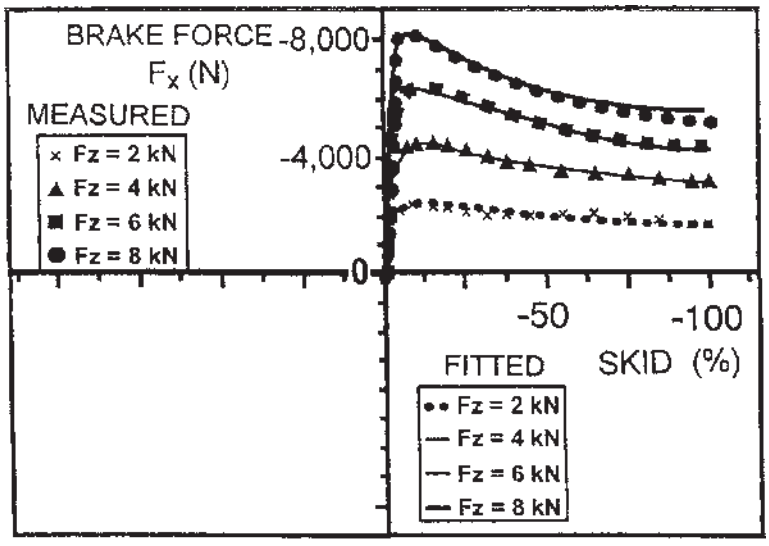

Fig. 1.46 Comparison of the measured and fitted relationships between braking force and skid using the Magic Formula. (Reprinted with permission from SAE paper No. 890087, © 1989 Society of Automotive Engineers, Inc.)

TABLE 1.6 Values of the Coefficients in the Magic Formula for a Car Tire (Slip Angle in Degrees and Skid in Minus %)

	Load, F_z, kN	B	C	D	E	S_h	S_v	BCD
F_y, N	2	0.244	1.50	1936	−0.132	−0.280	−118	780.6
	4	0.239	1.19	3650	−0.678	−0.049	−156	1038
	6	0.164	1.27	5237	−1.61	−0.126	−181	1091
	8	0.112	1.36	6677	−2.16	0.125	−240	1017
M_z, N · m	2	0.247	2.56	−15.53	−3.92	−0.464	−12.5	−9.820
	4	0.234	2.68	−48.56	−0.46	−0.082	−11.7	−30.45
	6	0.164	2.46	−112.5	−2.04	−0.125	−6.00	−45.39
	8	0.127	2.41	−191.3	−3.21	−0.009	−4.22	−58.55
F_x, N	2	0.178	1.55	2193	0.432	0.000	25.0	605.0
	4	0.171	1.69	4236	0.619	0.000	70.6	1224
	6	0.210	1.67	6090	0.686	0.000	80.1	2136
	8	0.214	1.78	7711	0.783	0.000	104	2937

Source: Reference 1.24.

For cornering stiffness (i.e., the initial slope of the cornering force–slip angle curve):

$$BCD = a_3 \sin[a_4 \arctan (a_5 F_z)] \tag{1.81}$$

where a_3, a_4, and a_5 are empirical coefficients.

For aligning stiffness (i.e., the initial slope of the self-aligning torque–slip angle curve) or longitudinal stiffness (i.e., the initial slope of the braking effort–skid curve):

$$BCD = \frac{a_3 F_z^2 + a_4 F_z}{e^{a_5 F_z}} \tag{1.82}$$

The shape factor C appears to be practically independent of F_z, and the average values for the particular car tire tested may be taken as follows (based on the data shown in Table 1.6):

For the cornering force–slip angle relationship, $C = 1.30$

For the self-aligning torque–slip angle relationship, $C = 2.40$

For the braking effort–skid relationship, $C = 1.65$

The stiffness factor B can be derived from

$$B = \frac{BCD}{CD} \tag{1.83}$$

TABLE 1.7 Values of Coefficients a_1 to a_8 for a Car Tire (F_z in kN)

	a_1	a_2	a_3	a_4	a_5	a_6	a_7	a_8
F_y, N	−22.1	1011	1078	1.82	0.208	0.000	−0.354	0.707
M_z, N · m	−2.72	−2.28	−1.86	−2.73	0.110	−0.070	0.643	−4.04
F_x, N	−21.3	1144	49.6	226	0.069	−0.006	0.056	0.486

Source: Reference 1.24.

The curvature factor E as a function of normal load F_z is given by

$$E = a_6 F_z^2 + a_7 F_z + a_8 \tag{1.84}$$

where a_6, a_7, and a_8 are empirical coefficients.

Table 1.7 gives the values of coefficients a_1 to a_8 for the same tire as in Table 1.6. It should be noted that in Eqs. 1.80–1.84, F_z is in kN.

Camber angle γ is found to have an influence on the relationships between cornering force and slip angle and self-aligning torque and slip angle, in the form of horizontal and vertical shifts, S_h and S_v [1.24]. The additional shifts due to camber angle γ may be expressed by

$$\begin{aligned} \Delta S_h &= a_9 \gamma \\ \Delta S_v &= (a_{10} F_z^2 + a_{11} F_z)\gamma \end{aligned} \tag{1.85}$$

where a_9, a_{10}, and a_{11} are empirical coefficients.

The change in stiffness factor ΔB is obtained by multiplying B by $(1 - a_{12}\ |\gamma|)$:

$$\Delta B = (1 - a_{12}|\gamma|)B \tag{1.86}$$

where a_{12} is an empirical coefficient.

The value of the self-aligning torque at high slip angles will change due to this change in stiffness factor B. To compensate for this effect, the curvature factor E for self-aligning torque M_z must be divided by $(1 - a_{13}\ |\gamma|)$.

The values of coefficients a_9 to a_{13} for the same tire as in Table 1.6 are given in Table 1.8.

TABLE 1.8 The Values of Coefficients a_9 to a_{13} for a Car Tire (Camber Angle in Degrees)

	a_9	a_{10}	a_{11}	a_{12}	a_{13}
F_y, N	0.028	0.000	14.8	0.022	0.000
M_z, kN	0.015	−0.066	0.945	0.030	0.070

Source: Reference 1.24.

When brakes are applied during a turning maneuver, the tires on a vehicle develop both slip angles and skids. Under these circumstances, Eqs. 1.78 and 1.79 are inadequate for characterizing tire behavior. To characterize the combined effects of slip angle and skid on the cornering force, self-aligning torque, or braking effort, empirical weighting functions G are introduced, which when multiplied by the original functions given in Eqs. 1.78 and 1.79 produce the interactive effects of skid on cornering force and self-aligning torque, or of slip angle on braking effort [1.26–1.28]. When the tire operates only with slip angle or skid, the weighting functions G take the value of one. However, when a tire operates under a given slip angle and at the same time its skid gradually increases, then the weighting function for cornering force F_y may first show a slight increase in magnitude, then reach its peak, followed by a continuous decrease. The weighting function G takes the following form:

$$G = D' \cos[C' \arctan\ (B'x)] \tag{1.87}$$

where B', C', and D' are empirical coefficients, and x is either slip angle or skid. For instance, if Eq. 1.87 represents the weighting function for determining the effect of skid on the cornering force F_y at a given slip angle, then x in Eq. 1.87 represents the skid of the tire. For details concerning the characterization of tire behavior under the combined effects of slip angle and skid, please refer to references 1.26–1.28.

The discussions presented above are for characterizing the steady-state cornering behavior of tires. When a vehicle is in transient motion, such as when the steering wheel angle and/or braking effort vary with time during a turning maneuver, the slip angle and/or skid of the tire is in a transient state. The equations given previously may be inadequate for characterizing the transient response of the tire. Studies on the transient cornering behavior of tires have been made [1.27, 1.29, 1.30].

Example 1.2. Using the Magic Formula, estimate the braking effort developed by a tire with a normal load of 6 kN (1349 lb), at a skid of −25%, and having empirical coefficients B, C, D, E, S_h, and S_v shown in Table 1.6.

Solution. For this case, the variables Y and X in the Magic Formula, Eqs. 1.78 and 1.79, represent the braking effort F_x and skid i_s, respectively. Note that skid i_s in the Magic Formula is expressed in percentage and considered to be a negative value and that the value of the arctan function should be expressed in radians.

$$F_x = D \sin\ [C \arctan\ (B(i_s + S_h) - E\{B(i_s + S_h) - \arctan\ [B(i_s + S_h)]\})] + S_v$$

Using the appropriate values of the empirical coefficients for a normal load of 6 kN (1349 lb) given in Table 1.6, the braking effort at a skid of −25% is calculated as follows:

$$\begin{aligned} F_x &= 6090 \sin [1.67 \arctan (0.210 (-25 + 0) - 0.686\{0.210(-25 + 0) \\ &\quad - \arctan [0.210(-25 + 0)]\})] \\ &\quad + 80.1 \\ &= 6090 \sin \{1.67 \arctan [-5.25 - 0.686(-5.25 + 1.3826)]\} \\ &\quad + 80.1 = -5433 \text{ N } (-1221 \text{ lb}) \end{aligned}$$

1.5 PERFORMANCE OF TIRES ON WET SURFACES

The behavior of tires on wet surfaces is of considerable interest from a vehicle safety point of view, as many accidents occur on slippery roads. The performance of tires on wet surfaces depends on the surface texture, water depth, tread pattern, tread depth, tread material, and operating mode of the tire (i.e., free-rolling, braking, accelerating, or cornering). To achieve acceptable performance on wet surfaces, maintaining effective contact between the tire tread and the road is of importance, and there is no doubt about the necessity of removing water from the contact area as much as possible.

To maintain effective contact between the tire and the road, the tire tread should have a suitable pattern to facilitate the flow of fluid from the contact area, and the surface of the pavement should have an appropriate texture to facilitate drainage as well. To provide good skid resistance, road surfaces must fulfill two requirements: an open macrotexture to facilitate gross draining, and microharshness to produce sharp points that can penetrate the remaining water film [1.31].

The effects of tread pattern and speed on the braking performance of tires on various wet surfaces have been studied experimentally by a number of investigators. Figures 1.47 and 1.48 show the variations of the peak values μ_p and the sliding values μ_s of the coefficient of road adhesion with speed for a smooth tire, a tire with ribs, and a tire with ribs and sipes on wet quartzite, asphalt, gravel, and concrete [1.31]. It can be seen that there is a marked difference in the coefficient of road adhesion between patterned tires, including the ribbed and siped tires, and smooth tires on wet asphalt and concrete surfaces. The tread pattern increases the value of the coefficient of road adhesion and reduces its speed dependency. In contrast, there is little pattern effect on wet quartzite surfaces, and a high level of road adhesion is maintained over the entire speed range. Thus, it can be concluded that the advantages of a patterned tire over a smooth tire are pronounced only on badly drained surfaces.

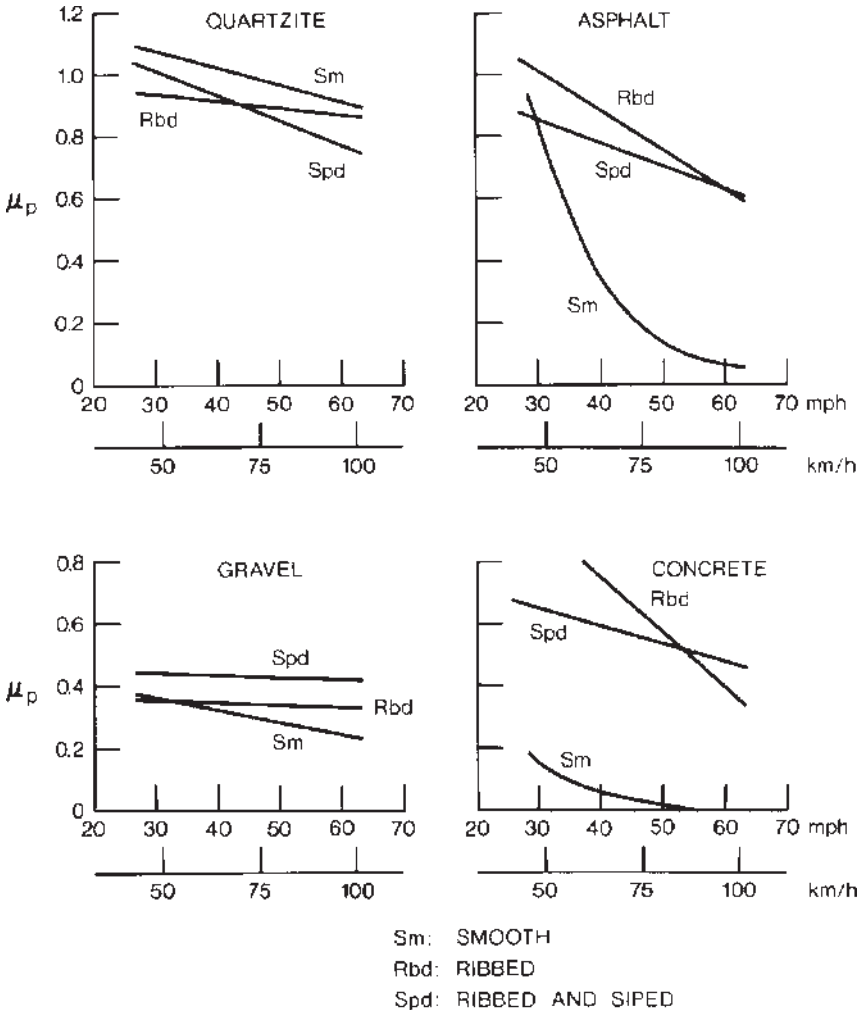

Fig. 1.47 Effect of tread design on the peak value of road adhesion coefficient μ_p over wet surfaces. (Reproduced with permission from *Mechanics of Pneumatic Tires,* edited by S.K. Clark, Monograph 122, National Bureau of Standards, 1971.)

Tread pattern can function satisfactorily on a wet road only when the grooves and sipes constitute a reservoir of sufficient capacity, and its effectiveness decreases with the wear of the tread or the tread depth. The decline in value of the coefficient of road adhesion with the decrease of tread depth is more pronounced on smooth than on rough roads, as rough roads can provide better drainage.

When a pneumatic tire is braked over a flooded surface, the motion of the tire creates hydrodynamic pressure in the fluid. The hydrodynamic pressure

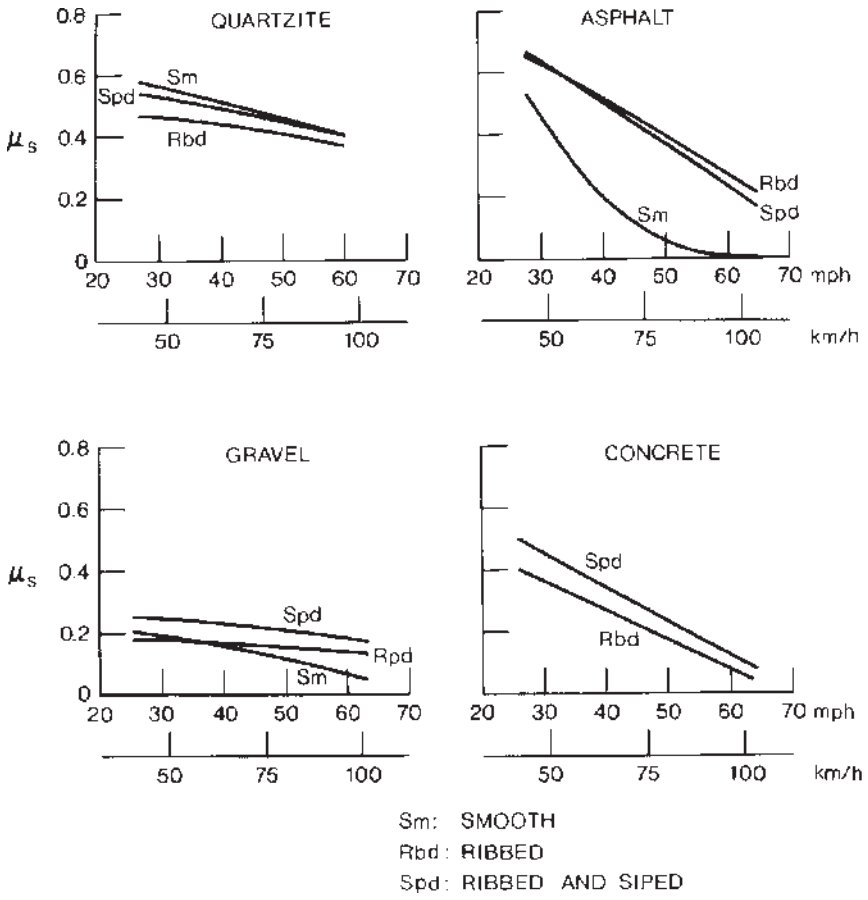

Fig. 1.48 Effect of tread design on the sliding value of road adhesion coefficient μ_s over wet surfaces. (Reproduced with permission from *Mechanics of Pneumatic Tires,* edited by S.K. Clark, Monograph 122, National Bureau of Standards, 1971.)

acting on the tire builds up as the square of speed of the tire, and tends to separate the tire from the ground. At low speeds, the front part of the tire rides on a wedge or a film of fluid. This fluid film extends backward into the contact area as the speed of the tire increases. At a particular speed, the hydrodynamic lift developed under the tire equals the vertical load, the tire rides completely on the fluid, and all contact with the ground is lost. This phenomena is usually referred to as "hydroplaning" and is illustrated in Fig. 1.49 [1.32].

For smooth or close-patterned tires that do not provide escape paths for water and for patterned tires on flooded surfaces with a fluid depth exceeding the groove depth in the tread, the speed at which hydroplaning occurs may be determined based on the theory of hydrodynamics. It can be assumed

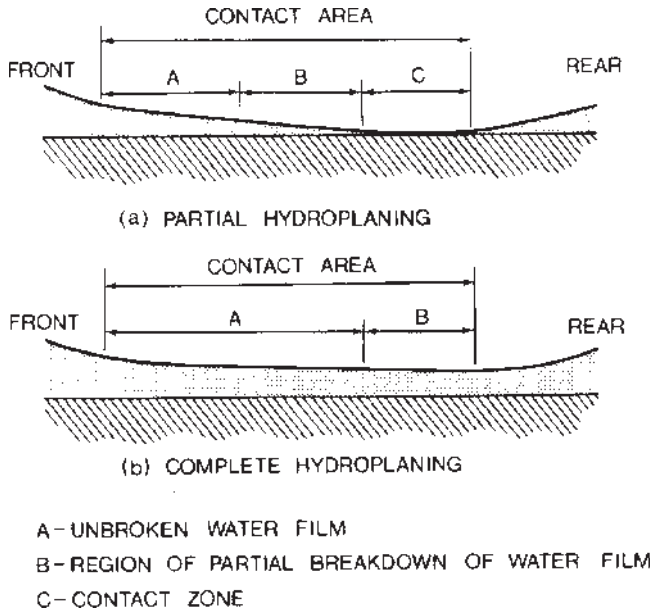

Fig. 1.49 Hydroplaning of a tire on flooded surfaces. (Reproduced with permission from *Mechanics of Pneumatic Tires,* edited by S.K. Clark, Monograph 122, National Bureau of Standards, 1971.)

that the lift component of the hydrodynamic force F_h is proportional to the tire–ground contact area A, fluid density ρ_f, and the square of the vehicle speed V [1.33, 1.34]:

$$F_h \propto \rho_f A V^2 \tag{1.88}$$

When hydroplaning occurs, the lift component of the hydrodynamic force is equal to the vertical load acting on the tire. The speed at which hydroplaning begins, therefore, is proportional to the square root of the nominal ground contact pressure W/A, which is proportional to the inflation pressure of the tire p_i. Based on this reasoning and on experimental data shown in Fig. 1.50 [1.34], the following formula was proposed by Horne and Joyner for predicting the hydroplaning speed V_p:

$$V_p = 10.35\sqrt{p_i}\,\text{mph} \tag{1.89}$$

or

$$V_p = 6.34\sqrt{p_i}\,\text{km/h} \tag{1.90}$$

where p_i is the inflation pressure of the tire in psi for Eq. 1.89 and in kPa for Eq. 1.90.

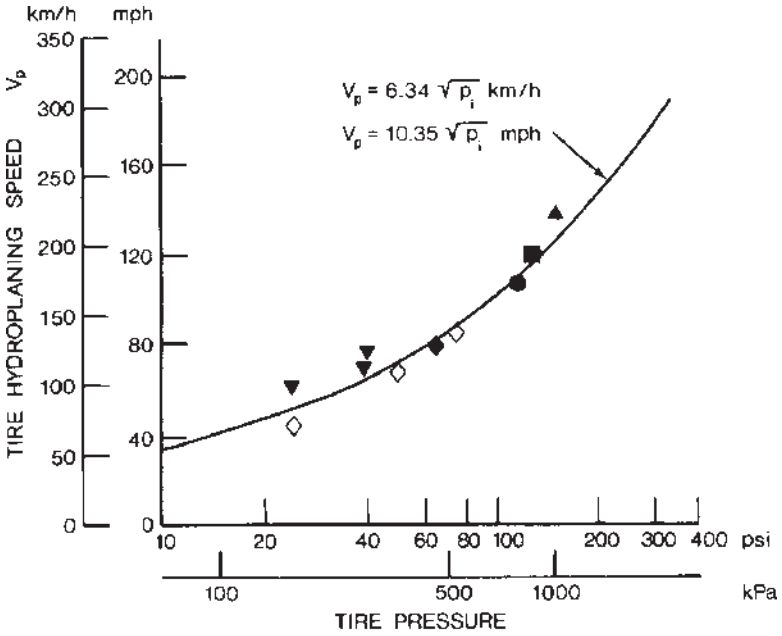

TIRE	LOAD PER TIRE lb	kN	VEHICLE
● 32 × 8.8 VII	9400	41.8	AIRCRAFT
■ 44 × 13.0 VII	22,000	97.8	AIRCRAFT
◆ 17.0–20 III	10,000	44.5	C–123
4.9 in. × 17 in.			AIRCRAFT
124 mm × 432 mm			
▲ 39 × 13 VII	17,300	76.9	880 JET
◇ 12.50–16	5600	24.9	FOUR WHEEL
38 in. × 12.5 in.			BOGIE
965 mm × 318 mm			
▼ 6.70 – 15	925	4.1	AUTOMOBILE

Fig. 1.50 Variation of hydroplaning speed with inflation pressure of tires. (Reproduced with permission of the Society of Automotive Engineers from reference 1.34.)

For passenger car tires, the inflation pressure is usually in the range 193–248 kPa (28–36 psi). According to Eq. 1.90, the hydroplaning speed V_p for a tire at an inflation pressure of 193 kPa (28 psi) is approximately 88 km/h (54.7 mph), which is well within the normal operating range for passenger cars. For heavy trucks, the inflation pressure is usually in the range 620–827 kPa (90–120 psi). From Eq. 1.90, the hydroplaning speed V_p for a tire at an inflation pressure of 620 kPa (90 psi) is approximately 158 km/h (98 mph), which is beyond the normal range of operating speed for heavy trucks. This would suggest that hydroplaning may not be possible for heavy truck tires

under normal circumstances. However, the tractive performance of truck tires is still significantly influenced by the presence of fluid on wet pavements.

For patterned tires on wet surfaces where the fluid depth is less than the groove depth of the tread, the prediction of the hydroplaning speed is more complex, and a generally accepted theory has yet to be evolved. The parameters found to be of significance to hydroplaning are pavement surface texture, pavement fluid depth, fluid viscosity, fluid density, tire inflation pressure, tire normal load, tire tread pattern, and tire tread depth.

The most important effect of hydroplaning is the reduction in the coefficient of road adhesion between the tire and the ground. This affects braking, steering control, and directional stability. Figure 1.51 shows the degradation of the

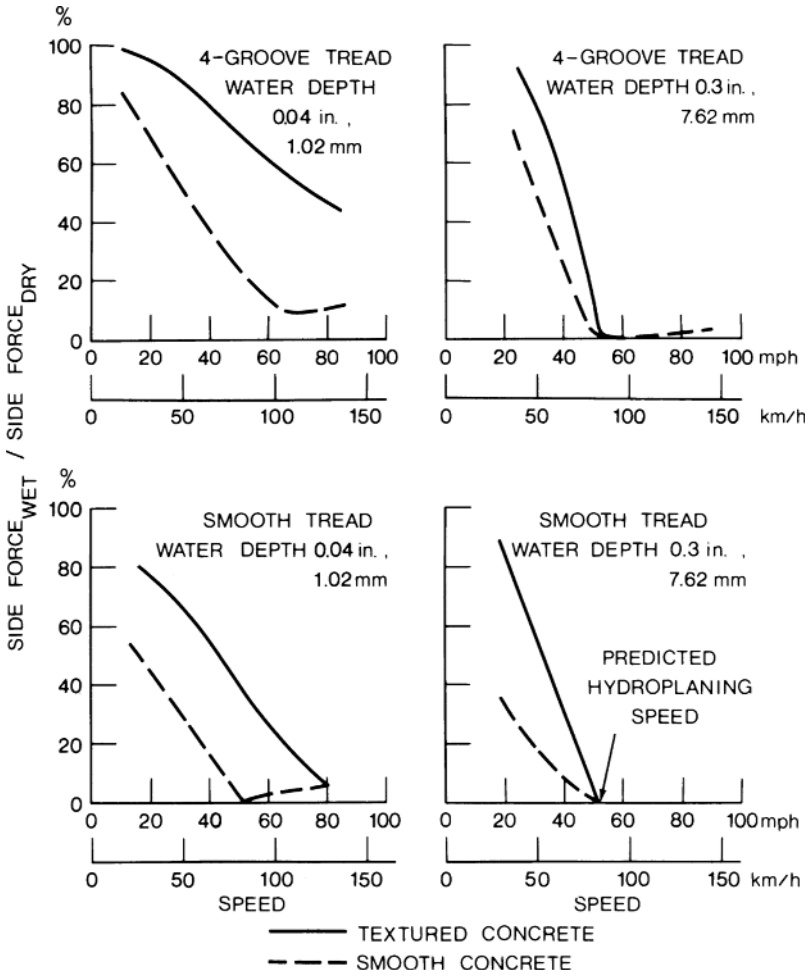

Fig. 1.51 Effect of tread design and surface conditions on the degradation of cornering capability of tires on wet surfaces. (Reproduced with permission of the Society of Automotive Engineers from reference 1.34.)

cornering force of passenger car tires on two different wet surfaces at various speeds [1.33].

Because of the difference in design priorities, a noticeable difference in traction on wet pavements between truck and passenger car tires is observed. Figure 1.52 shows a comparison of the peak value μ_p and sliding value μ_s of the coefficient of road adhesion on wet pavements of a sample of three radial-ply truck tires and a corresponding sample of radial-ply passenger car tires with different tread depths [1.8]. It can be seen that the tractive performance of the truck tires tested is substantially poorer than that of the passenger car tires.

In the design of heavy truck tires, greater emphasis is placed on tread life. As a result, tread patterns and tread compounds for truck tires are different from those for passenger car tires. For instance, natural rubber as the base polymer for the tread is widely used for truck tires, whereas synthetic rubber-based compounds are universally adopted for passenger car tires. As mentioned previously, while natural rubber compounds offer higher abrasion resistance and lower hysteresis losses, synthetic rubber compounds provide a fundamentally higher value of coefficient of road adhesion, particularly on wet pavements. The substantial difference in tractive performance between car and truck tires results in a significant difference in stopping distance. For instance, it has been reported that on a wet, slippery road, the stopping distance for a heavy truck with tires ranging from the best available to the worst, but of a fairly typical type could be 1.65–2.65 times longer than that of a passenger car with normal high-grip tires [1.1].

1.6 RIDE PROPERTIES OF TIRES

Supporting the weight of the vehicle and cushioning it over surface irregularities are two of the basic functions of a pneumatic tire. When a normal load is applied to an inflated tire, the tire progressively deflects as the load increases. Figure 1.53 shows the static load–deflection relationship for a 5.60 $\times$ 13 bias-ply tire at various inflation pressures [1.35]. The type of diagram shown in Fig. 1.53 is usually referred to as a lattice plot, in which the origin of each load–deflection curve is displaced along the deflection axis by an amount proportional to the inflation pressure. The relationship between the load and the inflation pressure for constant deflection can also be shown in the lattice plot. Figure 1.54 shows the interrelationship among the static load, inflation pressure, and deflections for a 165 $\times$ 13 radial-ply passenger car tire. The lattice plots of the load–deflection data at various inflation pressures for tractor tires 11-36 and 7.50-16 are shown in Figs. 1.55 and 1.56, respectively [1.36]. The load–deflection curves at various inflation pressures for a terra tire 26 $\times$ 12.00-12 are shown in Fig. 1.57. The vertical load–deflection curves are useful in estimating the static vertical stiffness of tires.

In vehicle vibration analysis and ride simulation, the cushioning characteristics of a pneumatic tire may be represented by various mathematical

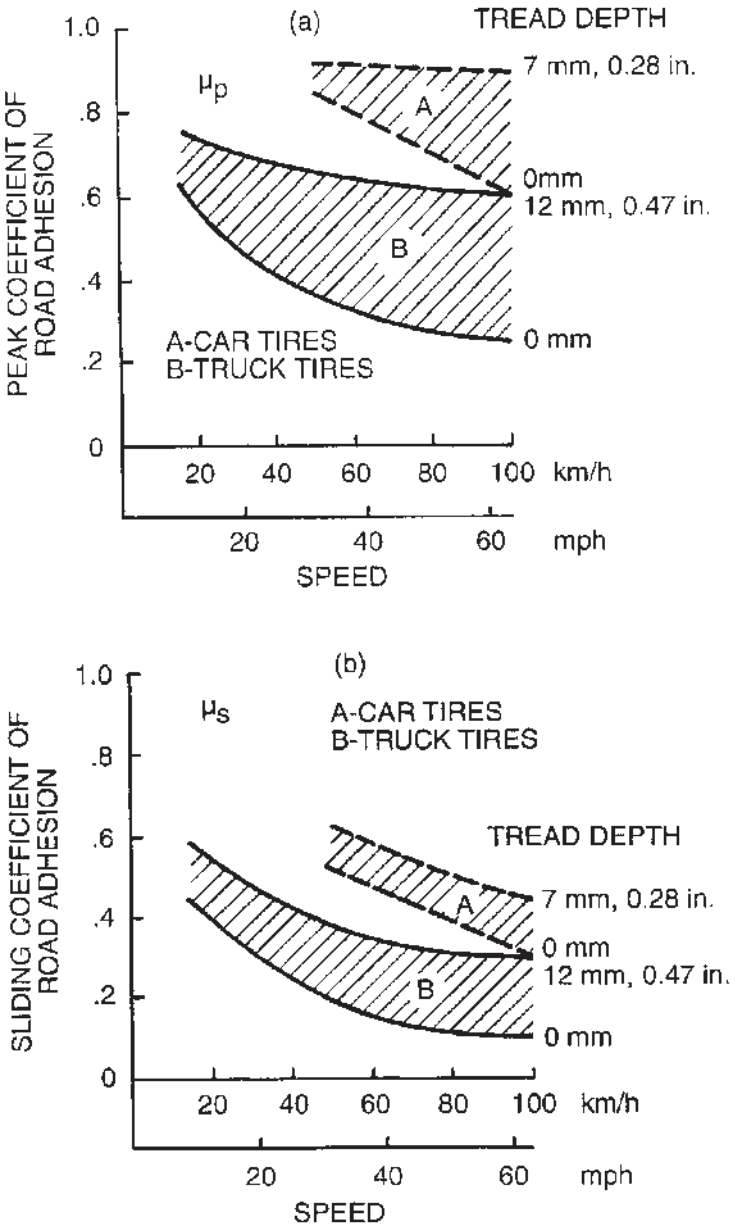

Fig. 1.52 Comparison of (a) the peak value of road adhesion coefficient μ_p and (b) the sliding value of road adhesion coefficient μ_s of car and truck tires on wet surfaces. (Reproduced with permission from reference 1.8.)

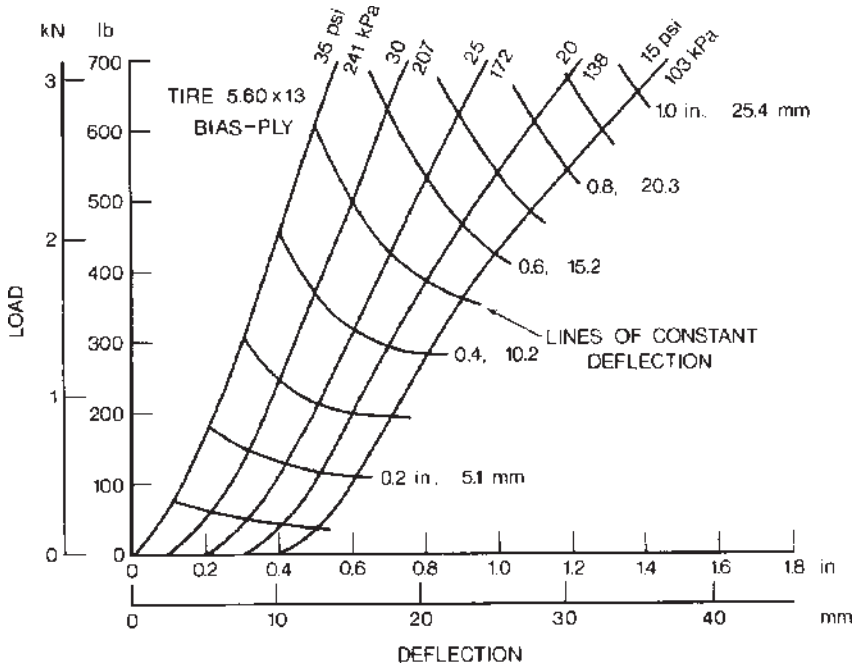

Fig. 1.53 Static load–deflection relationship of a bias-ply car tire. (Reproduced with permission of the Council of the Institution of Mechanical Engineers from reference 1.35.)

models. The most widely used and simplest model representing the fundamental mode of vibration of the pneumatic tire consists of a mass element and a linear spring in parallel with a viscous damping element, as shown in Fig. 1.58. Other models, such as the so-called "viscoelastic" model shown in Fig. 1.58, have also been proposed.

Depending upon the test conditions, three distinct types of tire vertical stiffness may be defined: static, nonrolling dynamic, and rolling dynamic stiffness.

Static Stiffness The static vertical stiffness of a tire is determined by the slope of the static load–deflection curves, such as those shown in Figs. 1.53–1.57. For a given inflation pressure, the load–deflection characteristics for both radial- and bias-ply tires are more or less linear, except at relatively low values of load. Consequently, it can be assumed that the tire vertical stiffness is independent of load in the range of practical interest. Figure 1.59 shows the variation of the stiffness with inflation pressure for the 165 × 13 radial-ply tire. The values of stiffness shown are derived from the load–deflection curves shown in Fig. 1.54 [1.35]. The values of the static vertical stiffness of the tractor tires 11-36 and 7.5-16, and those of the terra tire 26 × 12.00-12 at various inflation pressures are given in Table 1.9.

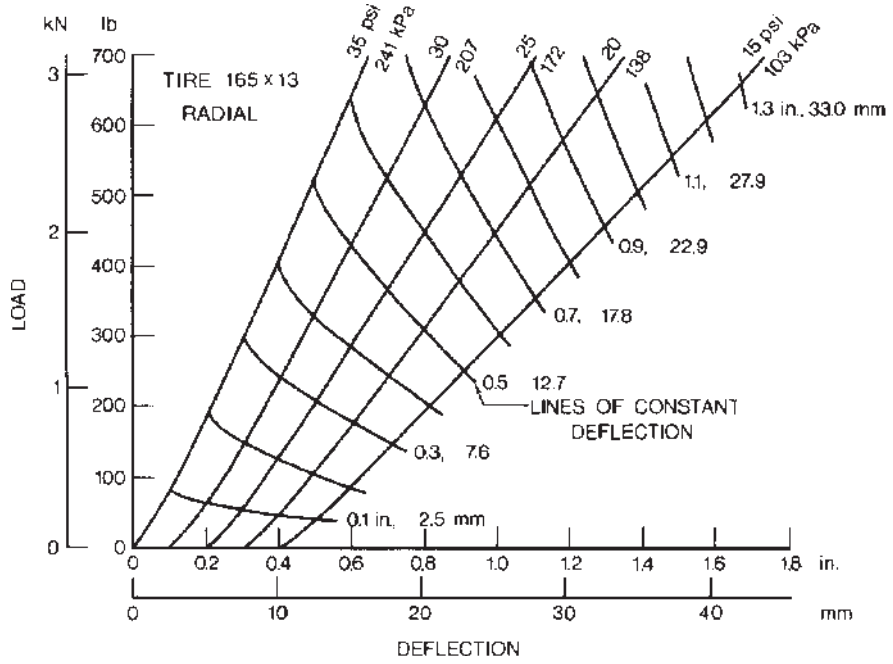

Fig. 1.54 Static load–deflection relationship of a radial-ply car tire. (Reproduced with permission of the Council of the Institution of Mechanical Engineers from reference 1.35.)

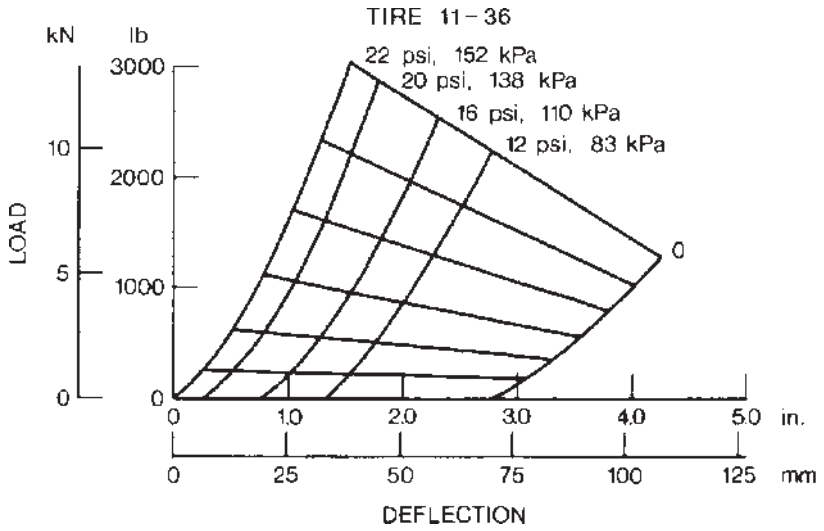

Fig. 1.55 Static load–deflection relationship of a tractor tire 11-36. (Reproduced with permission of the *Journal of Agricultural Engineering Research* from reference 1.36.)

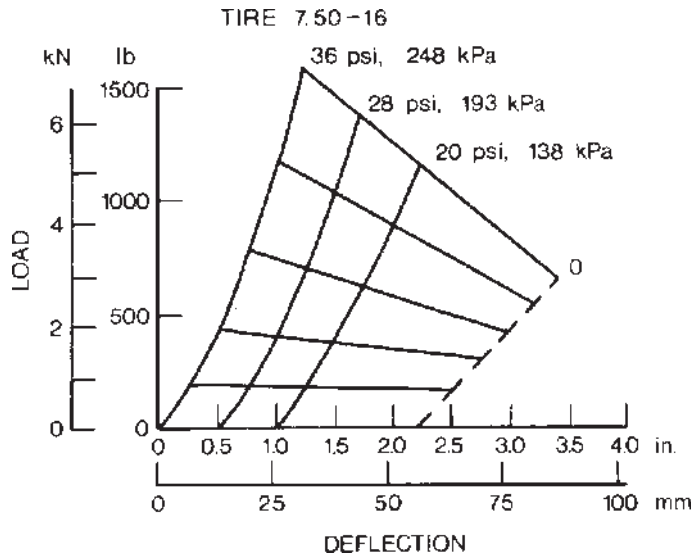

Fig. 1.56 Static load–deflection relationship of a tractor tire 7.50-16. (Reproduced with permission of the *Journal of Agricultural Engineering Research* from reference 1.36.)

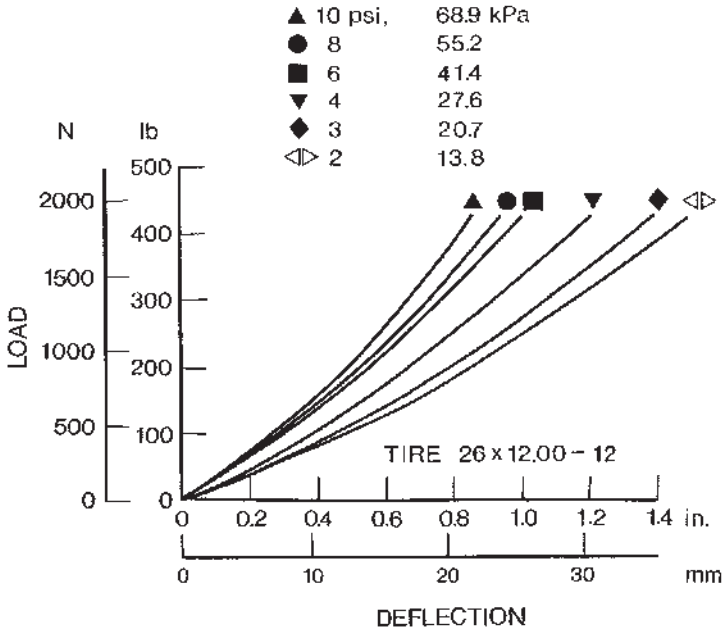

Fig. 1.57 Static load–deflection relationship of a terra tire 26 × 12.00-12 for all-terrain vehicles.

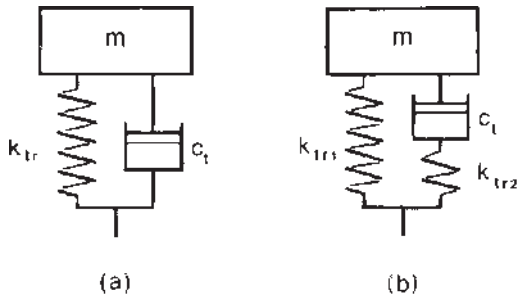

Fig. 1.58 (a) A linear model and (b) a viscoelastic model for tire vibration analysis.

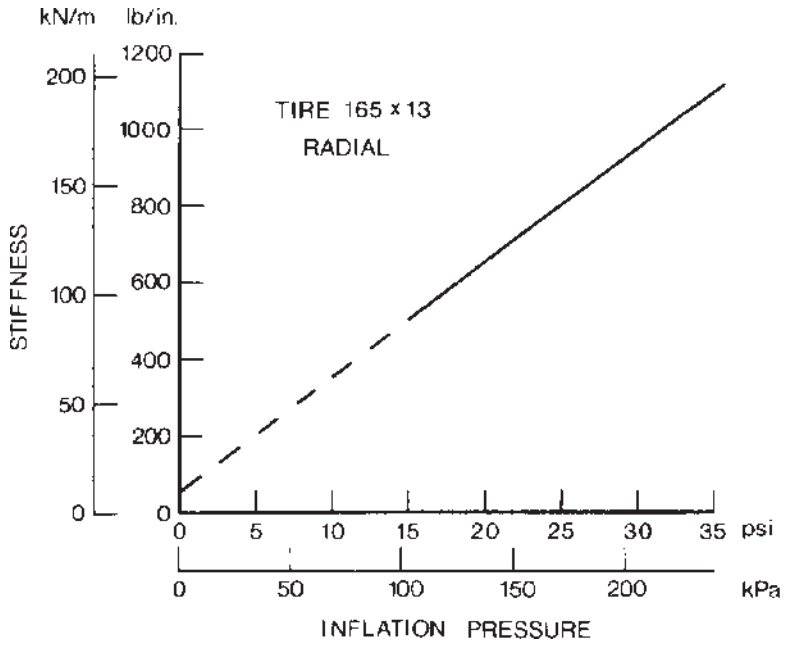

Fig. 1.59 Variation of static stiffness with inflation pressure for a radial-ply car tire. (Reproduced with permission of the Council of the Institution of Mechanical Engineers from reference 1.35.)

Nonrolling Dynamic Stiffness The dynamic stiffness of a nonrolling tire may be obtaining using various methods. One of the simplest is the so-called drop test. In this test, the tire with a certain load is allowed to fall freely from a height at which the tire is just in contact with the ground. Consequently, the tire remains in contact with the ground throughout the test. The transient response of the tire is recorded. A typical amplitude decay trace

TABLE 1.9 Vertical Stiffness of Off–road Tires

Tire	Inflation pressure	Load	Static stiffness	Nonrolling dynamic stiffness (average)	Damping coefficient
11-36 (4-ply)	82.7 kPa (12 psi)	6.67 kN (1500 lb)	357.5 kN/m (24,500 lb/ft)	379.4 kN/m (26,000 lb/ft)	2.4 kN·s/m (165 lb·s/ft)
		8.0 kN (1800 lb)	357.5 kN/m (24,500 lb/ft)	394.0 kN/m (27,000 lb/ft)	2.6 kN·s/m (180 lb·s/ft)
		9.34 kN (2100 lb)	—	423.2 kN/m (29,000 lb/ft)	3.4 kN·s/m (230 lb·s/ft)
	110.3 kPa (16 psi)	6.67 kN (1500 lb)	379.4 kN/m (26,000 lb/ft)	394.0 kN/m (27,000 lb/ft)	2.1 kN·s/m (145 lb·s/ft)
		8.0 kN (1800 lb)	386.7 kN/m (26,500 lb/ft)	437.8 kN/m (30,000 lb/ft)	2.5 kN·s/m (175 lb·s/ft)
		9.34 kN (2100 lb)	394.0 kN/m (27.000 lb/ft)	423.2 kN/m (29,000 lb/ft)	2.5 kN·s/m (175 lb·s/ft)
7.5-16 (6-ply)	138 kPa (20 psi)	3.56 kN (800 lb)	175.1 kN/m (12,000 lb/ft)	218.9 kN/m (15,000 lb/ft)	0.58 kN·s/m (40 lb·s/ft)
		4.45 kN (1000 lb)	175.1 kN/m (12,000 lb/ft)	233.5 kN/m (16,000 lb/ft)	0.66 kN·s/m (45 lb·s/ft)
		4.89 kN (1100 lb)	182.4 kN/m (12,500 lb/ft)	248.1 kN/m (17,000 lb/ft)	0.80 kN·s/m (55 lb·s/ft)
	193 kPa (28 psi)	3.56 kN (800 lb)	218.9 kN/m (15,000 lb/ft)	233.5 kN/m (16,000 lb/ft)	0.36 kN·s/m (25 lb·s/ft)
		4.45 kN (1100 lb)	226.2 kN/m (15,500 lb/ft)	262.7 kN/m (18,000 lb/ft)	0.66 kN·s/m (45 lb·s/ft)
		4.89 kN (1300 lb)	255.4 kN/m (17,500 lb/ft)	277.3 kN/m (19,000 lb/ft)	0.73 kN·s/m (50 lb·s/ft)
26 × 12.00-12 (2-ply)	15.5 kPa (2.25 psi)	1.78 kN (400 lb)	51.1 kN/m (3500 lb/ft)	—	0.47 kN·s/m (32 lb·s/ft)
	27.6 kPa (4 psi)	1.78 kN (400 lb)	68.6 kN/m (4700 lb/ft)	—	0.49 kN·s/m (34 lb·s/ft)

Source: Reference 1.36.

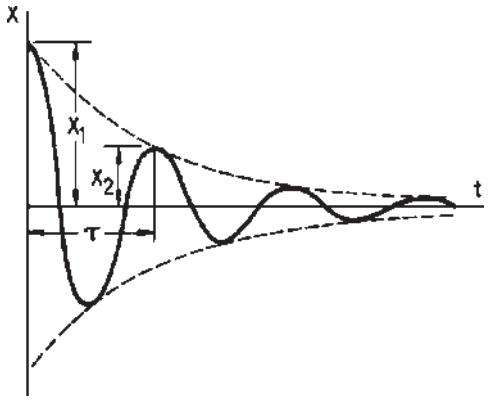

Fig. 1.60 An amplitude decay record of a nonrolling tire obtained from a drop test.

is shown in Fig. 1.60. The values of the equivalent viscous damping coefficient c_{eq} and the dynamic stiffness k_z of the tire can then be determined from the decay trace using the well-established theory of free vibration for a single-degree-of-freedom system:

$$c_{\text{eq}} = \sqrt{\frac{4m^2\omega_d^2\delta^2/(\delta^2 + 4\pi^2)}{1 - [\delta^2/(\delta^2 + 4\pi^2)]}} \tag{1.91}$$

and

$$k_z = \frac{m\omega_d^2}{1 - \delta^2/(\delta^2 + 4\pi^2)} \tag{1.92}$$

ω_d is the damped natural frequency of the tire with mass m, and can be identified from the amplitude decay trace shown in Fig. 1.60:

$$\omega_d = 2\pi/\tau \tag{1.93}$$

where τ is the period of damped oscillation shown in Fig. 1.60.

δ is the logarithmic decrement, which is defined as the natural logarithm of the ratio of any two successive amplitudes, such as x_1 and x_2, shown in Fig. 1.60:

$$\delta = \ln(x_1/x_2) \tag{1.94}$$

The drop test may also be performed utilizing a tire endurance testing machine consisting of a beam pivoted at one end, which carries the test tire loaded against a drum. To initiate the test, the beam is displaced and the

TABLE 1.10 Damping Coefficient of Car Tires

Tire	Inflation pressure	Damping coefficient
Bias-ply	103.4 kPa (15 psi)	4.59 kN·s/m (315 lb·s/ft)
5.60 × 13	137.9 kPa (20 psi)	4.89 kN·s/m (335 lb·s/ft)
	172.4 kPa (25 psi)	4.52 kN·s/m (310 lb·s/ft)
	206.9 kPa (30 psi)	4.09 kN·s/m (280 lb·s/ft)
	241.3 kPa (35 psi)	4.09 kN·s/m (280 lb·s/ft)
Radial-ply	103.4 kPa (15 psi)	4.45 kN·s/m (305 lb·s/ft)
165 × 13	137.9 kPa (20 psi)	3.68 kN·s/m (252 lb·s/ft)
	172.4 kPa (25 psi)	3.44 kN·s/m (236 lb·s/ft)
	206.9 kPa (30 psi)	3.43 kN·s/m (235 lb·s/ft)
	241.3 kPa (35 psi)	2.86 kN·s/m (196 lb·s/ft)

Source: Reference 1.35.

system is set in angular oscillation about the pivot of the beam. A decay trace for the amplitude of angular displacement is recorded. A set of equations for this torsional system, similar to that for a single-degree-of-freedom linear system described above, can be derived for determining the equivalent damping coefficient and nonrolling dynamic stiffness for the tire from the decay trace.

Table 1.9 shows the values of the nonrolling dynamic stiffness and the damping coefficient for the tractor tires 11-36 and 7.5-16 [1.36], and the damping coefficient for the terra tire 26 × 12.00-12. The values of the damping coefficient for the 5.60 × 13 bias-ply and the 165 × 13 radial-ply car tires are given in Table 1.10 [1.35].

Rolling Dynamic Stiffness The rolling dynamic stiffness is usually determined by measuring the response of a rolling tire to a known harmonic excitation. The response is normally measured at the hub, and the excitation is given at the tread. By examining the ratio of output to input and the phase angle, it is possible to determine the dynamic stiffness and the damping coefficient of a rolling tire.

An alternative method for determining the dynamic stiffness of a tire is to measure its resonant frequency when rolling on a drum or belt. Figure 1.61 shows the values of the dynamic stiffness for various types of car tire obtained using this method [1.6]. It is shown that the dynamic stiffness of car tires decreases sharply as soon as the tire is rolling. However, beyond a speed of approximately 20 km/h (12 mph), the influence of speed becomes less important.

Table 1.11 shows the values of vertical stiffness of a sample of truck tires at rated loads and inflation pressures [1.19]. They were obtained when the tires were rolling at a relatively low speed. Values of the vertical stiffness for the truck tires tested range from 764 to 1024 kN/m (4363 to 5850 lb/in.), and that the vertical stiffness of radial-ply truck tires is generally lower than that of bias-ply tires of similar size.

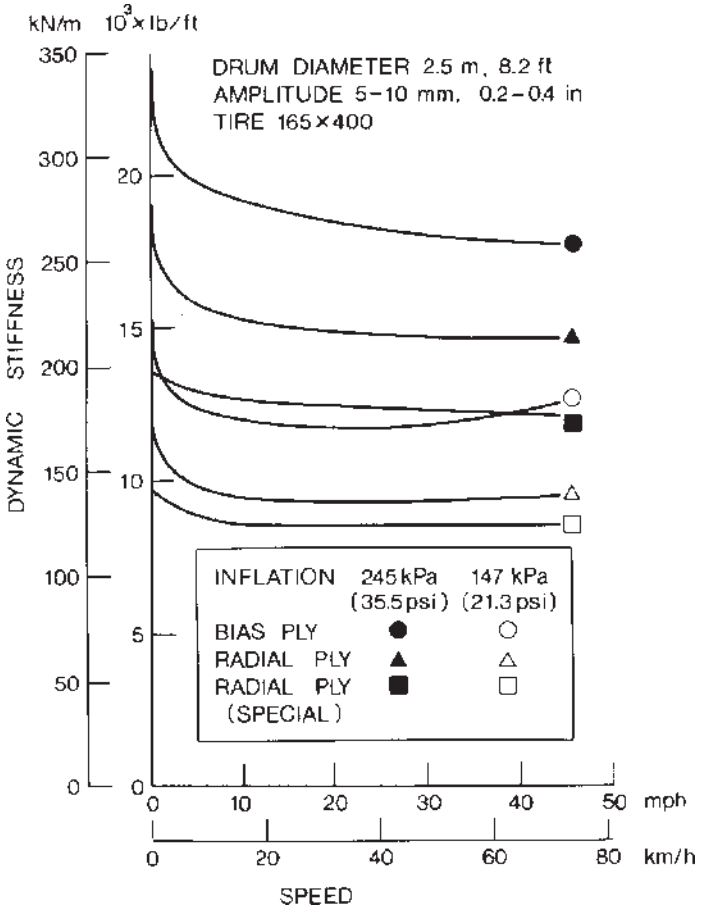

Fig. 1.61 Effect of speed on rolling dynamic stiffness of car tires. (Reproduced with permission from *Mechanics of Pneumatic Tires*, edited by S.K. Clark, Monograph 122, National Bureau of Standards, 1971.)

Figure 1.62 shows the variation of the dynamic stiffness of a 13.6 × 38 radial tractor tire with speed [1.37]. The static load on the tire was 18.25 kN (4092 lb), and the inflation pressure was 138 kPa (20 psi). The dynamic stiffness of the tractor tire decreases sharply as soon as the tire begins rolling, similar to that for passenger car tires shown in Fig. 1.61. The effects of inflation pressure on the dynamic stiffness of the same tire are shown in Fig. 1.63. The variation of the damping coefficient with speed for the tractor tire is shown in Fig. 1.64. It can be seen that beyond a speed of 1 km/h (0.6 mph), the damping coefficient drops rapidly until a speed of 5 km/h (3.1 mph) is reached, and then approaches an asymptote. The effects of inflation pressure on the damping coefficient are shown in Fig. 1.65.

TABLE 1.11 Vertical Stiffness of Truck Tires at Rated Loads and Inflation Pressures

Tire type	Tire construction	Vertical stiffness kN/m	Vertical stiffness lb/in.
Unspecified 11.00-22/G	Bias-ply	1024	5850
Unspecified 11.00-22/F	Bias-ply	977	5578
Unspecified 15.00 × 22.5/H	Bias-ply	949	5420
Unspecified 11.00-20/F	Bias-ply	881	5032
Michelin Radial 11 R22.5 XZA (1/3 tread)	Radial-ply	874	4992
Michelin Radial 11 R22.5 XZA (1/2 tread)	Radial-ply	864	4935
Michelin Radial 11 R22.5 XZA	Radial-ply	831	4744
Unspecified 10.00-20/F	Bias-ply	823	4700
Michelin Radial 11 R22.5 XZA	Radial-ply	809	4622
Michelin Pilote 11/80 R22.5 XZA	Radial-ply	808	4614
Unspecified 10.00-20/F	Bias-ply	788	4500
Michelin Pilote 11/80 R22.5 XZA	Radial-ply	774	4418
Unspecified 10.00-20/G	Bias-ply	764	4363

Source: UMTRI, reference 1.19.

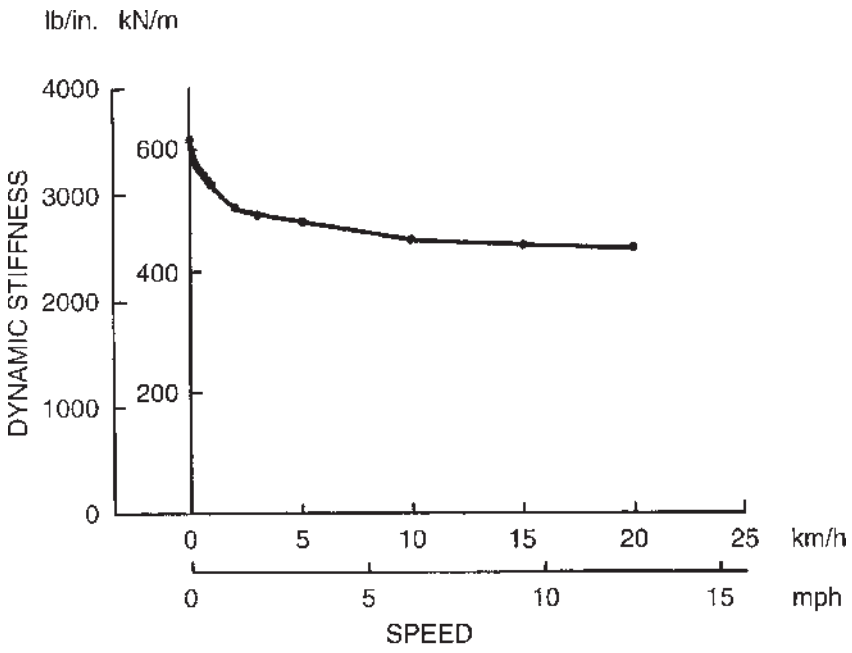

Fig. 1.62 Effect of speed on rolling dynamic stiffness of a radial-ply tractor tire 13.6 × 38. (Reproduced with permission from reference 1.37.)

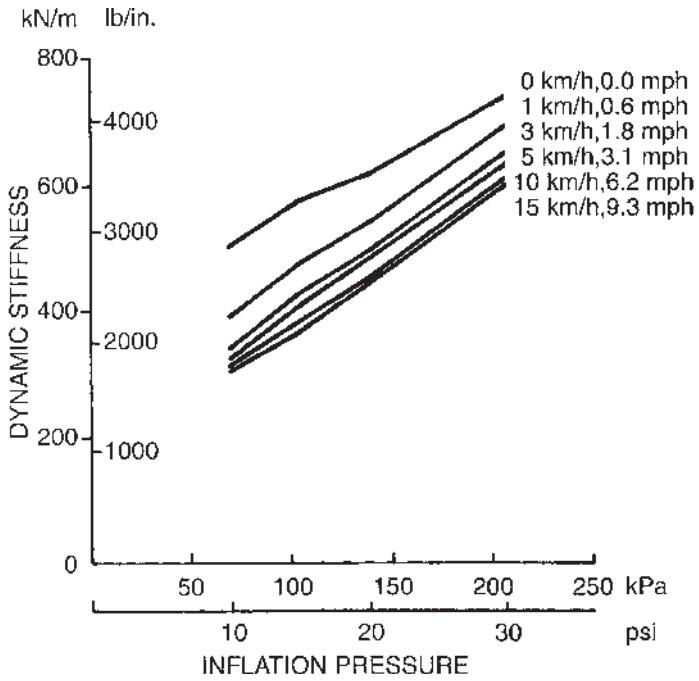

Fig. 1.63 Effect of inflation pressure on rolling dynamic stiffness at various speeds of a radial-ply tractor tire 13.6 × 38. (Reproduced with permission from reference 1.37.)

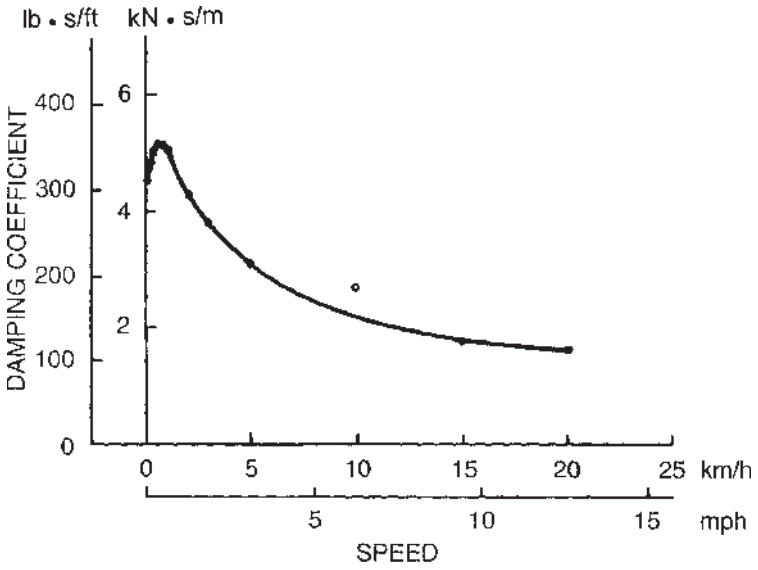

Fig. 1.64 Effect of speed on damping coefficient of a radial-ply tractor tire 13.6 × 38. (Reproduced with permission from reference 1.37.)

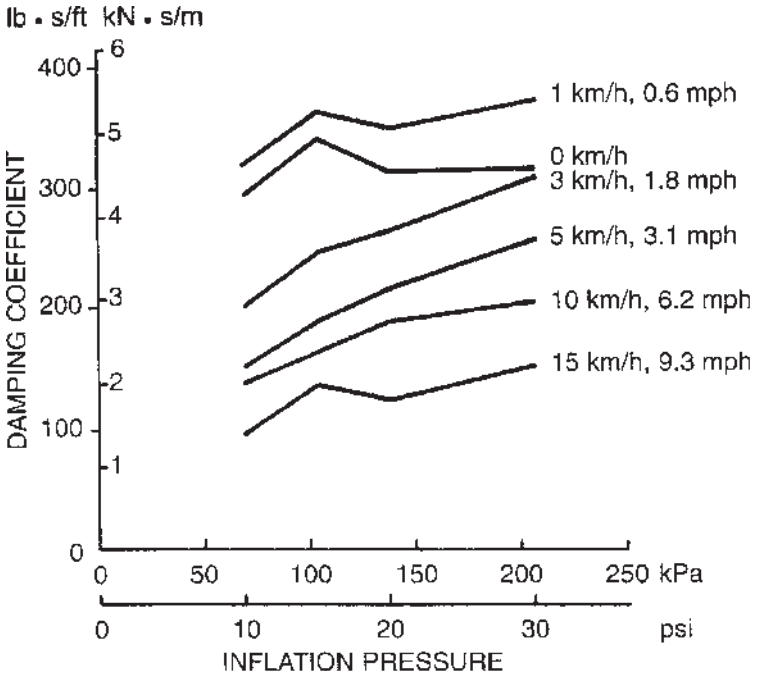

Fig. 1.65 Effect of inflation pressure on damping coefficient at various speeds of a radial-ply tractor tire 13.6 × 38. (Reproduced with permission from reference 1.37.)

Attempts to determine the relationship between the static and dynamic stiffness of tires have been made, but no general conclusions have been reached. Some reports indicate that for passenger car tires, the rolling dynamic stiffness may be 10–15% less than the stiffness derived from static load–deflection curves, whereas for heavy truck tires, the dynamic stiffness is approximately 5% less than the static value. For tractor tires, it has been reported that the dynamic stiffness may be 26% lower than the static value. In simulation studies of vehicle ride, the use of the rolling dynamic stiffness is preferred.

Among various operation parameters, inflation pressure, speed, normal load, and wear have a noticeable influence on tire stiffness. Tire design parameters, such as the crown angle of the cords, tread width, tread depth, number of plies, and tire material, also affect the stiffness.

The damping of a pneumatic tire is mainly due to the hysteresis of tire materials. Generally speaking, it is neither Coulomb-type nor viscous-type damping, and it appears to be a combination of both. However, an equivalent viscous damping coefficient can usually be derived from the dynamic tests mentioned previously. Its value is subject to variation, depending on the design and construction of the tire, as well as operating conditions. The damping of pneumatic tires made of synthetic rubber compounds is considerably less than that provided by a shock absorber.

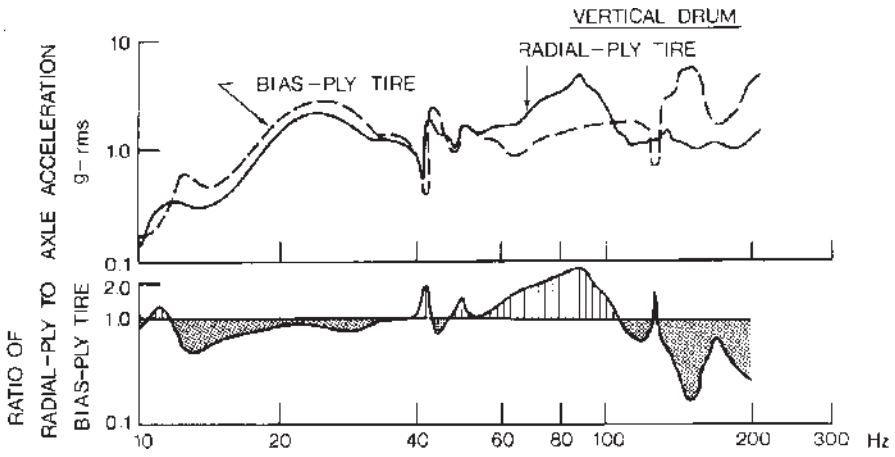

Fig. 1.66 Vibration characteristics of a bias-ply and a radial-ply car tire subject to sinusoidal excitation. (Reproduced with permission of the Council of the Institution of Mechanical Engineers from reference 1.38.)

To evaluate the overall vibrational characteristics of tires, tests may be carried out on a variable-speed rotating drum. The profile of the drum may be random, sinusoidal, square, or triangular. Experience has shown that the use of a periodic type of excitation enables rapid assessments to be made. Figure 1.66 shows the wheel hub acceleration as a function of frequency for a radial-ply and a bias-ply tire over a sinusoidal profile with 133 mm (5.25 in.) pitch and 6 mm (0.25 in.) peak-to-peak amplitude [1.38]. The transmissibility ratios in the vertical direction over a wide frequency range of a radial-ply and a bias-ply tire are shown in Fig. 1.67 [1.38]. This set of results has been obtained using a vibration exciter. The vibration input is imparted to the tread of a nonrolling tire through a platform mounted on the vibration exciter.

It can be seen from Figs. 1.66 and 1.67 that the transmissibility ratio for vertical excitation of the radial-ply tire is noticeably higher than that of the bias-ply tire in the frequency range of 60–100 Hz. Vibrations in this frequency range contribute to the passenger's sensation of "harshness." On the other hand, the bias-ply tire is significantly worse than the radial-ply tire in the frequency range of approximately 150–200 Hz. In this frequency range, vibrations contribute to induced tire noise, commonly known as "road roar" [1.1].

Tire noise is generated by the following major mechanisms [1.23]:

1. *Air pumping effect* As the tire rolls, air is trapped and compressed in the voids between the tread and the pavement. Noise is generated when the compressed air is released at high speed to the atmosphere at the exit of the contact patch.
2. *Tread element vibrations* Tread elements impact the pavement as the tire rolls. When the elements leave the contact patch, they are released from

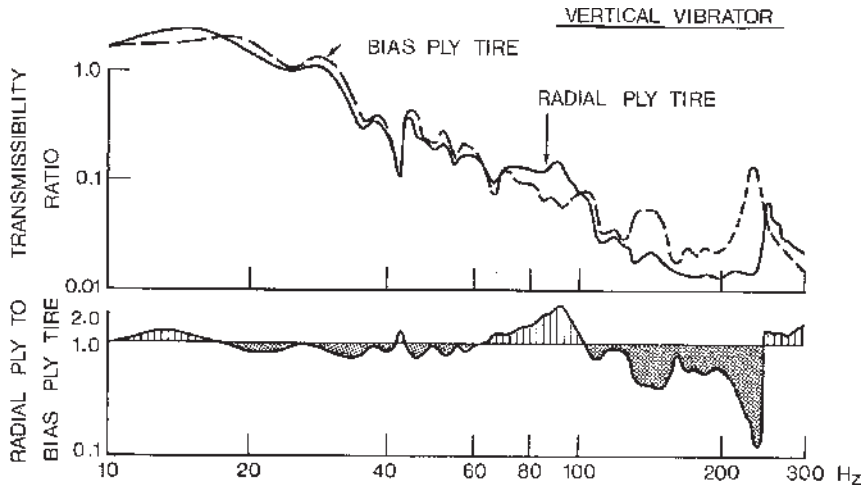

Fig. 1.67 Transmissibility ratio of a bias-ply and a radial-ply car tire. (Reproduced with permission of the Council of the Institution of Mechanical Engineers from reference 1.38.)

a highly stressed state. These induce vibrations of the tread, which form a major source of tire noise. Carcass vibrations and the grooves and lug voids in the tread acting like resonating pipes also contribute to noise radiation from the tire.

Since the air pumping effect, the vibrations of tread elements and carcass, etc., are related to speed, the noise level generated by a tire is a function of operating speed. Figure 1.68 shows the variations of noise level with speed for various types of truck tire on a smooth pavement [1.23]. The results were obtained following the SAE J57 test procedure. The effect of pavement texture on the noise level generated by a bias-ply, ribbed truck tire at 80 km/h (50 mph) is shown in Table 1.12 [1.23].

TABLE 1.12 Effect of Pavement Texture on Noise Level Generated by a Bias-ply Truck Tire

Road surface	Noise level dB (A)
Moderately smooth concrete	70
Smooth asphalt	72
Worn concrete (exposed aggregate)	72
Brushed concrete	78

Source: Reference 1.23.

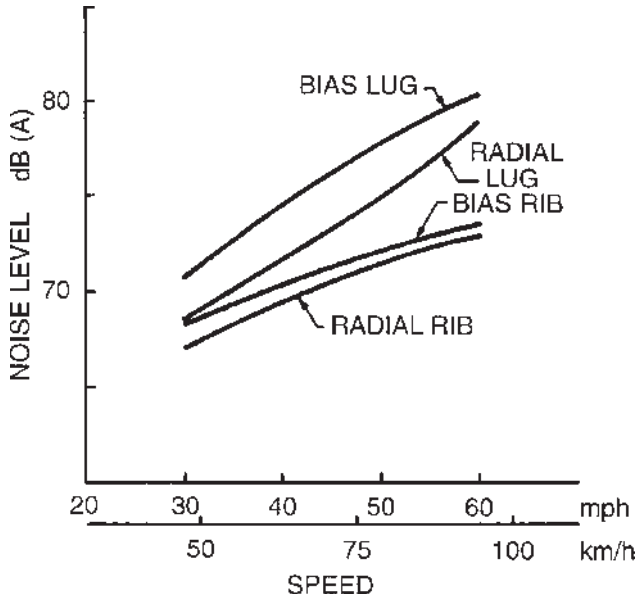

Fig. 1.68 Effect of speed on noise generated by bias-ply and radial-ply truck tires. (Reproduced with permission of the Society of Automotive Engineers from reference 1.23.)

REFERENCES

1.1 T. French, *Tire Technology.* Bristol, UK: Adam Hilger, 1989.

1.2 V.E. Gough, "Structure of the Tire," in S.K. Clark, Ed., *Mechanics of Pneumatic Tires,* Monograph 122. Washington, DC: National Bureau of Standards, 1971.

1.3 D.F. Moore, *The Friction of Pneumatic Tyres.* Amsterdam: Elsevier, 1975.

1.4 *Vehicle Dynamics Terminology,* SAE J670e, Society of Automotive Engineers, 1978.

1.5 T. French, "Construction and Behaviour Characteristics of Tyres," in *Proc. of the Institution of Mechanical Engineers, Automobile Division,* AD 14/59, 1959.

1.6 H.C.A. van Eldik and Thieme and H.B. Pacejka, "The Tire as a Vehicle Component," in S.K. Clark, Ed., *Mechanics of Pneumatic Tires,* Monograph 122. Washington, DC: National Bureau of Standards, 1971.

1.7 *Automotive Handbook,* 2nd ed. Robert Bosch, 1986.

1.8 L. Segel, "The Mechanics of Heavy-duty Trucks and Truck Combinations," presented at the Engineering Summer Conferences, University of Michigan, Ann Arbor, 1984.

1.9 J.D. Hunt, J.D. Walter, and G.L. Hall, "The Effect of Tread Polymer Variations on Radial Tire Rolling Resistance," Society of Automotive Engineers, Special Publications, P-74, *Tire Rolling Losses and Fuel Economy—An R&D Planning Workshop,* 1977.

1.10 L.W. DeRaad, "The Influence of Road Surface Texture on Tire Rolling Resistance," Society of Automotive Engineers, Special Publication P-74, *Tire Rolling Losses and Fuel Economy—An R&D Planning Workshop,* 1977.

1.11 B.L. Collier and J.T. Warchol, "The Effect of Inflation Pressure on Bias, Biasbelted and Radial Tire Performance," Society of Automotive Engineers, paper 800087, 1980.

1.12 J.J. Taborek, "Mechanics of Vehicles," *Machine Design*, May 30–Dec. 26, 1957.

1.13 J.D.C. Hartley and D.M. Turner, "Tires for High-performance Cars," *SAE Transactions,* vol. 64, 1956.

1.14 M.L. Janssen and G.L. Hall, "Effect of Ambient Temperature on Radial Tire Rolling Resistance," Society of Automotive Engineers, paper 800090, 1980.

1.15 R. Hadekel, "The Mechanical Characteristics of Pneumatic Tyres," S&T Memo No. 10/52, Ministry of Supply, London, 1952.

1.16 P.S. Fancher and P. Grote, "Development of a Hybrid Simulation for Extreme Automobile Maneuvers," in Proc. 1971 Summer Computer Simulation Conf., Boston, MA, 1971.

1.17 J.L. Harned, L.E. Johnston, and G. Sharpf, "Measurement of Tire Brake Force Characteristics as Related to Wheel Slip (Antilock) Control System Design," *SAE Transactions,* vol. 78, paper 690214, 1969.

1.18 R.D. Ervin, "Mobile Measurement of Truck Tire Traction," in *Proc. Symposium on Commercial Vehicle Braking and Handling,* Highway Safety Research Institute, University of Michigan, Ann Arbor, 1975.

1.19 P.S. Fancher, R.D. Ervin, C.B. Winkler, and T.D. Gillespie, "A Fact Book of the Mechanical Properties of the Components for Single-unit and Articulated Heavy Trucks," Report No. DOT HS 807 125, National Highway Traffic Safety Administration, U.S. Department of Transportation, 1986.

1.20 V.E. Gough, "Practical Tire Research," *SAE Transactions,* vol. 64, 1956.

1.21 D.L. Nordeen and A.D. Cortese, "Force and Moment Characteristics of Rolling Tires," Society of Automotive Engineers, paper 713A, 1963.

1.22 J.R. Ellis, *Vehicle Handling Dynamics.* London: Mechanical Engineering Publications, 1994.

1.23 T.L. Ford and F.S. Charles, "Heavy Duty Truck Tire Engineering," *The Thirty-Fourth L. Ray Buckendale Lecture,* Society of Automotive Engineers, SP-729, 1988.

1.24 E. Bakker, L. Nyborg, and H.B. Pacejka, "Tyre Modelling for Use in Vehicle Dynamic Studies," Society of Automotive Engineers, paper 870421, 1987.

1.25 E. Bakker, H.B. Pacejka, and L. Lidner, "A New Tire Model with an Application in Vehicle Dynamic Studies," Society of Automotive Engineers, paper 890087, 1989.

1.26 H.B. Pacejka, "The Tyre as a Vehicle Component," in *Proc. XXVI FISITA Congress, Prague, June 16–23,* 1996 (CD-ROM).

1.27 H.B. Pacejka and I.J.M. Besselink, "Magic Formula Tyre Model with Transient Properties," in F. Bohm and H.-P. Willumeit, Eds., *Proc. 2nd Int. Colloquium on Tyre Models for Vehicle Dynamic Analysis,* Berlin: Lisse, The Netherlands: Swets & Zeitlinger, 1997.

1.28 P. Bayle, J.F. Forissier, and S. Lafon, "A New Tyre Model for Vehicle Dynamics Simulations," in *Automotive Technology International '93.* U.K. & International Press, 1993.

1.29 A. van Zanten, W.D. Ruf, and A. Lutz, "Measurement and Simulation of Transient Tire Forces," Society of Automotive Engineers, paper 890640, 1989.

1.30 J. Zhou, J.Y. Wong, and R.S. Sharp, "A Multi-Spoke, Three Plane Tyre Model for Simulation of Transient Behavior," *Vehicle System Dynamics,* vol. 31, no. 1, 1999.

1.31 A. Schallamach, "Skid Resistance and Directional Control," in S.K. Clark, Ed., *Mechanics of Pneumatic Tires,* Monograph 112. Washington, DC: National Bureau of Standards, 1971.

1.32 S.K. Clark, "The Contact Between Tire and Roadway," in S.K. Clark, Ed., *Mechanics of Pneumatic Tires,* Monograph 122. Washington, DC: National Bureau of Standards, 1971.

1.33 W.B. Horne and R.C. Dreher, "Phenomena of Pneumatic Tire Hydroplaning," NASA TND-2056, Nov. 1963.

1.34 W.B. Horne and U.T. Joyner, "Pneumatic Tire Hydroplaning and Some Effects on Vehicle Performance," Society of Automotive Engineers, paper 650145, 1965.

1.35 J.A. Overton, B. Mills, and C. Ashley, "The Vertical Response Characteristics of the Non-rolling Tire," in *Proc. Institution of Mechanical Engineers,* vol. 184, part 2A, no. 2, 1969–1970.

1.36 J. Matthews and J.D.C. Talamo, "Ride Comfort for Tractor Operators, III: Investigation of Tractor Dynamics by Analogue Computer Simulation," *Journal of Agricultural Engineering Research,* vol. 10, no. 2, 1965.

1.37 J.A. Lines and N.A. Young, "A Machine for Measuring the Suspension Characteristics of Agricultural Tyres," *Journal of Terramechanics,* vol. 26, no. 3/4, 1989.

1.38 C.W. Barson, D.H. James, and A.W. Morcombe, "Some Aspects of Tire and Vehicle Vibration Testing," *Proc. Institution of Mechanical Engineers,* vol. 182, part 3B, 1967–1968.

PROBLEMS

1.1 Compare the power required to overcome the rolling resistance of a passenger car weighing 15.57 kN (3500 lb) and having radial-ply tires with that of the same vehicle, but having bias-ply tires in the speed range 40–100 km/h (25–62 mph). The variations of the coefficient of rolling resistance of the radial-ply and bias-ply passenger car tire with speed are described by Eqs. 1.1 and 1.2, respectively.

1.2 A truck tire with vertical load of 24.78 kN (5570 lb) travels on a dry concrete pavement with a peak value of coefficient of road adhesion $\mu_p = 0.80$. The longitudinal stiffness of the tire during braking C_s is 224.64 kN/unit skid (55,000 lb/unit skid). Using the simplified theory described

in Section 1.3, plot the relationship between the braking force and the skid of the tire up to skid $i_s = 20\%$.

1.3 Using the simplified theory described in Section 1.4.4, determine the relationship between the cornering force and the slip angle in the range 0–16° of the truck tire described in Problem 1.2. The cornering stiffness of the tire C_α is 132.53 kN/rad (520 lb/deg). Assume that there is no braking torque applied to the tire.

1.4 Determine the available cornering force of the truck tire described in Problems 1.2 and 1.3 as a function of longitudinal skid at a slip angle of 4°, using the simplified theory described in Section 1.4.4. Plot the cornering force of the tire at a slip angle of 4° versus skid in the range 0–40%. The coefficient of road adhesion is 0.8.

1.5 A passenger car travels over a flooded pavement. The inflation pressure of the tires is 179.27 kPa (26 psi). If the initial speed of the car is 100 km/h (62 mph) and brakes are then applied, determine whether or not the vehicle will be hydroplaning.

1.6 An all-terrain vehicle weighs 3.56 kN (800 lb) and has four terra tires, each of which has a vertical stiffness of 52.54 kN/m (300 lb/in.) at an inflation pressure of 27.6 kPa (4 psi), and a stiffness of 96.32 kN/m (550 lb/in.) at a pressure of 68.9 kPa (10 psi). Estimate the fundamental natural frequencies of the vehicle in the vertical direction at the two inflation pressures. The vehicle has no spring suspension.

1.7 Using the Magic Formula described in Section 1.4.4, estimate the cornering force of a car tire at a normal load of 6 kN (1349 lb) with a slip angle of 5°. The values of the empirical coefficients in the Magic Formula for the tire are given in Table 1.6.